FACULTY OF ENGINEERING AND ARCHITECTURE

Experimental study and kinetic modelling of combined deep hydrodenitrogenation and olefin saturation

Klaus Jacobs Cruz
Student Number: 02007302

Supervisors: Prof. Dr. Ir. Joris Thybaut, Prof. Dr. Ir. Kevin Van Geem
Councellors: Ir. Cesar Pernalete

Master's dissertation submitted in order to obtain the academic degree of
Master of Science in Chemical Engineering

Academic Year 2021-2022

GHENT UNIVERSITY

FACULTY OF ENGINEERING AND ARCHITECTURE

Experimental study and kinetic modelling of combined deep hydrodenitrogenation and olefin saturation

Klaus Jacobs Cruz

Student Number: 02007302

Supervisors: Prof. Dr. Ir. Joris Thybaut, Prof. Dr. Ir. Kevin Van Geem

Councellors: Ir. Cesar Pernalete

Master's dissertation submitted in order to obtain the academic degree of
Master of Science in Chemical Engineering

Academic Year 2021-2022

GHENT UNIVERSITY

Acknowledgements

This dissertation is the result of 12 months of hard work which could not have been possible to do by my own. As such, I would like to spend some words to those who were in a supporting role during the making of this study.

First and most importantly I would like to thank my coach Cesar as well as my supervisors Joris and Kevin. They helped me through knowledge, advice and active action during the whole experimental campaign. I would like to give special thanks to Cesar. He was very active in both the experimental campaign and the analysis of the results. Without his involvement it wouldn't have been possible to obtain even one result. He was always besides me and helping me to overcome the many difficulties and setbacks while using the set-up. His creativity and experience was extremely valuable to solve every problem. For certain, some problems I would not have been able to solve by myself. He always kept his cool even when the situation was looking grim as the set-up just didn't want to work and by adapting his original idea to the limitations of the set-up relevant results were obtained. Another person who deserves special thanks is Jessica. She arrived to work on her thesis which is going to be made in the same set-up and became an active participant of this thesis. Without her help, the data that was collected wouldn't have been possible.

Other persons who deserve acknowledgement are the persons in the technical department. I wish to thank Michaël, Wim, Brecht, Lambert, Hans, Erwin, Tom and Bert. I came into many and frequent technical problems, both small and big. Without their direct and rapid involvement, the set-up would have never worked. They were always willing to help.

The corona crisis was very hard on me as it caught me on an unknown country with unknown people. As a result, I would like to thank the people with whom I shared the master student room for the last 12 months. It was fun to share all the difficulties, disappointments, successes and achievements and to remind me that I was not alone in the struggle. Special thanks to Felix, Frederik, Joren, Marteen and Guillaume for reminding me what was life before corona.

Lastly but most importantly, I would like to thank my family. Without the support of my mother, father and brother it would not have been possible to have this experience in Belgium. You are the reason that have brought me to this point and will be forever grateful.

Klaus Jacobs Cruz

FACULTY OF ENGINEERING AND ARCHITECTURE

Permission of use on loan

June 18, 2022

Remark on the master's dissertation and the oral presentation

This master's dissertation is part of an exam. Any comments formulated by the assessment committee during the oral presentation of the master's dissertation are not included in this text

Experimental study and kinetic modelling of combined hydrodenitrogenation and olefin saturation

Klaus Jacobs Cruz*

Ir. Cesar Pernalete**, Prof. Dr. Ir. Joris Thybaut***, Prof. Dr. Ir. Kevin Van Geem***

Master's dissertation submitted in order to obtain the academic degree of

Master of Science in Chemical Engineering

Academic Year 2021-2022

Abstract

Chemical recycling via conversion refers to the use of a chemical process to convert plastic waste into an oil like hydrocarbon stream. In schemes where thermal pyrolysis is the conversion route the product is a pyrolysis oil typically with a very high nitrogen and olefins content. Further processing of this pyrolysis oil in the refining/petrochemical industry requires a previous hydrodenitrogenation step in order to guarantee product specifications and protect catalyst in downstream processes. To get a deeper understanding on the combined hydrodenitrogenation, and the consequent olefin saturation, an experimental study and kinetic modelling of the hydrotreating of a mixture containing hexadecene, octadecene and quinoline. The experiments were done using a commercially available $NiMoP/Al_2O_3$ catalyst (HR-348 from PROCATALYSE) in a three phase Robinson Mahoney reactor. Operating conditions were set at a fixed H_2/HC ratio of 890 $Nm^3\ m^{-3}$ and pressure of 90 bar while temperature ranged between 300 and 350°C and LHSV varied between 0.4 and1 h^{-1}. It was observed that olefin conversion decreases dramatically with LHSV at 300 C being the lowest between 70% and 75% at the lowest LHSV tested value. The higher the temperature the less pronounced the contribution of LHSV on conversion. At 350 C olefin conversion was always above 95%. Quinoline conversion was always higher than 95%. However, the maximum achieved conversion towards non-nitrogenated compounds was only 15%. The hydrogenated intermediate 1,2,3,4 tetrahydroquinoline (14THQ) was identified as the major product in all cases. Other intermediates including 5,6,7,8 tetrahydroquinoline (58THQ) and decahydroquinoline (DHQ) were also identified but in smaller concentrations. The more severe the operating conditions the lower the selectivity towards 14THQ confirming that quinoline follows a sequential hydrodenitrogenation process with an initial hydrogenation mainly towards 14THQ. This intermediate could follow a ring opening reaction, producing either orto-propylaniline (OPA) by direct ring opening without hydrogenation of the benzene ring ,and finally denitrogenation producing propylbenzene (PB). Another path of reaction could be initialhydrogenation of the benzene ring of 14THQ and later ring opening producing the intermediate propylcyclohexylamine (PCHA) and finally propylcyclohexane (PCH) via denitrogenation. The results of the kinetic modelling were inconclusive as low F-values were obtained but this may be due to the low number of experiments performed and the chosen experimental conditions were not appropriate for parameter estimation. By comparing these results with the ones on the literatures it can be deduced that olefin saturation interferes with the hydrogenation and ring opening reactions of the intermediates of quinoline hydrodenitrogenation as lower nitrogen conversions than in the literature at similar operating conditions were obtained.

Keywords: chemical recycling, pyrolysis oil, olefin saturation, quinoline hydrodenitrogenation, hydrotreating

---

*Student Number: 02007302, **Counselor, ***Supervisor

1. Introduction

Plastics are used in a wide range of industrial processes, from packaging applications to automotive or electronics parts production, due to the versatility of their mechanical properties. As a result, the global consumption of plastics has grown from 1.5 Mt in 1950 to 359 Mt in 2018 [1]. A major issue associated with plastics production is its end-of-life management. Some plastics could have a long service life, up to 50 years as in aerospace applications, while others have a service life that range from a few days to a few months, such as in packaging applications. Since packaging has a share of 40% in the end use market of plastics in Europe [2], it represents a big environmental problem. It is estimated that from 4 to 12 Mt/y of waste plastics end up in the ocean [3]. The effects of this situation on marine life and, in consequence, on the human being is of increasing concern.

From a general point of view, plastics recycling can be achieved using two methods: mechanical and chemical. A schematic representation of the different methods for plastics recycling is shown in Figure 1. Mechanical recycling is a process where a plastic stream is reduced in size, melt, and reshaped to produce a new final product [4]. A big disadvantage of this method is that with each recycling cycle a lower quality product is produced until it has no practical use [5]. Chemical recycling refers to the use of a chemical process to convert the plastic waste weather into simpler compounds such as the 'constituents' monomer of the polymer, or an oil like hydrocarbon stream that can be used as feedstock in the refining/petrochemical industry [4].

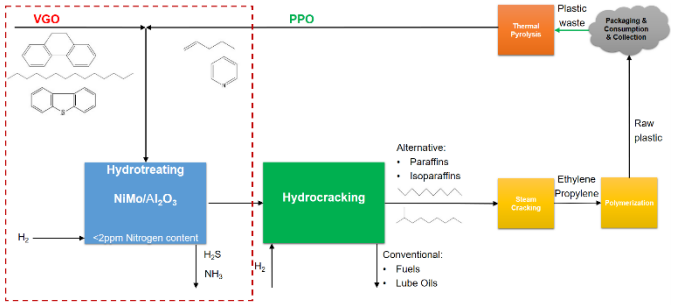

Figure 1 Schematic representation of a closed looping chemical recycling integrating steam cracking and hydroprocessing (hydrotreatment and hydrocracking)

Figure 1 shows a global scheme of chemical recycling that integrates traditional refining/petrochemical units such as hydrocracking and steam cracking with thermal pyrolysis. In this configuration the plastic waste is initially processed via thermal pyrolysis to obtain a hydrocarbon rich stream called plastic pyrolysis oil (PPO). PPO produced from plastic waste is a complex hydrocarbon mixture containing paraffins, naphthenes, aromatics and an elevated proportion of olefins, with a carbon range distribution between 3 and even more than 50 carbon atoms. A high content of nitrogen heterocompounds are also found in these streams. This unconventional stream is mixed with a conventional petroleum fraction, such as vacuum gas oil (VGO), and processed using an integration of hydroprocessing and steam cracking aiming to maximice the production of the building block for polymers ethylene andpropylene.After production of new plastics, the loop is closed when they are collected and pyrolized

.

Using the described configuration, it is possible either to produce fuels in a typical configuration for a hydrocracking unit or to produce a synthetic feed for a steam cracker. In any case, nitrogen compounds need to be removed to guarantee product specifications and to avoid inhibition effect in the downstream hydrocracking catalyst [6] for which a hydrotreating unit is used previous to the hydrocracking-steam cracking process sequence.Since virgin petroleum fractions do not contain olefins, hydrodenitrogenation is normally made in absence of olefins. Consequently literature on kinetics for hydrodenitrogenation combined with olefin saturation is very limited. The aim of this thesis is to perform an experimental study that allow to get a deeper understanding about the combined hydrodenitrogenation and saturation of long olefins, particularly in scenarios of high concentration of olefins. For this purpose, a combination of model molecules for nitrogen compounds and unsaturated compounds are hydroprocessed under typical operating conditions and catalyst for hydrodenitrogenation. Finally, different kinetic models for both olefin saturation and denitrogenation reactions are proposed and compared against the generated experimental data.

2. Experimental section

2.1. Catalyst and reactants

A commercial NiMoP in all the experiments. The theoretical catalyst composition by weight is: 10.7% Mo, 2.5% Ni and 2.64% P while the reported BET surface area is 164 m^2 g^{-1} [7]. The catalyst pellets were crushed and sieved to get a particle size between 600 and 720 µm. Theolefins selected as model molecules were: synthesis grade 1-Hexadecene with a purity of ≥92 wt.% and unspecified impurities, technical grade 1-Octadecene with a purity of ≥90% and 2-octyl-1-decene, n-octadecane, 2-butyl-1-tetradecene, 2-hexyl dodecene as impurities of unspecified composition. The selected nitrogenated heterocompound was synthesis grade quinoline with a purity of ≥97 wt.%. As solvent a mixture of C_9-C_{14} paraffins commercially called Halpasol was used. The GC/FID analysis of this solvent yielded the following composition in wt.%: 0.15% n-nonane, 7.71% n-decane, 33.29% n-undecane, 22.00% n-dodecane, 36.49% tridecane and 0.46% tetradecane. DMDS was used as a sulfiding agent for the catalyst activation procedure and to keep a sulfur

*Student Number: 02007302, **Counselor, ***Supervisor

environment in the system and keep the catalyst in the active sulfided state during all the experimental campaign.

1.1. Equipment

All the experiments were performed in a Robinson-Mahoney reactor, a gradient-less three phase continuously stirred tank reactor (CSTR) which makes it ideal for studying the hydroprocessing of petroleum fractions such as light gas oil (LGO) and VGO.. A simplified block diagram of the set-up is shown in Figure 2.

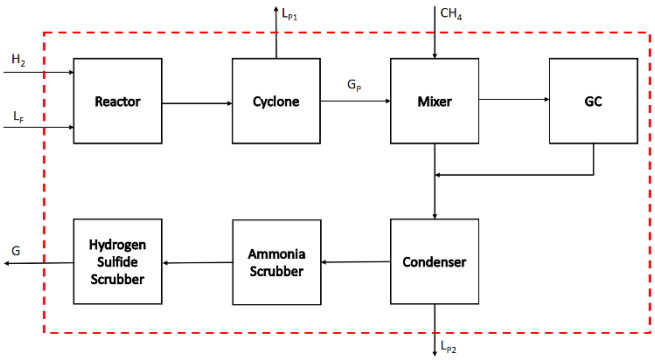

Figure 2 General mass balance scheme of the set-up

Initially the reactor is fed with a liquid feed (L_F) and hydrogen (H_2) while the product stream is sent to a cyclone where the main liquid product L_{p1} is separated. The gas stream (G_p) exiting the cyclone is mixed with the internal standard 'methane' in the mixer and is partially sent to the GC for online analysis. The total gas effluent from the mixer enters the condenser where any condensable hydrocarbon is recovered (L_{p2}). H_3PO_4 and NaOH aqueous solutions were used to neutralize NH_3 and H_2S respectively in the scrubbing section after the condenser.

The set-up is equipped with a gas chromatograph Trace 1310 from Thermo Scientific. The GC has three detectors, two TCDs and one FID. The FID detector is attached to a detailed hydrocarbon analysis (DHA) column of dimensions 100m x 0.25mm and a liquid injector module and uses helium as carrier gas. The Front TCD is attached to a RT-Volamine column of dimensions 30m x 0.32mm and also uses helium as carries gas. The Aux TCD is attached to a Molsieve 5A, 60-80 of dimensions 3m x 1/16 SS and a Hayesep Q, 60-80 of dimensions 1m x 1/16 SS and uses argon as carrier gas.

1.2. Data acquisition and parameter estimation

The catalyst activation process was performed based on the procedure proposed by Ancheyta [8] and it is, in general, divided into three steps: drying, soaking and sulfiding. The drying consist of using hot hydrogen to remove any trace of water from the catalyst pores that can expand at high temperatures and mechanically affect the catalyst. The soaking with a hydrocarbon mixture is made to ensure that the entire catalyst surface is in touch with the liquid phase. The sulfiding step is made to ensure that the molybdenum oxide transforms to molybdenum sulphide which is the active phase of the catalyst for hydrotraeating. For this a sulfiding feed consisting of a mixture of Halpasol (98%) and DMDS (3%) was used. It was left to sulphide for 150 min. Afterwards, the temperature was increased to 310°C and maintained for 194 min at 20 bar.

The composition of the feed was chosen assuming a 58 wt.% olefin content in PPO, a mixture of 80 wt.% VGO and 20 wt.% PPO, a total nitrogen content of 1 wt.% and a H_2S/Nitrogenated hetero-compounds ratio of 0.2 mol mol^{-1} [9]. Consequently, the L_F composition in wt. % was 0.12% n-nonane, 6.02% n-decane, 25.99% n-undecane, 17.18% n-dodecane, 28.41% n-tridecane, 0.36% n-tetradecane, 9.23% quinoline, 6.01% hexadecene, 6.02% octadecene and 0.67% DMDS.

The investigated range of experimental operating conditions is shown in Table 1 at fixed H_2/HC ratio of 890 Nm^3 m^{-3}. The total amount of experiments amounted to 16. After 1 h stabilization of the reactor, liquid samples were taken at a 30 min time frame.

Table 1 Experimental operating conditions

OPERATING CONDITION	VALUE
TEMPERATURE	300-317-334-350°C
PRESSURE	90 bar
LHSV	0.4-0.7-1 h^{-1}
LIQUID FEED FLOW	1-1.75-2.5 ml min^{-1}
H_2 FLOW	53.4-90.45-133.5 NL h^{-1}

The experimental conversions of quinoline, hexadecene and octadecene were calculated considering that the reactions take place in the completely wetted catalyst [10]. As a consequence, the fraction of liquid reactant that vaporize is excluded from participating in the reaction. Therefore, given a molar feed rate $L_{F,i}$, the molar rate that is in contact with the catalyst is $L_{F,i}$-$L_{P2,i}$ where $L_{P2,i}$ is the molar flow that is condensed from the product gas stream G_P. Consequently, the conversion of the olefins is defined in Eq. 1.

$$X_i = \frac{L_{F,i} - L_{P1,i} - L_{P2,i}}{L_{F,i} - L_{P2,i}} \qquad 1$$

The conversion of the products is calculated according to Eq. 2.

$$X_i = \frac{L_{P1,i} + L_{P2,i}}{L_{F,i} - L_{P2,i}} \qquad 2$$

Experimental production rates/rate of disappearance R_i, is calculated dividing the conversion X_i by the space time. Due to the assumption made for the calculation of the conversion space time is defined as the mass of the catalyst W divided

*Student Number: 02007302, **Counselor, ***Supervisor

by the molar flow rate that is in contact with the catalyst [10]. Consequently, the experimental production rates R_i were calculated according to Eq. 3 where $L_{F,j}$-$L_{P2,j}$ is the molar rate of the olefin or quinoline that is in contact with the catalyst

$$R_i = \frac{X_i}{\frac{W}{L_{F,j} - L_{P2,j}}} \qquad 3$$

The experimental selectivity of the products of the hydrodenitrogenation of Quinoline were calculated according to Eq. 4. where S_i is the selectivity with reference to Quinoline, $L_{P1,i}$ is the molar flow of compound "i" in the liquid product, $L_{F,Q}$ is the molar flow of Quinoline in the liquid feed, $L_{P1,Q}$ is the unreacted Quinoline in the liquid product and $L_{P2,Q}$ is the unreacted Quinoline in the condensed gas product.

$$S_i = \frac{L_{P1,i} + L_{P2,i}}{L_{F,Q} - L_{P1,Q} - L_{P2,Q}} \qquad 4$$

Athena visual studio was used to estimate the model parameters by minimizing the objective function shown in Eq. 5 employing a non-linear least square algorithm.

$$SSQ = \sum_{i=1}^{nob} \sum_{j=1}^{nresp} \left(R_{i,j} - \widehat{R_{i,j}}\right)^2 \rightarrow Min \qquad 5$$

3. Experimental results and kinetic model

3.1. Olefin saturation

Olefin conversion results are shown in Figure 3. At a LHSV of 1 h^{-1} the olefins conversion ranged between 72% and 95% for hexadecene while for octadecene varied between 74% and 96%. The lowest conversion was observedat 300°C while the highest conversion was

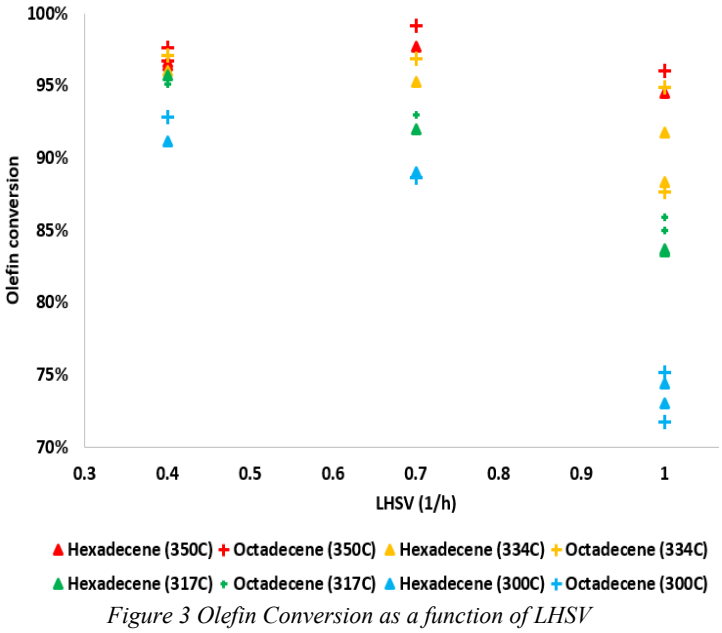

Figure 3 Olefin Conversion as a function of LHSV

observed at 350°C. As the reaction temperature increased, the olefin conversion increased as expected. In Figure 3 it can also be observed that temperature has a strong effect on olefin conversion with respect to LHSV. These trends are in agreement with the work of Xin, et al. [11] where temperatures in a range of (100-300°C) and pressures in the range of (14-28 bar) were used to hydrogenate C_7 olefins. In the work of Xin, 100% conversion is achieved at 300°C, 21 bar, and an LHSV of 1.5 h^{-1} . Since in this work conversions between 72% and 75% were obtained at 300°C for C_{16} and C_{18} n-olefins the comparison with the work of Xie suggest that the hydrogenation of olefins is negatively correlated with the chain length of the olefin. From Figire 3 can also be observed that the temperature specific contribution to olefins conversion is less pronounced at lower LHSV values. At a LHSV = 0.4 1 h^{-1} the lowest conversion was 91% at 300°C while the highest conversion was 97% at 350°C. At 0.7 h^{-1} the lowest conversion was 89% at 300°C while at the highest conversion was 99% at 350°C. The increase in the conversion as the LHSV decreases is due to higher retention times of the olefin inside the reactor [11]. An optimal conversion of 99.1% was obtained at 350°C and LHSV = 0.7 h^{-1}.

The total olefin content in the hydrotreated product (L_{P1} + L_{P2}) at a LHSV of 1 h^{-1} decreased from a maximal value of 3.5 wt.% at 300°C to a minimal value 0.57 wt.% at 350°C from an initial total olefin content of 12 wt.%. These results are also in agreement with the other work of Xin, et al [12]. The olefin content of a light fraction of a thermally processed bitumen decreased from 6 wt.% in the feed to 0.5 wt.% in the hydrotreated product at 300°C. From these results it can be inferred that in order to obtain near full olefins saturation conversion with carbon of 16 or higher at industrially relevant space velocities temperatures of 350°C or higher are needed. At LHSV of 0.4 and 0.7 h^{-1}, the olefin content in the hydrotreated product was observed to be between 0.18 wt.% and 0.53% at temperatures of 334°C and 350°C. At LHSV=1 h^{-1} the olefin content in the product varied from 3.5 wt.% at 300°C to 0.57% at 350°C It is worth saying, that working at too low LHSV may present productivity issues that might affect the economics of the process rendering the process not viable. Olefin content in PPO ranges from C_{10} to C_{20} [13] and since PPO can be separated into light and heavy fractions, the choice of operating conditions in a PPO/VGO mixture if the objective is to saturate the olefins of the mixture will depend on the amount of PPO added to the mixture and carbon range of the PPO fraction. Adding lighter PPO fractions to VGO will need less severe conditions than adding heavy PPO fractions. Another important factor is the source in the PPO. The composition of the pyrolysis product will depend on the composition of the plastic feed stream of the pyrolysis process [14]. Knowledge of the composition of the PPO

*Student Number: 02007302, **Counselor, ***Supervisor

added to the VGO becomes a prerequisite if conventional hydrocracking is to be desired.

3.2. Quinoline hydrodenitrogenation

Quinoline conversion varied only between 95.1% and 96.2% for all the studied experimental conditions. These results are in agreement with the results obtained by Luan et al. [15] and Tu et al [16] in a batch reactor at 350°C and 30 bar using a NiMo catalyst. The temperature seems to have a low influence on quinoline conversion because at temperature above the ones used in this work; conversions only rise until 98% [15]. The effect of temperature on product selectivities is more pronounced as shown in Figure 4. For every studied LHSV conditions the principal product was 1,4THQ. For every studied temperature, the selectivity towards this product decreased from 93.9% at 300°C to 76.2% at 350°C at 1 h^{-1}. LHSV does not appear to have a strong effect on quinoline conversion as conversions varied between 95.1% and 97.9% at 0.4 h^{-1} and 0.7 h^{-1} but it does have a strong effect on 1,4THQ selectivity. At 0.4 h^{-1}, 14THQ selectivity decreased from 84.1% to 59.6%.

Other major products were OPA and PCHA in which the selectivities increased from 1.9% and 2.3% at 300°C to 6.4% and 8.0% at 350°C respectively at a LHSV of 1 h^{-1}. As the LHSV decreased, the selectivity towards these intermediates increased to 10.0% and 10.9% at 350°C and 0.4 h^{-1}. Minor intermediate products were 58THQ and DHQ whose selectivities increased from 0.2% and 0.4% at 300°C to 2.4% and 1.6% at 350°C at 1 h^{-1} respectively. LHSV doesn't have a strong effect on the selectivity of those minor intermediates. The detected denitrogenated products were PCH and PB with selectivities that increased from 0.1% and 0.2% at 300°C to 3.6% and 1.4% at 350°C respectively. LHSV does have a strong effect on PCH and PB selectivities. At 0.4 h^{-1} there was an increase from 2.2% and 1.0% at 300°C to 10.9% and 4.0% at 350°C. PCHE was not detected in none of the experimental runs. It is possible that PCHE was eluting at the same retention time as PB or that it is easily hydrogenated into PCH. The results show that 14THQ is the main product of quinoline HDN, this is in accord with the results of Tian, et al. [17], Luan, et al. [15], Nguyen, et al. [18] and Tu, et al. [16]. Since quinoline conversion is independent of temperature at the tested temperature range, it can be deduced that it is easily hydrogenated into 14THQ while hydrogenation of 14THQ is a more difficult reaction. The hydrogenation of the hetero-cyclic aromatic ring is the prefer path towards quinoline HDN as the production 58THQ is much lower than that of 14THQ. Once 14THQ is produced, the HDN can take two different pathways. One pathway (PW1) is the subsequent hydrogenation of the benzene ring to form DHQ which then undergoes ring opening through C_{sp3}-N cleavage to form PCHA. Finally, the C-N is broken to form PCH releasing NH_3. The other pathway (PW2) according to the results is the direct hydrogenolysis of 14THQ to form OPA which is then either hydrogenated into PCHA or it can go into direct C_{sp2}-N bond cleavage to form PB releasing NH_3. According to the selectivity analysis as a function of temperature, PW1 is the prefer path towards quinoline HDN as the temperature increases. The PCH to PB ratio increases from 0.43 at 300°C to 2.60 at 350°C. Due to the high production of 14THQ, it can be deduced that the slowest steps from PW1 and PW2 are the benzene ring hydrogenation to DHQ and the direct hydrogenolysis to OPA respectively. DHQ and PCH shows lower selectivities than PCHA which means that ring opening is faster step than C-N cleavage however, DHQ is also being consumed in the equilibrium reaction with 58THQ as shown by the increase in selectivity of 58THQ. Since quinoline conversion is not changing with temperature, it means that the other only possible pathway towards 58THQ formation is that as temperature increases the equilibrium shifts to the left and hence 58THQ is formed. OPA selectivity is lower is than PCHA selectivity which means that either ring opening of 14THQ is more difficult than the benzene ring hydrogenation or that as temperature increases more OPA is being consumed towards PCHA.

Despite the high quinoline conversion, the total nitrogen conversion is low as shown in Figure 4. However, temperature have a strong effect on nitrogen conversion. There is an exponential increase from 0.25% at 300°C to 4.8% at 350°C at a LHSV of 1 h^{-1} and a maximal nitrogen conversion of 15.1% at 350°C and 0.4 h^{-1}. These results are much lower than those presented by Luan, et al. [15]. According to the authors, at a space time of 1.12 min which means a LHSV of 0.018 h^{-1}, at 350°C there is a nitrogen conversion of around 70%. It is worth noticing that the strong effect of temperature is also evidenced. Yet, the operating conditions and the catalyst (NiW) were different. Ferdous, et al. [19] hydrorteated a heavy gas oil containing 0.3% nitrogen at operating conditions similar to the ones tested in this work. At 356°C, 94 bar and a LHSV of 0.8 h^{-1}, they obtained a 49.3% nitrogen conversion which is a value much higher than the one obtained at similar conditions in this work. While the operating conditions were similar, the catalyst used was a NiMoB catalyst and the feed was a complex mixture which does not contains olefins. As a result, the feed contains a mixture of basic and non-basic nitrogen containing hetero-compounds. As explained in the selectivity analysis, HDN follows sequential hydrogenation, ring opening and denitrogenation. As a consequence, the presence of olefins in the feed may affect the hydrogenation of the intermediate HDN products due to competitive effects and/or hydrogen availability. Since hydrogenation of the benzene ring of a heterocyclic compound is a fundamental pathway for nitrogen removal, olefin presence may inhibit this step and consequently decreasing the total nitrogen conversion.

*Student Number: 02007302, **Counselor, ***Supervisor

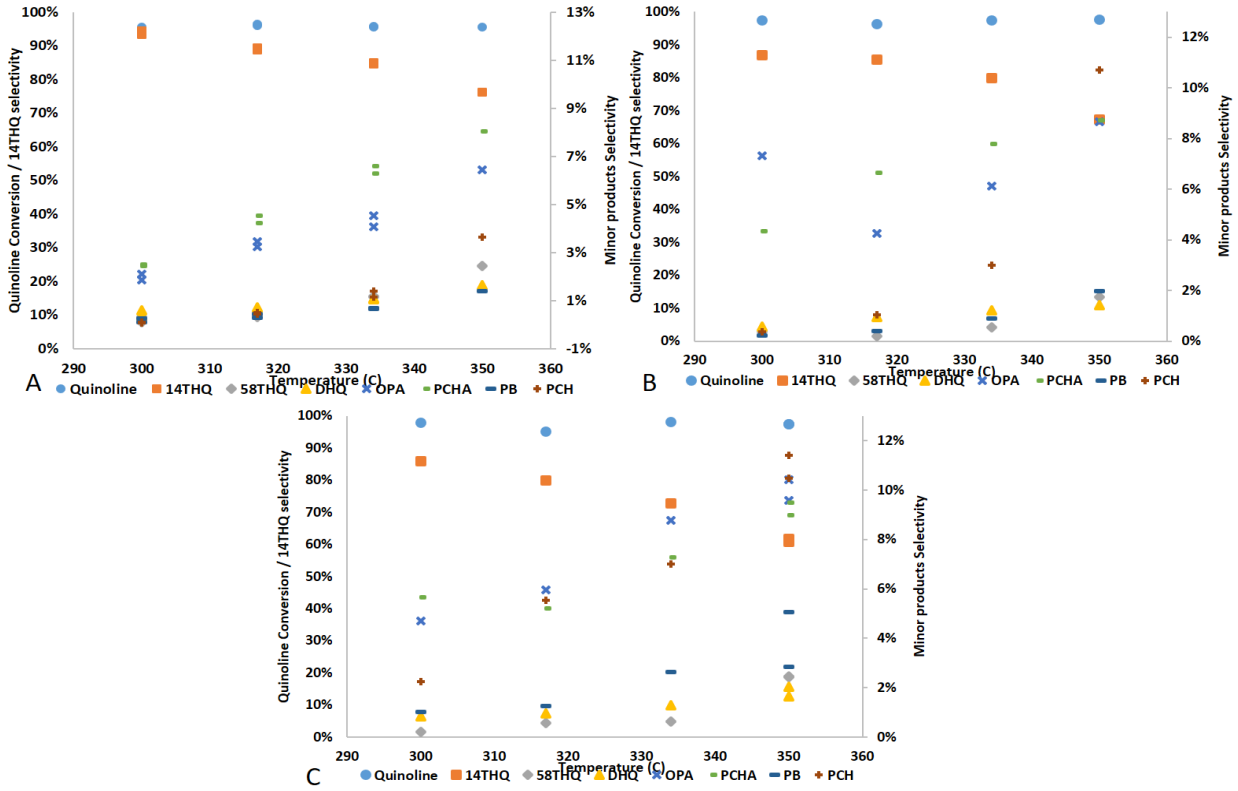

Figure 4 Quinoline conversion and close products selectivity as a function of temperature. 14THQ=1,2,3,4 tetrahydroquinoline, 58THQ= 5,6,7,8 tetrahydroquinoline, OPA=orto-propylaniline, DHQ=decahydroquinoline, PCHA= propyl-cyclohexylamine, PB=propylbenzene. A: LHSV=1, B: LHSV=0.7, C: LHSV=0.4

3.3. Kinetic Model

3.3.1. Olefin saturation kinetic model

Two different kinetic models for the olefin hydrogenation were proposed. Both of them are based on the studies of Thybaut, et al. [20] and Mattson, et al. [21]. As both of these studies are based on the Horiuti-Polanyi mechanism the difference between the proposed models are on the assumptions made. The proposed reaction mechanism for the first kinetic model on olefin hydrogenation (OHKM1). The assumptions made on this reaction mechanism are as follow:

- H_2 dissociative chemisorption and olefin reactant chemisorb at identical sites (competitive chemisorption)
- First (OHKM1) or second (OHKM2) hydrogenation step is the rate-limiting step and irreversible
- Other surface reactions are at a quasi-equilibrated state
- Alkane desorption is very fast, chemisorbed species coverage is negligible

OHKM1 is shown in Eq. 6 while OHKM2 is shown in Eq. 7.

$$r_{OHKM1} = \frac{k_1\sqrt{C_{H_2}K_{H_2}}\Theta_T{}^2 K_{OH_2}{}^2 C_{H_2}K_{H_2}K_O C_O}{\left(K_{OH}(C_O K_O + 1)\sqrt{C_{H_2}K_{H_2}} + C_{H_2}K_{H_2}K_{OH} + K_{OH_2}C_{OH_2}\right)^2} \quad 6$$

$$r_{OHKM2} = \frac{\mathrm{k}_1 K_{H_2}\mathrm{C}_{\mathrm{H}_2}\Theta_T{}^2 K_O \mathrm{C}_\mathrm{O} K_{OH}}{\left(K_O \mathrm{C}_\mathrm{O} K_{OH}\sqrt{K_{H_2}\mathrm{C}_{\mathrm{H}_2}} + K_O \mathrm{C}_\mathrm{O} + \sqrt{K_{H_2}\mathrm{C}_{\mathrm{H}_2}} + 1\right)^2} \quad 7$$

3.3.2. Quinoline hydrodenitrogenation kinetic model

A kinetic model for the quinoline HDN is proposed based on the reaction scheme shown in Figure 5. The assumptions and mechanisms of this model are based on the work of Nguyen, et al. [18]. The assumptions are as follow:

- Coverages of H_2S and NH_3 are negligible
- Same active site for hydrogenation and C-N cleavage
- Surface reactions are rate limiting steps
- No consideration on solvent adsorption
- Generalized Langmuir-Hinshelwood formalism to To express the coverage of the relevant species

Consequently, the reaction rate for the reactions shown in Figure 5 is described in Eq. 8

$$\mathrm{r_i} = \frac{\mathrm{k_i K_i C_i C_{H_2}}}{\left(1 + \sum_{\mathrm{j=1}}^{\mathrm{n}} \mathrm{K_j C_j}\right)^2} \quad 8$$

**Student Number: 02007302, **Counselor, ***Supervisor*

As a result, 58 parameters must be estimated which is too high for so few experiments. By assuming th consumption rates of hexadecene and octadecene are equal and simplifying the reaction scheme in Figure 5 by lumping 58THQ, 14THQ and DHQ into one pseudo-compound (HYDROG), OPA and PCHA into another pseudo-compound (RO), PB and PCH into another pseudo-compound (HC) and assuming that quinoline hydrodenitrogenation occurs in sequential and irreversible hydrogenation, ring opening and denitrogenation steps, it was possible to reduce the total number of parameters to 24.

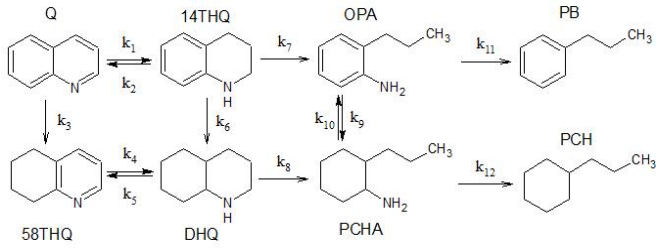

Figure 5 Proposed quinoline hydrodenitrogenation reaction scheme

The results of the parameter estimation for the two proposed model for olefin saturation are shown in Table 2. Activation energies for both models are around 20000 kmol kJ^{-1} with an estimated rate constant ktm at the average temperature Tm of 598.15K of 0.8 kmol m^{-3} h^{-1} and 4.1 kmol m^{-3} h^{-1} for OHKM1 and OHKM2 respectively however no t-value was estimated for ktm in both models. For OHKM2, only the Ea was statistically significant and the adsorption constant at Tm of the first hydrogenation step. OHKM1 estimated that the Ea, adsorption enthalpies of H_2, olefin, the chemisorbed alkane, the adsorption constants at Tm of hydrogen and olefin are statistically significant. Figure 6 shows the parity plots for OHKM1 (Top) and OHKM2 (Bottom). Neither of the models achieve an accurate prediction of the consumption rates of olefins. However, OKHM1 has a better performance than OHKM2 as evidenced by their F-values of 81 and 20 respectively but are low values for both models. The difficulty to predict the consumption rate may be due to the low number of experiments and to the fact that the operating conditions achieved high conversions on all experiments.

Table 2 Olefin saturation parameter estimation results

	OHKM1			OHKM2		
Parameter	**Value**	**t-value**	**95% CI**	**Value**	**t-value**	**95% CI**
ktm (kmol kg_{cat}^{-1} h^{-1})	0.8	n.e.	n.e.	4.1	n.e.	n.e.
Ea (kmol kJ^{-1})	20420.6	34.4	10260.0	19464.8	47.6	409.3
$AtmH_2$ (m^3 $kmol^{-1}$)	367.7	n.e.	n.e.	1773.8	n.e.	n.e.
ΔH_2 (kmol kJ^{-1})	-369415.0	-2.7	1313.0	-943.5	n.e.	n.e.
AtmO (m^3 $kmol^{-1}$)	311.6	3.5	195.8	0.1	n.e.	n.e.
ΔHO (kmol kJ^{-1})	-39666.5	-2.5	17780.0	-36.5	n.e.	n.e.
AtmOH (m^3 $kmol^{-1}$)	53.0	n.e.	n.e.	134.7	5.5	134.7
ΔHOH (m^3 $kmol^{-1}$)	-28675.0	n.e.	n.e.	-29.1	n.e.	n.e.
$AtmOH_2$ (kmol m^{-3})	134.4	n.e.	n.e.	n.a.	n.a.	n.a.
ΔHOH_2 (m^3 $kmol^{-1}$)	-42106.5	-3.2	29190.0	n.a.	n.a.	n.a.

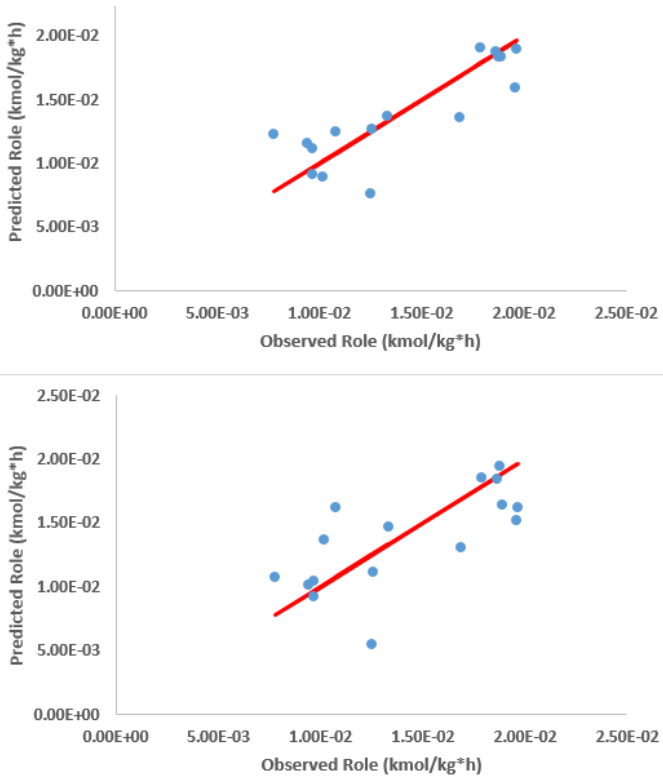

Figure 6 Parity plots for olefin saturation. Top: OHKM1, Bottom: OHKM2

Table 3 shows the parameter estimation for the quinoline hydrodenitrogenation model. No activation energy for quinoline hydrogenation was estimated. This was probably due to the fact that as shown in the experimental results, the quinoline conversion was constant independent of the temperature. The adsorption constant at Tm and adsorption enthalpy of quinoline was found to be not statistically significant as well as the adsorption enthalpy of the HYDROG pseudo-compounds. Activation energies from reaction 2 and 3 which are the ring opening of the HYDROG pseudo-compound and the denitrogenation reactions were found to be lower than the value presented by Nguyen, et al. [18]. The values of the rate constants are in the same order of magnitude however the values of the adsorption constants at Tm are 3 order of magnitude higher than those presented by Nguyen, et al [18] while the adsorption enthalpy of Q is 1 order of magnitude lower and the adsorption enthalpy of HYDROG was negligible. Adsorption enthalpies for RO and HC are in the same order of magnitude.

The parity plots (Figures 7 and 8) show that the model cannot predict accurately the consumption/production rates evidenced by a low F-value of 210. The low number of experiments, the limited operating conditions tested,

*Student Number: 02007302, **Counselor, ***Supervisor

experimental errors and the simplification made on the reaction scheme contribute to the failure of the mode. More experiments at less and more severe conditions are needed in order to observe the accurate behaviour of quinoline consumption and hydrocarbon production as a function of temperature. Lumping the intermediates and final products into pseudo-compounds may also not had been the best way to reduce the number of parameters. Maybe by equalling reaction constants of similar reactions would have been a better strategy.

Table 3 Parameter estimation for quinoline hydrodenitrogenation

Parameter	*Value*	*t-value*	*95% CI*
ktm_1 (kmol kg_{cat}^{-1} h^{-1})	186.36	3.15	118.70
Ea_1 (kmol kJ^{1})	0.00	n.e.	n.e.
ktm_2 (kmol kg_{cat}^{-1} h^{-1})	53.89	1.91	36.62
Ea_2 (kmol kJ^{1})	51550.32	2.27	8118.00
ktm_3 (kmol kg_{cat}^{-1} h^{-1})	5.48	2.72	15.20
Ea_3 (kmol kJ^{1})	92126.54	2.44	41590.00
Atm_Q (m^3 $kmol^{-1}$)	100000.00	n.e.	n.e.
ΔH_Q (kmol kJ^{1})	-1345.75	n.e.	n.e.
Atm_{HYDROG} (m^3 $kmol^{-1}$)	1880.46	2.30	2901.00
ΔH_{HYDROG} (kmol kJ^{1})	0.00	n.e.	n.e.
Atm_{RO} (m^3 $kmol^{-1}$)	26701.64	5.19	10320.00
ΔH_{RO} (kmol kJ^{1})	-34678.36	-2.27	30630.00
Atm_{HC} (m^3 $kmol^{-1}$)	36306.15	3.46	21020.00
ΔH_{HC} (kmol kJ^{1})	-80256.40	-2.44	65960.00

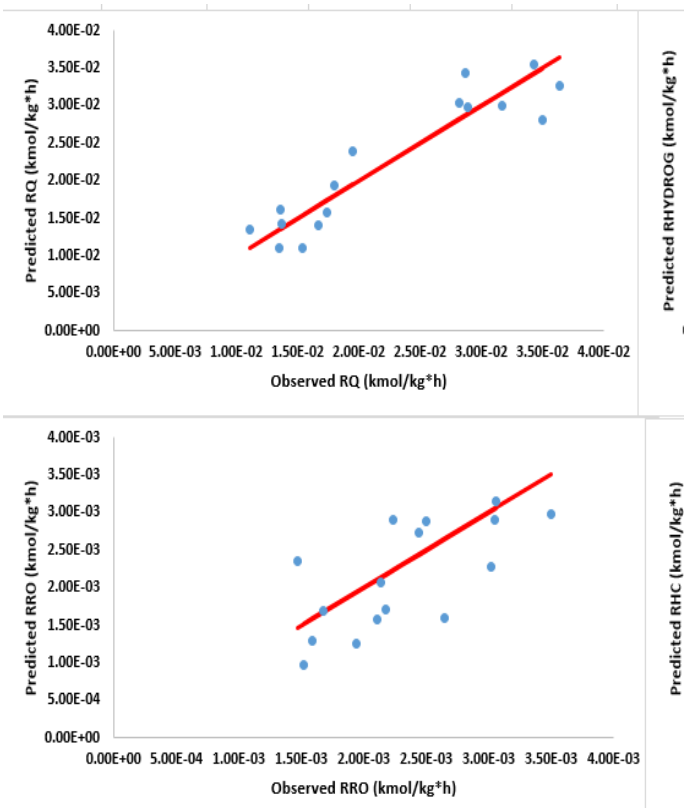

Figure 7 Parity plots for quinoline and HYDROG pseudo-compund

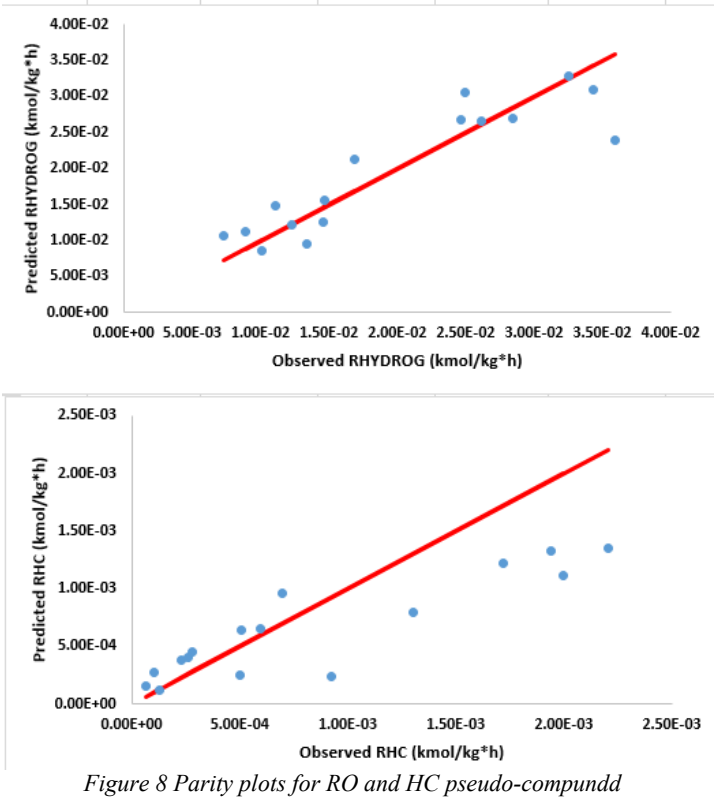

Figure 8 Parity plots for RO and HC pseudo-compundd

4. Conclusion

At the tested operating conditions, high but not full olefin conversions were obtained. There was no difference

*Student Number: 02007302, **Counselor, ***Supervisor

between the conversions of the selected olefins. High temperatures and low LHSV favor the conversion of olefins. Deep hydrodenitrogenation was not successfully achieved. Conditions more severe than the limits of the set-up are needed or not industrially relevant LHSV as low LHSV and high temperature favors the denitrogenation process. However, from the experimental results can be concluded that the quinoline hydrodenitrogenation follows a sequential hydrogenation, ring opening and denitrogenation process. The most difficult reaction appears to be the ring opening of 14THQ. The results of the kinetic modelling, while not successful are inconclusive as there were too few experiments at operating conditions that didn't allowed the best data for kinetic analysis.

The experimental results are relevant to understanding the hydrotreating and hydrocracking of mixtures of VGO and PPO. Not negligible amounts of olefins and low nitrogen conversions are obtained at typical hydrotreating operating conditions. Consequently, feeding a mixture of VGO and PPO which was hydrotreated at typical operating conditions to a hydrocracking unit may have a negative effect on a standard hydrocracking process. It is important to keep researching on how mixing VGO with PPO affects hydrotreating at typical operating conditions. Unconventional nitrogen hetero-compounds such as nitriles are present in PPO, thus understanding the hydrodenitrigenation of nitriles is of relevance as well as oxygenated hetero-compounds which are not usually found in VGO. Model compounds offer a simpler way to understanding reaction mechanisms that can be used in simulation models. The effect of combined aromatic and olefin saturation must also be researched as well as combined with hydrodesulphurization and hydrodenitrogenation. Understanding these effects becomes a necessity in order to maximize the paraffin yield in the hydrocracking process as well as avoid catalyst deactivation.

5. References

[1] *"Global plastic production 1950-2020," Statista. https://www.statista.com/statistics/282732/global-production-of-plastics-since-1950/ (accessed Oct. 25, 2021).*

[2] *"Publicaciones :: PlasticsEurope," Plastic Europe, 2019. https://www.plasticseurope.org/es/resources/publications/1804-plastics-facts-2019 (accessed Apr. 29, 2021).*

[3] *J. R. Jambeck et al., "Plastic waste inputs from land into the ocean," Science, vol. 347, no. 6223, pp. 768–771, Feb. 2015, doi: 10.1126/science.1260352.*

[4] *K. Ragaert, L. Delva, and K. Van Geem, "Mechanical and chemical recycling of solid plastic waste," Waste Management, vol. 69, pp. 24–58, Nov. 2017, doi: 10.1016/j.wasman.2017.07.044.*

[5] *UNEP, "Plastic Waste Background Report," UNEP, Basel, Feb. 2020.*

[6] *D. Almeida and M. de F. Marques, "Thermal and catalytic pyrolysis of plastic waste," Polímeros, vol. 26, pp. 44–51, Mar. 2016, doi: 10.1590/0104-1428.2100.*

[7] *E. Kordouli, B. Pawelec, C. Kordulis, A. Lycourghiotis, and J. L. G. Fierro, "Hydrodeoxygenation of phenol on bifunctional Ni-based catalysts: Effects of Mo promotion and support," Applied Catalysis B: Environmental, vol. 238, pp. 147–160, Dec. 2018, doi: 10.1016/j.apcatb.2018.07.012.*

[8] *J. Ancheyta, Experimental Methods for Evaluation of Hydrotreating Catalysts, 1st ed. Mexico City: Wiley, 2020. Accessed: Mar. 28, 2022. [Online]. Available: https://www.wiley.com/en-be/Experimental+Methods+for+Evaluation+of+Hydrotreating+Catalysts-p-9781119517993*

[9] *C. S. Raghuveer, J. W. Thybaut, R. De Bruycker, K. Metaxas, T. Bera, and G. B. Marin, "Pyridine hydrodenitrogenation over industrial NiMo/γ-Al2O3 catalyst: Application of gas phase kinetic models to liquid phase reactions," Fuel, vol. 125, pp. 206–218, Jun. 2014, doi: 10.1016/j.fuel.2014.02.017.*

[10] *V. Vanrysselberghe and G. F. Froment, "Hydrodesulfurization of Dibenzothiophene on a CoMo/Al2O3 Catalyst: Reaction Network and Kinetics," Ind. Eng. Chem. Res., vol. 35, no. 10, pp. 3311–3318, Jan. 1996, doi: 10.1021/ie960099b.*

[11] *Q. Xin, A. Alvarez-Majmutov, H. D. Dettman, and J. Chen, "Hydrogenation of Olefins in Bitumen-Derived Naphtha over a Commercial Hydrotreating Catalyst," Energy Fuels, vol. 32, no. 5, pp. 6167–6175, May 2018, doi: 10.1021/acs.energyfuels.8b00344.*

[12] *Q. Xin, A. Alvarez-Majmutov, R. Gieleciak, J. Chen, and H. Dettman, "Hydrotreating of Olefins in Thermally Processed Bitumen under Mild Conditions," Energy & Fuels, vol. 33, Mar. 2019, doi: 10.1021/acs.energyfuels.9b00157.*

[13] *H. Dao Thi, M. R. Djokic, and K. M. Van Geem, "Detailed Group-Type Characterization of Plastic-Waste Pyrolysis Oils: By Comprehensive Two-Dimensional Gas Chromatography Including Linear, Branched, and Di-Olefins," Separations, vol. 8, no. 7, Art. no. 7, Jul. 2021, doi: 10.3390/separations8070103.*

[14] *M. Kusenberg et al., "A comprehensive experimental investigation of plastic waste pyrolysis oil quality and its dependence on the plastic waste composition," Fuel Processing Technology, vol. 227, p. 107090, Mar. 2022, doi: 10.1016/j.fuproc.2021.107090.*

[15] *"Hydrodenitrogenation of quinoline and its intermediates over sulfided NiW/γ-Al2O3 in the absence and presence of H2S - Luan - 2009 - Asia-Pacific Journal of Chemical Engineering - Wiley Online Library." https://onlinelibrary.wiley.com/doi/10.1002/apj.322 (accessed Mar. 31, 2022).*

[16] *C. Tu, S. Liu, C. Liu, X. Wu, Q. Chen, and W. Huang, "Single-Pot Synthesis of NiMo-Al2O3 Catalyst for Quinoline Hydrodenitrogenation," Energy Fuels, vol. 35, no. 2, pp. 1120–1128, Jan. 2021, doi: 10.1021/acs.energyfuels.0c03186.*

[17] *S. Tian, X. Li, A. Wang, Y. Chen, H. Li, and Y. Hu, "Hydrodenitrogenation of Quinoline and Decahydroquinoline Over a Surface Nickel Phosphosulfide Phase," Catal Lett, vol. 148, no. 6, pp. 1579–1588, Jun. 2018, doi: 10.1007/s10562-018-2370-z.*

[18] *M.-T. Nguyen, M. Tayakout-Fayolle, G. D. Pirngruber, F. Chainet, and C. Geantet, "Kinetic Modeling of Quinoline Hydrodenitrogenation over a NiMo(P)/Al2O3 Catalyst in a Batch Reactor," Ind. Eng. Chem. Res., vol. 54, no. 38, pp. 9278–9288, Sep. 2015, doi: 10.1021/acs.iecr.5b02175.*

[19] *D. Ferdous, A. K. Dalai, and J. Adjaye, "Hydrodenitrogenation and Hydrodesulfurization of Heavy Gas Oil Using NiMo/Al2O3 Catalyst Containing Boron: Experimental and Kinetic Studies," Ind. Eng. Chem. Res., vol. 45, no. 2, pp. 544–552, Jan. 2006, doi: 10.1021/ie050094r.*

[20] *J. Thybaut, M. Saeys, and B. Marin, "Hydrogenation kinetics of toluene on Pt/ZSM-22," Chemical Engineering Journal, vol. 90, pp. 117–129, Nov. 2002, doi: 10.1016/S1385-8947(02)00073-6.*

[21] *B. Mattson et al., "Heterogeneous Catalysis: The Horiuti-Polanyi Mechanism and Alkene Hydrogenation," Journal of Chemical Education, vol. 90, pp. 613–619, May 2013, doi: 10.1021/ed300437k.*

**Student Number: 02007302, **Counselor, ***Supervisor*

Sustainability reflection

Plastic contamination of the biospheres, especially on the oceans and by extension to the marine life is an increasingly concerning problem due to the possible health effects on the long run to the human beings. But plastics are a fundamental part of our modern way of life, they are used from everyday items such as packaging applications to speciality applications such as in the exploration of the solar system. Eliminating plastics from our way of life is just not an option because there are no other materials available which provides such versatility in their mechanical, chemical and electrical properties apart from the possible economic and social consequences that eliminating the plastic industry would have on the world's nations.

The solution to the plastic contamination is to recycle the plastic and bring it into a context of circular economy. Plastic recycling brings many political, logistical, economic and social challenges but most pressingly are the technical challenges to plastic recycling. Actually, there is no process available which can effectively recycle all of the plastic wastes that are produced. Mechanical recycling, while the simpler method on paper is not an option of plastic recycling massification due to the limitations that this method has as during the physical transformations that the plastic undergoes the plastic changes its properties. This leaves chemical recycling as the best option for plastic recycling massification. Depolimerization is conceptually the best option as bringing down the polymer to their respective monomers and back to polymers again sounds the perfect idea. But there are limitations to this method which prevents it from recycling all plastic wastes. First, not all polymers can be effectively depolimerized. For example, polyethylene and polypropylene which are the most produced polymers cannot be depolimerized with a high yield due to the mechanisms in which the polymer is cracked into smaller molecules. Second, depolimerizing a stream of mixtures of different polymers is not possible so a completely new logistical chain would need to be built in order to separate the mixture of polymers. Gasification for electricity production or syngas production is a viable option from a technical point of view but there are economic challenges to overcome. Besides, gasification cannot be brought into a circular economy context. Pyrolysis is the most versatile option available but the pyrolysis oil produced from the plastic does not have much value by itself such as a conventional oil source. Both are complex mixtures of hydrocarbons which need to be treated in order to produce a valuable product from it. Most importantly, all the infrastructure needed to process these complex mixtures of hydrocarbons already exists as oil fractions from conventional sources are processed every day in the many refineries around the world. Conceptually, it would be possible to incorporate the plastic pyrolysis oil to already proven oil refining processes such as hydrocracking. One option would be to mix a conventional hydrocracking feed such as vacuum gas oil with plastic pyrolysis. That mixture can

be then hydrocracked to produce a highly paraffinic product which then can be steam cracked to produce ethylene and propylene who can be polymerized to produce plastic. Under this configuration the production and consumption loop is closed.

While conceptually possible, this configuration also presents many challenges to overcome. While both vacuum gas oil and plastic pyrolysis oil are complex mixtures of hydrocarbons, their compositions are fundamentally different. Vacuum gas oil does not contain olefins while in plastic pyrolysis oil from plastic mixtures olefins are an important constituent. The effect of the presence of olefins in hydrocracking is not well known. Nitrogen content in plastic pyrolysis can be significantly higher than in vacuum gas oil due to the presence of polymers which contain nitrogen such as polyamides or due to the different additives and colorants added in the polymerization process. Nitrogen is known to contaminate the hydrocracking catalyst. A hydrotreating unit before the hydrocracking unit becomes a necessity in order to remove the nitrogen from the mixture and to hydrogenate the olefins so the hydrocracking process can be done without modifications. Yet, literature on olefin hydrogenation is very limited because as previously stated conventional oil fractions do not contain olefins. While literature un nitrogenated hetero-compounds hydrodenitrogenation is abundant, the literature on combined olefin saturation and hydrodenitrogenation is inexistent. Consequently, the possible effects that such reactions can have on conventional hydrotreating is not known.

As a result, the study of combined olefin saturation and hydrodenitrogenation is brought into relevance. Experimental studies are needed in order to determine if at typical operating conditions and catalyst the olefins can be fully saturated and bring down the nitrogen content to acceptable levels. Kinetic studies are needed in order to better understand the processes so accurate simulations on this process can be performed. The experimental results of this study show that at typical hydrotreating operating condition and catalyst near but not full olefin saturation is achieved while no deep hydrodenitrogenation was possible. Apparently, olefin saturation does have an effect on hydrodenitrogenation as nitrogen conversions much lower than those presented in the literature were obtained. The kinetic results were inconclusive as there were too few experiments and at operating conditions which were not the best for kinetic studies. Further studying of combined olefin saturation and hydrodenitrogenation is important to make massification of plastic recycling a reality in the context of a circular economy.

Table of content

List of Tables:

List of Figures:

List of abbreviations

Abbreviation	*Meaning*
PPO	Plastic Pyrolysis oil
VGO	Vacuum gas oil
PE	Polyethylene
PP	Polyproylene
PET	Polyethylene terephthalate
PVC	Polyvinyl chloride
PS	Polystyrene
LDPE	Low density polyethylene
HDPE	High density polyethylene
GC	Gas chromatography
FID	Flame ionization detector
TCD	Thermal conductivity detector
MPO	Mixed polyolefins
HDN	Hydrodenitrogenation
HDS	Hydrodesulphurization
Q	Quinoline
14THQ	1,2,3,4 tetrahydroquinoline
58THQ	5,6,7,8 tetrahydroquinoline
OPA	Orto-propylaniline
DHQ	Decahydroquioline
PCHA	Propylcyclohexilamine
PCHE	Propylcyclohexene
PB	Propylbenzene
PCH	Propylcyclohexane
CF	Calibration factor
PA	Peak area
Ea	Activation energy (kJ $kmol^{-1}$)
H	Enthalpy (kJ $kmol^{-1}$)
K	adsorption constant (m^3 $kmol^{-1}$)
k	reaction constant (kmol m^{-3} h^{-1})
R	net reaction rate (kmol kg_{cat}^{-1} h^{-1})
r	reaction rate (kmol kg_{cat}^{-1} h^{-1})
Θ	Surface fractional coverage
L	Liquid molar flow (kmol h^{-1})
G	Gas molar flow (kmol h^{-1})
C	Concentration (kmol m^{-3})

1. Introduction

Plastics are used in a wide range of industrial processes, from packaging applications to automotive or electronics parts production, due to the versatility of their mechanical properties. As a result, the global consumption of plastics has grown from 1.5 Mt in 1950 to 359 Mt in 2018 [1]. A major issue associated with plastics production is its end-of-life management. Some plastics could have a long service life, up to 50 years as in aerospace applications, while others have a service life that range from a few days to a few months, such as in packaging applications. Since packaging has a share of 40% in the end use market of plastics in Europe [2], it represents a big environmental problem. It is estimated that from 4 to 12 Mt/y of waste plastics end up in the ocean [3]. The effects of this situation on marine life and, in consequence, on the human being is of increasing concern.

The solution to the adverse effects that the irresponsible deposition of plastics has on the wildlife and human life requires an effective strategy for plastic wastes recycling. For this is necessary to overcome the challenges that post-consumer plastics recycling involves such as: the uncertainty of the material to be processed in terms of variability of the polymers composition of the mixture, the degree of contamination with other substances or additives, and the existence of materials different to polymers. Consequently, currently in Europe only around 30% of post-consumer plastics are effectively being recycled, 40% are burnt using the flue gas for heat recovery and the rest is landfilled [2]. This situation is even less favourable in not fully developed regions. As an example, in South America, the plastics waste recycling ratio is less than 20% [4].

From a general point of view, plastics recycling can be achieved using two methods: mechanical and chemical. A schematic representation of the different methods for plastics recycling is shown in Figure 1. Mechanical recycling is a process where a plastic stream is reduced in size, melt, and reshaped to produce a new final product [5]. A big disadvantage of this method is that with each recycling cycle a lower quality product is produced until it has no practical use [6]. Chemical recycling refers to the use of a chemical process to convert the plastic waste weather into simpler compounds such as the ‘constituents’ monomer of the polymer, or an oil like hydrocarbon stream that can be used as feedstock in the refining/petrochemical industry [5].

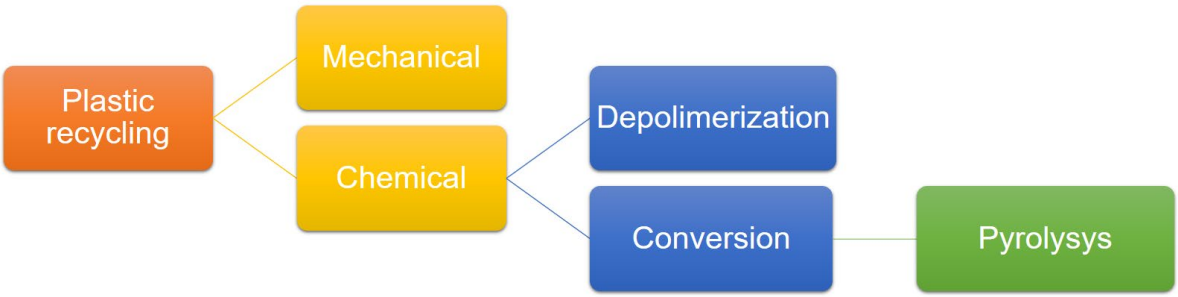

Figure 1 Paths for plastic recycling

There are different commercial technologies pointing towards the chemical recycling concept. Among the commercial technologies applying chemical recycling via conversion it is worthy to mention a technology developed by BASF called ChemCycling™ where a pyrolysis process is used to produce a pyrolysis oil which can be used as a feedstock in the conventional value chain of crude oil [7]. In addition, Anallotech developed the Plas-TCat™ process where through a catalytic process any mixed plastic stream, including composite plastics, can be converted into valuable chemicals [8]. A similar process is described in the patent US9200207B2 submitted by Huang, et al. where it is claimed that a liquid hydrocarbon fuel can be produced by reacting a waste plastic stream with a metal hydride using a supported catalyst [9]. Regarding chemical recycling via polymerization depending on the plastic to be treated different techniques are applied. Polyethylene terephthalate (PET) can be depolymerized by treating it with methanol at relatively high temperatures (180 - 290 C) and pressures (20 – 40 atm) which yields up to 90% DMT and EG as main products [10]. Another technique is applied for Polystyrene (PS) that can be thermally depolymerized into styrene (ST) in a catalytic fluidized bed using magnesium aluminium silicate [11]. In case of polyolefin depolymerization is not possible because the degradation of the plastic as a consequence of the C-C random scission [10]. Finally polyvinyl chloride (PVC) is degraded at temperatures higher than 280 C and yields a gaseous chlorine which, apart from being harmful, produces damages in the employed equipment and contaminate catalysts. For this reasons, mechanical recycling is considered a better route for polyolefins and PVC [12]. These technological proposals indicate that from an industrial point of view the mixed plastics chemical recycling is currently focused on the production of a valuable hydrocarbon stream. Since each polymer needs a specific process to be depolymerized, this strategy is less flexible to process mixed plastics.

Figure 2 shows a global scheme of chemical recycling that integrates traditional refining/petrochemical units such as hydrocracking and steam cracking with thermal pyrolysis. In this configuration the plastic waste is initially processed via thermal pyrolysis to obtain some stream rich

in hydrocarbon compounds called plastic pyrolysis oil (PPO). Thermal pyrolysis is a process in which organic matter is thermally degraded in the absence of oxygen producing [13] a gas-liquid hydrocarbon mixture. The kinetics of the thermal degradation during pyrolysis is still a matter of study and discussion as the mechanisms involved in thermal degradation are overly complex. The compounds that normally constitute a PPO produced from plastic waste are a complex hydrocarbon mixture containing paraffins, naphthenes, olefins and aromatics from a carbon range distribution between 3 and more than 50 carbon atoms. A high content of nitrogen hetero compounds are also found in that streams which should be removed to avoid an inhibition effect in the hydrocracking catalyst [14].

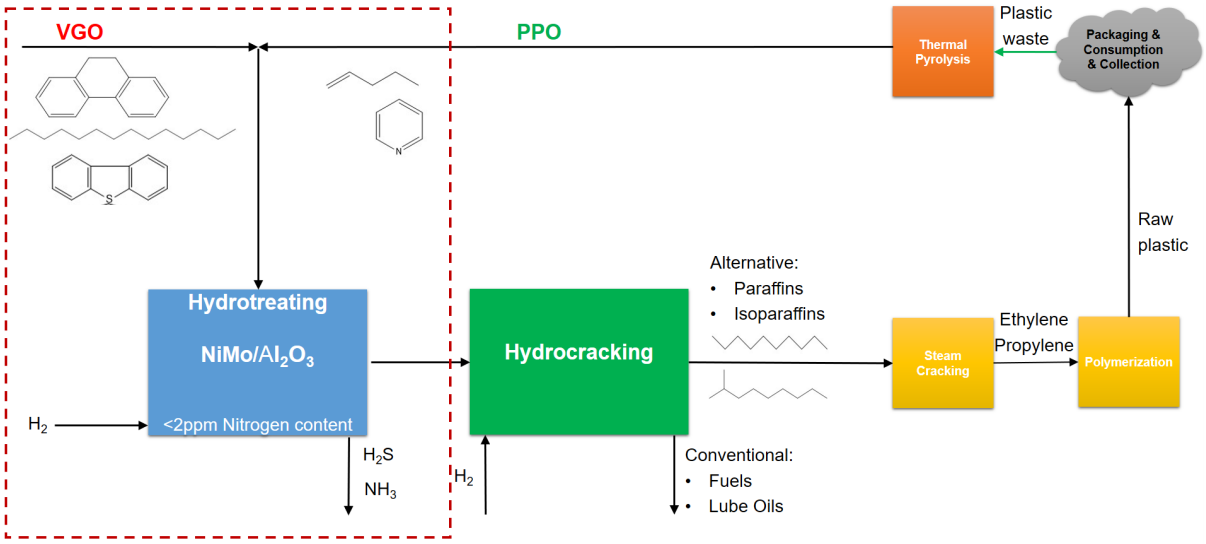

Figure 2 Schematic representation of a closed looping chemical recycling integrating steam cracking and hydroprocessing (hydrotreatment and hydrocracking)

The PPO produced in thermal pyrolysis can be feed to a steam cracking unit whose main duty is to produce ethylene and propylene, key building blocks that serve as feed for polymerization processes to produce polyethylene (PE) and polypropylene (PP). High yields of ethylene and propylene can be produced in a steam cracker with highly saturated feedstocks, especially rich in paraffins while aromatic ring produces fuel oil and tar [15]. Since the content of olefins and aromatics in a PPO is normally high, a pre-conditioning of this type of feed could significantly improve the yields towards ethylene and propylene [15]. An alternative option to directly feed the PPO to the steam cracker, is to mix it with vacuum gas oil (VGO) and feed into a hydrocracking unit [16][17] under normal operating conditions. With this configuration it is possible either to produce fuels in a typical configuration for a hydrocracking unit or to produce a synthetic feed for a steam cracker. This last option allows to adequate the PPO by maximizing the yield of saturated compounds, specially paraffins and iso paraffins [18] making the hydrocracked product a better suited feed for steam cracking. Under this alternative not only the production-consumption loop of plastics is closed, as in the first case, but also a gain in flexibility and yield maximization of the desired products is also expected.

A hydrotreating unit previous to the hydrocracking unit becomes a necessity in order to remove nitrogen compounds to avoid inhibition of the hydrocracking catalyst. If PPO is co-fed to the hydrocracking unit, the composition of the combined stream will contain olefins. Since virgin petroleum fractions do not contain olefins, literature on kinetics of olefin saturation combined with hydrodenitrogenation is very limited. The aim of this thesis is to perform an experimental study that allow to get a deeper understanding about the combined saturation of olefins and hydrodenitrogenation in scenarios of high concentration of olefins. For this purpose, a combination of model molecules for nitrogenated compounds and unsaturated compounds are hydroprocessed under typical operating conditions and catalyst for hydrodenitrogenation. Finally, different kinetic models for both olefin saturation and denitrogenation reactions are proposed and compared against the generated experimental data.

2. Theoretical Background

2.1. Thermal Pyrolysis of waste plastics

Thermal pyrolysis of plastic waste is a process where the plastic is converted to an oil-like stream via a complex network of chemical reactions that involve the cracking of long polymer molecules into simpler ones. This is a non-catalytic process that takes places at temperatures above 400°C and in the absence of oxygen [19]. This process is a suitable option for recycling polymers that are difficult to depolymerize or mechanically recycle such as mixtures of PE/PP/PS, polyolefins, multi-layered packaging and fibre-reinforced composites [5]. The major products obtained from plastic pyrolysis are a gas stream rich in light hydrocarbons, a liquid product called plastic pyrolysis oil and a solid product called char [20]. Figure 3 shows a process flow diagram (PFD) of a typical plastic pyrolysis plant with a vortex reactor. The gas product can be used as fuel for heat generation, the plastic pyrolysis oil can be distilled into different high value products such as a light oil, jet fuel and diesel while the char can be treated as a waste or be further transformed into a valuable carbon material.

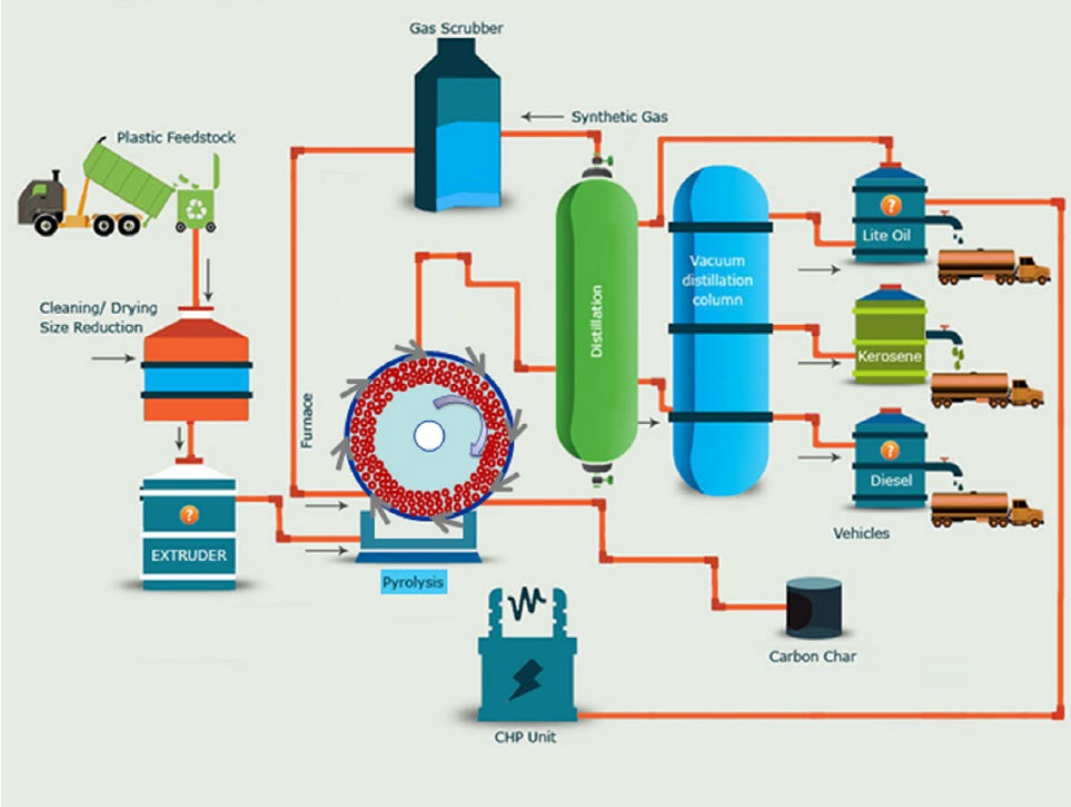

Figure 3 PFD of a typical plastic pyrolysis plant using a vortex reactor [5]

Depending on the desired product, thermal pyrolysis can be classified as slow, fast or flash. Slow pyrolysis is performed at temperatures ranging from 350°C to 550°C with heating rates from 1°C min^{-1} to 10°C min^{-1}, as a result the vapour has a longer residence time, and the major product is char [21]. Fast pyrolysis is performed at temperatures ranges from 500°C to 700°C while the heating rate is above 1000°C min^{-1} [22]. This process promotes plastic pyrolysis oil formation with yields up to 90% [23]. Flash pyrolysis of plastics is performed at temperatures above 700°C with residence times of milliseconds, favouring the formation of non-condensable vapours [24]. At temperatures rounding 1000°C gas yields for the pyrolysis of LDPE can reach up to 99% with monomer yields of 48% [25].

As mentioned before, reaction kinetics of thermal pyrolysis of plastics is very complex but it is generally accepted as a free radicals mechanism comprising the stages of initiation, propagation and termination [14]. For the thermal cracking of HDPE, the initiation reactions involve the homolytic rupture of a C-C bond, forming radicals via either end chain scission (Eq.1) or random scission (Eq.2) [26].

$$\sim CH_2 - CHX - CH_2 - CHX \rightarrow \sim CH_2 - \dot{C}HX + \dot{C}H_2 - CH_2X \quad (1)$$

$$\sim CH_2 - CHX - CH_2 - CHX\sim \rightarrow \sim CH_2 - \dot{C}HX + \dot{C}H_2 - CH_2X\sim \quad (2)$$

Propagation reactions are done by hydrogen chain transfer reactions, which can be intramolecular or intermolecular and β-cleavage. Intramolecular hydrogen chain transfer reactions form an olefinic species as shown in Eq.3 [27].

$$\sim CH_2 - CHX - CH_2 - CHX - \dot{C}H_2 \rightarrow \sim \dot{C}H_2 - CHX = CH - CHX - CH_3 \quad 3$$

Intermolecular hydrogen chain transfer can lead to either an olefinic species as shown in Eq.4 or a secondary radical can also be formed from hydrogen abstraction through a reaction between a primary radical and a polymeric fragment (Eq.5) [27].

$$\sim CH_2 - \dot{C}HX + \sim CH_2 - CHX - CH_2 - CHX - CH_2 \sim \rightarrow \sim CH_2 - CH_2X + \sim CH_2 - CHX - CH = CHX - \dot{C}H_2 \sim \quad 4$$

$$\sim CH_2 - \dot{C}HX + \sim CH_2 - CHX - CH_2 \sim \rightarrow \sim CH_2 - CH_2X + \sim CH_2 - \dot{C}X - CH_2 \sim \quad 5$$

Cracking reactions proceed via β-cleavage of secondary radicals which leads to an end-chain olefinic group and a primary radical (Eq.6) [27].

$$\sim CHX - CH_2 - \dot{C}X - CH_2 \sim \rightarrow \sim \dot{C}HX + CH_2 = CX - CH_2 \sim \quad 6$$

Termination is done by the coupling of two primary radicals (Eq. 7) or by disproportionation of the primary macroradicals (Eq.8) [27].

$$\sim CHX - \dot{C}H_2 + \dot{C}HX - CH_2 \sim \rightarrow \sim CHX - CH_2 - CHX - CH_2 \sim \quad 7$$

$$\sim CH_2 - CHX - \dot{C}H_2 + CHX - CH_2 - CH_2 \sim \rightarrow \sim CH_2 - CHX - CH_3 + CHX = CH - CH_2 \sim \quad 8$$

Thermal pyrolysis of polyolefins yields a broad range of carbon number distribution along their products, from C_5 to C_{80} composed mainly of dienes, paraffins and olefins [26]. Other polymers such as PTFE, PA, and PMMA can be fragmented through pyrolysis into products that are composed mostly on their respective monomer [5], [28]. The variability of the different products obtained in thermal pyrolysis of plastic waste depending on the composition of the inlet mixed solid plastic is one of the biggest challenges involved in this approach.

2.1.1 PPO Composition

Due to the reasons explained in section 2.1 the composition of a PPO is fundamentally different to the composition of VGO. As shown in Figure 4, a typical VGO composition comprises n and iso-paraffins,

mono, di, tri and tetra aromatics as well as mono, di, tri, and tetra naphthenic compounds. Olefins are compounds that do does not appear in the composition of VGO [29].

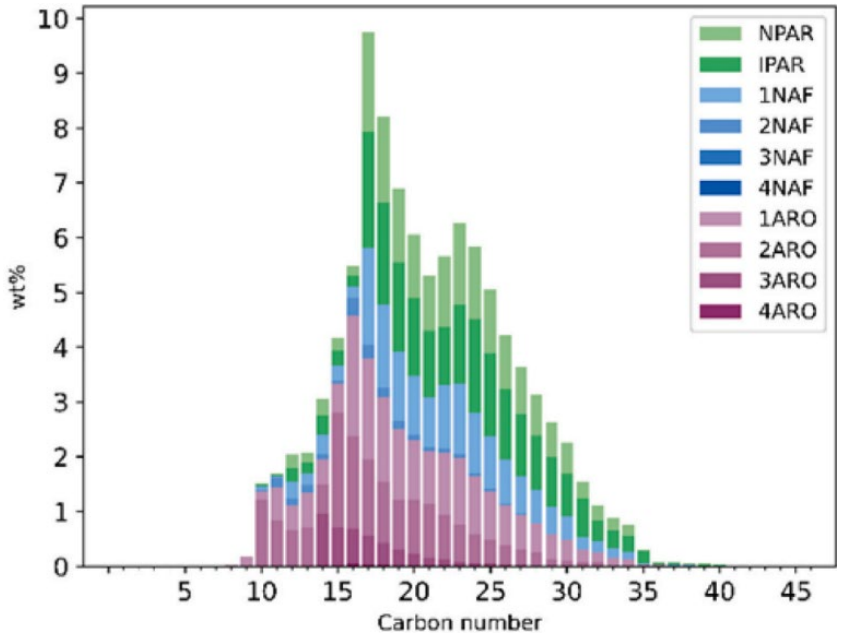

Figure 4 Typical VGO composition [29]

It is important to notice that the composition distribution of the different classes can vary between different VGOs. As the VGO is derived from a heavy fraction of atmospheric distillation, the composition of the VGO is also dependent on the crude oil composition which is dependent on the origin of the crude oil but what remains constant is the different classes of compounds that are present in the VGO [30].

A PPO produced of unspecified plastic composition and unspecified pyrolysis operating conditions was analysed using GCxGC by Thi, et al. and its composition is shown in Figure 4. From this Figure it can be observed that the main group of compounds present in this PPO are α-olefins (37 wt%), diolefins 4 wt% [31]and a carbon distribution between 9 and 21 carbon atoms. The composition of this PPO differs from the composition of the VGO shown in Figure 4 with regard to the distribution by family of compounds while the carbon number distribution is skewed more to the left .

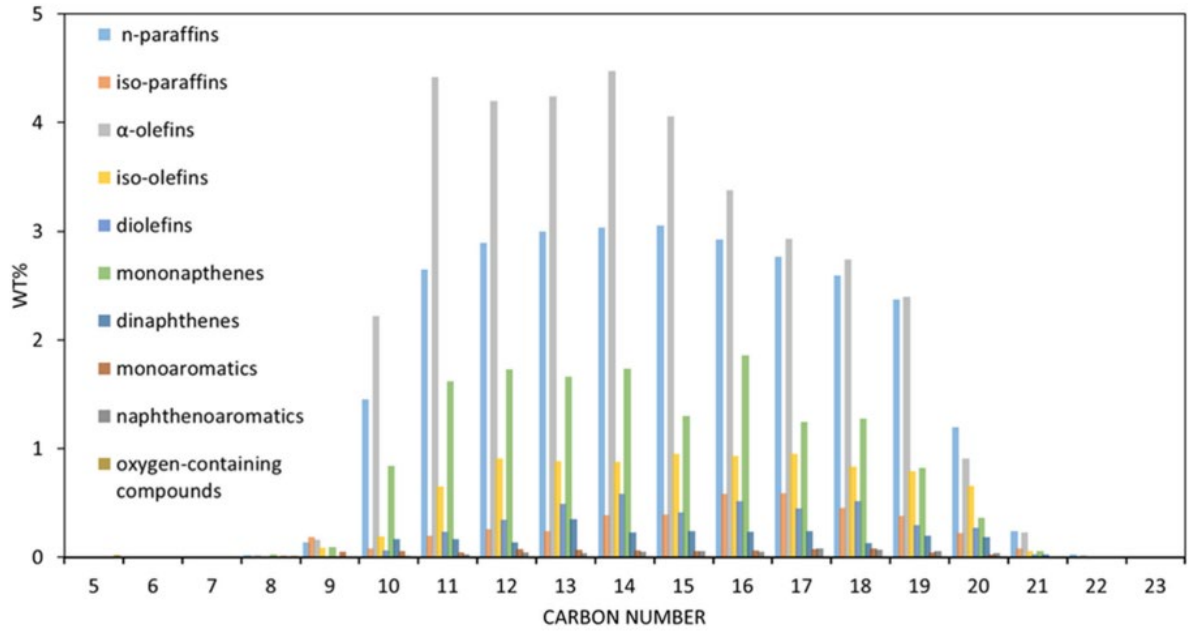

Figure 5 PPO composition of unspecified plastic origin [31]

Onwudili, et al. studied composition of PPO from LDPE and PS via GC/FID. For the pyrolysis of LDPE, the experiments were performed at temperatures from 425°C to 500°C and pressures from 1.60MPa to 6.31MPa being the results are shown in Table 1. Olefins are 13 wt% ot the mixture. The decrease in the olefin content with increase of the temperature can be attributed to the dehydrogenation of olefins to aromatics which is favoured by temperature increase [32]. In the same study, the pyrolysis of PS was performed at temperatures of 400°C to 500°C being the results shown in Table 2. It is shown that when PPO is produced from PS, a liquid product composed only of aromatic compounds are produced.

Table 1 Pyrolized LDPE, PPO compound classes composition [33]

	OPERATING CONDITIONS		
TEMPERATURE (°C)	425	450	500
PRESSURE (MPA)	1.60	2.45	4.31
COMPOUND CLASSES			
NAPHTENES	2,69	5.56	1.50
ALKANES	46.2	31.7	17.8
ALKENES	12.4	13.1	3.58
AROMATICS	12.0	22.9	68.0
UNKNOWNS	19.1	17.9	Nd

Table 2 Pyrolized PS, PPO compound composition [33]

	OPERATING CONDITIONS	
TEMPERATURE (°C)	400	500
PRESSURE (MPA)	1.14	1.60
COMPUNDS		
BENZENE	0.38	1.63
TOLUENE	21.7	28.4
ETHYLBENZENE	32.6	36.6
STYRENE	1.09	0.61
CUMENE	10.2	9.60
PROPYLBENZENE	0.6	1.29
METHYLSTYRENE	1.37	0.55
DIPHENYLMETHANE	0.91	1.61
1,2-DIPHENYLETHANE	1.44	0.37
PHENYLNAPHTALENE	0.98	1.25
1,2-DIPHENYLBENZENE	1.27	1.89
TRIPHENYLBENZENE	6.30	3.18

Pinto, et. al. studied the effect of plastic waste composition on pyrolysis products. The experiments were carried at 430°C and 3.5MPa. The results from Figure 6 show that the increase in PE content, increase the alkane content to around 70%, olefin content was a little more than 20% while aromatic content stayed just below 10% for pure PE. These results coincide with the results shown in Table 1. By increasing the PP content, the content of olefins is increased to more than 30% when pure PP is used while the aromatic content stays in the same range as when pure PE was used. When pure PS was used, the aromatic content increased to more than 90% which is also in agreement with the results shown in Table 2.

Jia, et. Al. studied the catalytic pyrolysis of PET at temperatures of 450°C and 600°C via NMR and FT-IR. Aromatic and aliphatic hydrocarbons are the main constituents of the PPO with 60 wt% and 20 wt% respectively, however carbonyls are also an important constituent of PET derived PPO with 15 wt% as it is shown in Figure 7 . Aromatics ethers were also detected with a proportion close to 5 wt%.

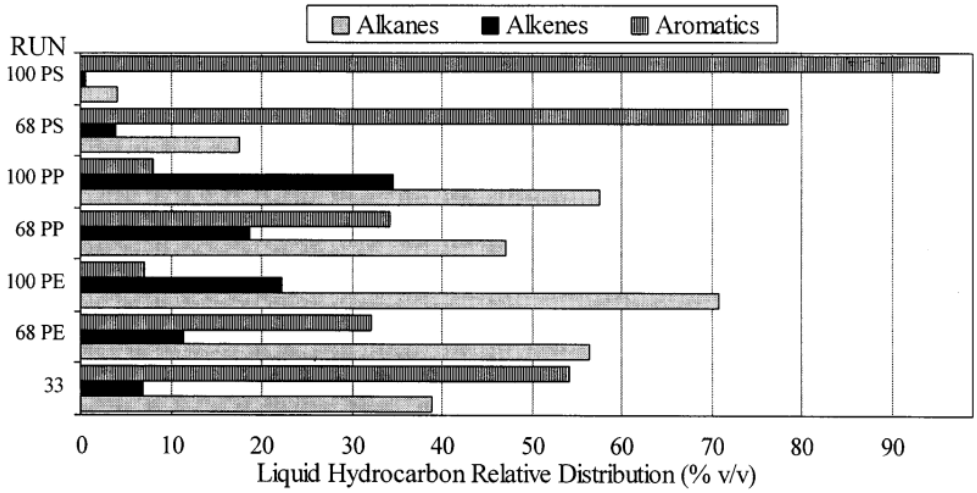

Figure 6 PE, PP, and PS derived PPO compound classes composition in % v/v [34]

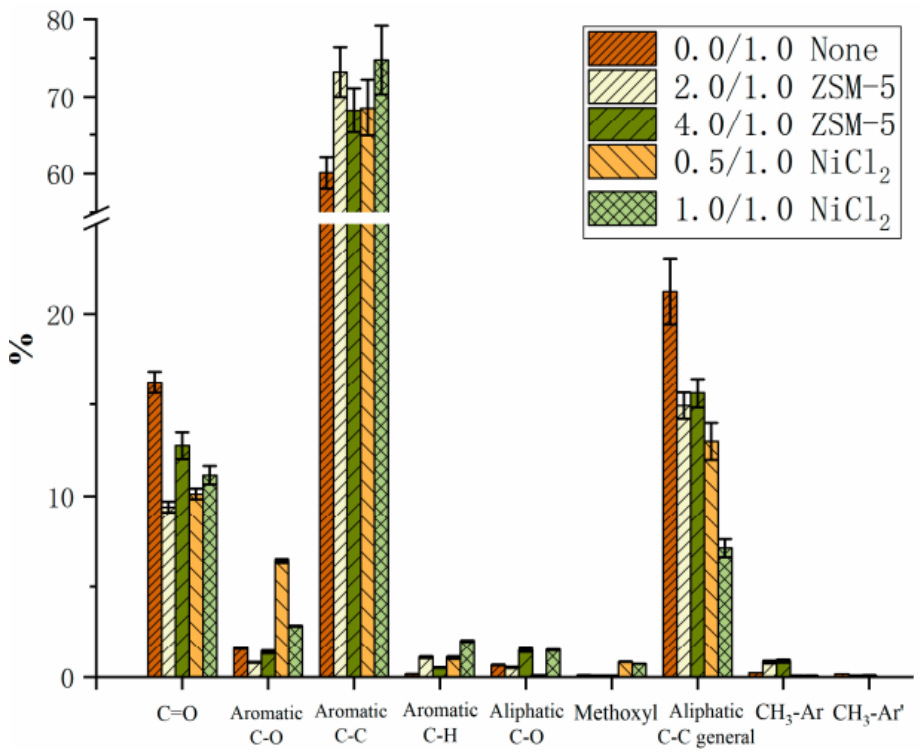

Figure 7 PPO composition of PET [35]

Kusenberg et al., [36] studied the composition of three different plastic wastes: rigid PP, mixed polyolefins (MPO) and PE films. The results are shown in Figure 8. PP rigids produce mostly isoolefins and diolefins with 62.7 wt. % and 19.5 wt. %. PE films produce mostly n-paraffins and α-olefins with 34.4 wt. % and 25.5 wt. % respectively while the MPO are somewhere in the middle.

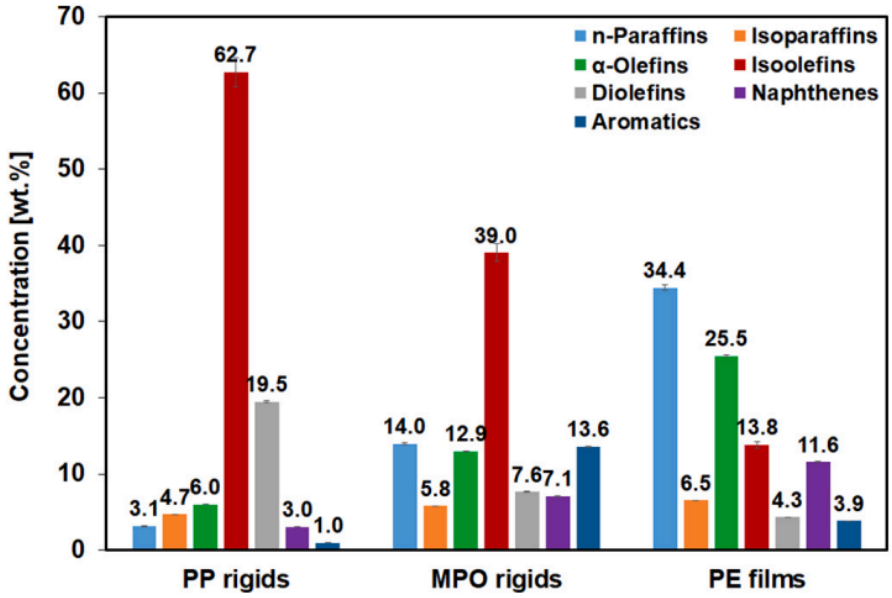

Figure 8 PPO composition of PP rigids, MPO rigids and PE films [36]

By comparing the results from Figure 5, Figure 6, Figure 7, Figure 8, Table 1 and Table 2, it can be deduced that PPO composition is highly dependent on the composition of the plastic feed to the pyrolysis unit. PE produces mostly alkanes but also olefins, PP produces mostly olefins but also alkanes, PS produces aromatics and PET produces mostly aromatics but also carbonyls. Consequently, hydrogenation of olefins is of special interest to this thesis.

2.2 Hydrotreating

Hydrotreating is a process designed to decrease the content of principally but not limited to, sulphur, nitrogen, olefins and aromatics from an oil fraction by reacting the oil fraction with hydrogen. Industrially it is used for the treatment of light oil fractions such as naphta for further processing in catalytic reformer units, for the treatment of heavier oil fractions like VGO to meet product specifications and/or to prepare the fraction for the use as a feed in subsequent units such as Hydrocracking units and to increase the quality of atmospheric and vacuum residues removing sulphur and organometallic compounds [16].

2.2.1 History

The history of hydrotreating processes start with the conversion of bituminous coal to a liquid product using hydriodic acid (HI) in 1869. In 1897 it was discovered by Sabatier and Senderens that unsaturated hydrocarbons could be hydrogenated using a Ni-based catalyst [37]. Three years later it was discovered

by Ipatieff that the range of possible hydrogenation reactions could be extended by using high hydrogen pressures [38]. Both of this discoveries combined with the rise of the automobile industry drove a rapid increase in the research on hydroconversion processes which lead to the first industrial plant for the hydrogenation of brown coal in 1927 in Leuna, Germany. Imposed mostly by military motivations there was an expansion of hydrogenation plants in the years before WW2 as western Europe does not have inland oil wells. During the war, Germany largely depended on hydrogenation processes to produce fuel for their war machine. In 1944, 3.5 million tons of fuel were produced using this technology. Outside of Europe there was little interest on hydrogenation processes as low-cost hydrogen sources was not a possibility [39]. During the 1950s, with the rise of catalytic reforming, hydrogen became a more accessible compound which lead to an increase in the interest on upgrading low quality petroleum. By 2020, the global capacity of hydrotreater units was 56921 Mbpd and is expected to reach 68438 Mbpd by 2025 [40].

2.2.2 Applications relevant to this work

2.2.2.1 *Hydrodenitrogenation (HDN)*

HDN of oil fractions is an application that is becoming more important with time due to the fact that hydrotreating units feeds usually contain less nitrogen than sulphur [41]. Since nitrogen is mostly found on the heaviest fractions of petroleum and the heavier the more complex the nitrogen-containing molecule is [39], there has been a rise in the interest on HDN due to the need of increasing the quality of low-quality oil fractions and the use of alternative hydrocarbon sources such as biomass. There is also an environmentally related interest in HDN as stricter legislations on fuels are being implemented across the world [42]. Hydrocracked products such as Diesel, when they are combusted release SO_x and NO_x gases into the atmosphere causing acid rain [43].

In general, oil fractions contain less than 1 wt % of N with the lightest fractions containing less than 0.25 wt % of N [44], while total nitrogen content in VGO can range from 467 ppm to 3136 ppm and basic nitrogen content from 140ppm to 920ppm depending on how heavy is the fraction [45] and up to 70% conversion can be achieve [46]. Parulkar et al. [47] studied the HDN of a VGO with 997ppm of nitrogen achieving 94% conversion over a typical hydrotreating catalyst at 370°C and 159bar and values as low as 12.2ppm of nitrogen in hydrotreated VGO under typical conditions and catalyst have being reported [48] which is below the threshold of 100ppm content of nitrogen in steam cracking feeds [36]. HDS usually reaches higher conversions because it is easier to remove and consumes less hydrogen than HDN and as result HDN is done under more severe conditions, e.g. higher hydrogen partial

pressures than HDS [44]. This is due to the fundamental differences between the mechanisms of HDS and HDN. In HDS, the sulphur is removed first and the intermediate molecule is then saturated while in HDN, the molecule which are usually five or six carbons aromatic ring structures, is first saturated and then the nitrogen is removed [39]. Typically, HDN comprises three stages: aromatic hydrogenation, hydrogenolysis and hydrodenitrogenation as shown in Eq. 9-11 respectively for the pyridine HDN [46].

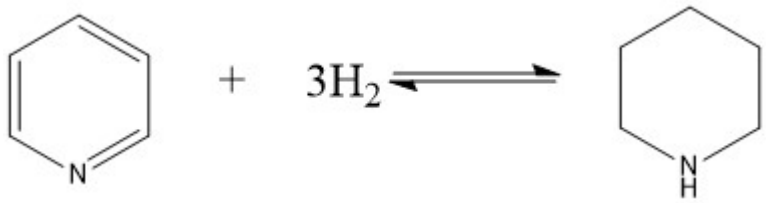

9

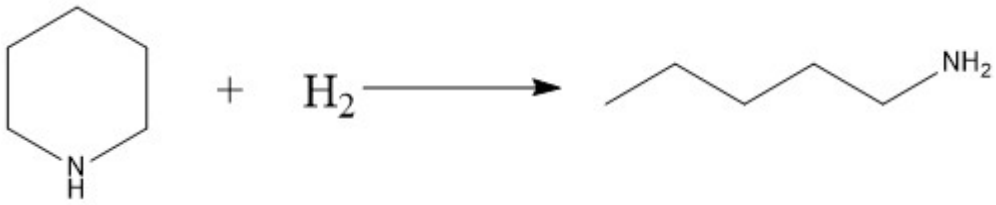

10

11

From easiest to hardest to remove, the typical nitrogen containing compounds found on oil fractions are listed. Pyridines, pyrroles, quinolines, indoles, benzoquinolines, carbazoles [16].

Nitrogen in oil fractions are mainly sourced to the well from where the original petroleum was extracted but nitrogen in PPO can be traced to different sources. Nitrogen in PPO can be traced to a specific polymer, such as in the polyamides family of polymers. Multi-layered polyolefins for packaging applications usually contain nylon in one of their layers [49]. Some plastics have additives that contain nitrogen, one of them is HALS (hindered amine light stabilizer) which act as a stabilizer for the polymer [50]. A final source of nitrogen in PPO the colorants used in plastic production, many of them are nitrogen containing compounds such as azoic pigments, phtalocyanine pigments, or several condensed heterocycles [51].

Total nitrogen content in PPO is can be higher than in oil fractions due to the multi-source origin of the nitrogen in the PPO. It can range from 2 wt % [52] to 6.4 wt % [53]. A PPO from MPO which doesn't

have any nitrogen-containing plastic can present 1144ppm of nitrogen [36]. These values are well above the allowed level of nitrogen in a steam cracking feed, however by diluting the PPO in VGO the hydrotreating unit should operate under more typical contents of nitrogen. While many of the nitrogen-containing compounds in PPO are the same as those found in oil fractions, there are some compounds such as nitriles and caprolactams which are not found in oil fractions [49], [53], [54].

Consequently, it is of special interest to investigate the HDN of nitriles and caprolactams as HDN of nitrogen containing compounds typically found on oil fractions is well researched. As model sample molecules, quinoline and indole are selected.

2.2.2.1.1 Quinoline HDN

Quinoline is a basic N-compound of industrial relevance as is commonly found on heavy oil fractions. It is also accepted that basic N-compounds gain a higher relevance than non-basic N-compounds as these compounds are easily hydrogenated into basic N-compounds [55].

Nguyen, et al. [56] studied the HDN of quinoline over a NiMo(P)/Al_2O_3 catalyst in a batch reactor. The experiments were done at temperatures of 340-360°C, pressure of 7 MPa, quinolone concentration of 1-2 wt. % and hydrogen partial pressures of 3.2-3.3 MPa. The proposed reaction scheme is shown in Figure 9. Due to the complexity of the reaction scheme other authors have work under assumptions of simplified schemes. Yang and Satterfield [57] worked with lumped compounds. The hydrocarbons PB, PCHE and PCH were lumped into one group, all of them with the same kinetic parameters. They also defined three groups with the same adsorption constant: the aromatic amines, the secondary amines and NH_3.

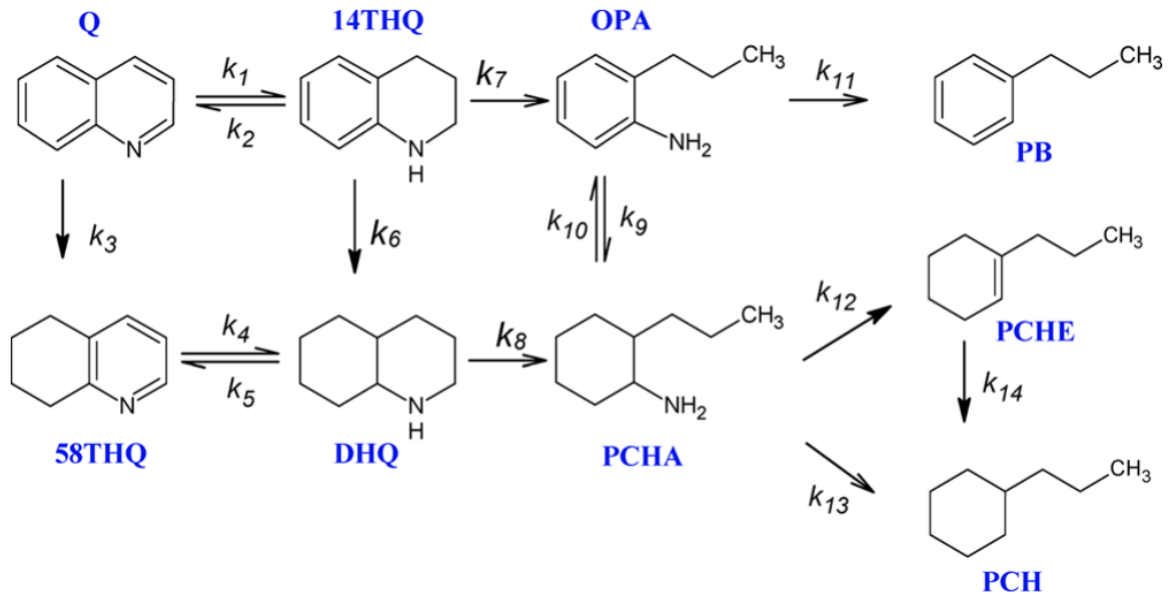

Figure 9 Quinoline HDN reaction scheme. Q=quinolone, 14THQ=1,2,3,4 tetrahydroquinoline, 58THQ= 5,6,7,8 tetrahydroquinoline, OPA=orto-propylaniline, DHQ=decahydroquinoline, PCHA= propyl-cyclohexylamine, PB=propylbenzene, PCHE=propylcyclohexene, PCH=propylcyclohexane [56]

The results of Nguyen, et al. work [56] are shown in Figure 10. The evolution of the reactant, intermediate products and main products show that PCH is the main product while the hydrogenation of 14THQ into DHQ is the rate determine step and that traces of the intermediate and byproducts are present. They also proved that after 9 h, 95% HDN conversion is obtained at a load of 1 wt.% but it decreased to 83% when the load was 2 wt.%. Luan, et al. [58] studied the HDN of quinoline in a continuous fixed bed reactor over a NiW/Al_2O_3 catalyst at temperatures of 300-420°C and pressures of 2-6 MPa. The results are shown in Figure 11. It is shown that temperature and pressure have an important effect on the denitrogenation conversion of quinolone while the hydrogenation is mostly affected by pressure. The results of the intermediate products are in agreement with the work of Nguyen, et al. [56] and Ancheyta, et al. [55]. It is proved that the preferred path of quinolone HDN is through the hydrogenation of 14THQ to DHQ. The reactions between quinolone, 14THQ, 58THQ and DHQ happen so fast that it is assumed that they are in quasi-equilibrium, however it is easier the hydrogenate an aromatic ring than a nitrogenated ring, consequently 14THQ to DHQ is the rate determine step [59]. Tian, et. al., [60] studied the HDN of quinolone over a Ni_2P catalyst at 340°C ad 40 bars in a tubular reactor. The HDN conversion increased from 10% to 40% by increasing the weight time (g min mol^{-1}). 14THQ was the main product while its concentration decreased from 70% to 40% by increasing the weight time.

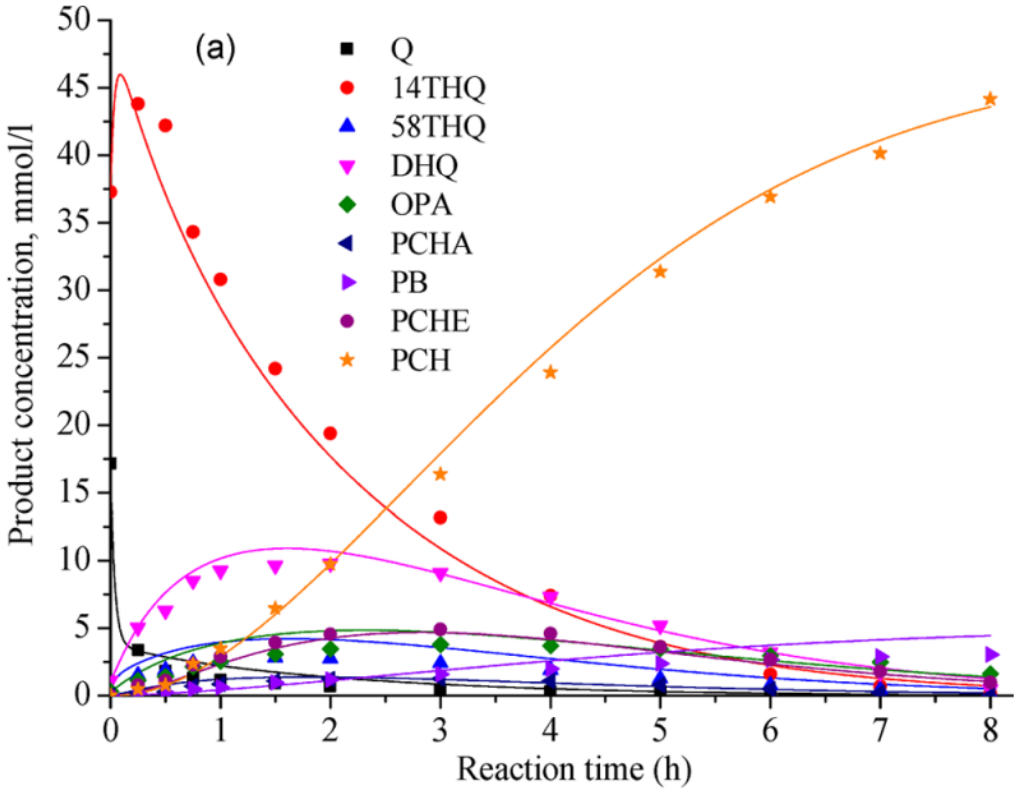

Figure 10 Quinoline HDN at 350°C and 1 wt. % load [56]

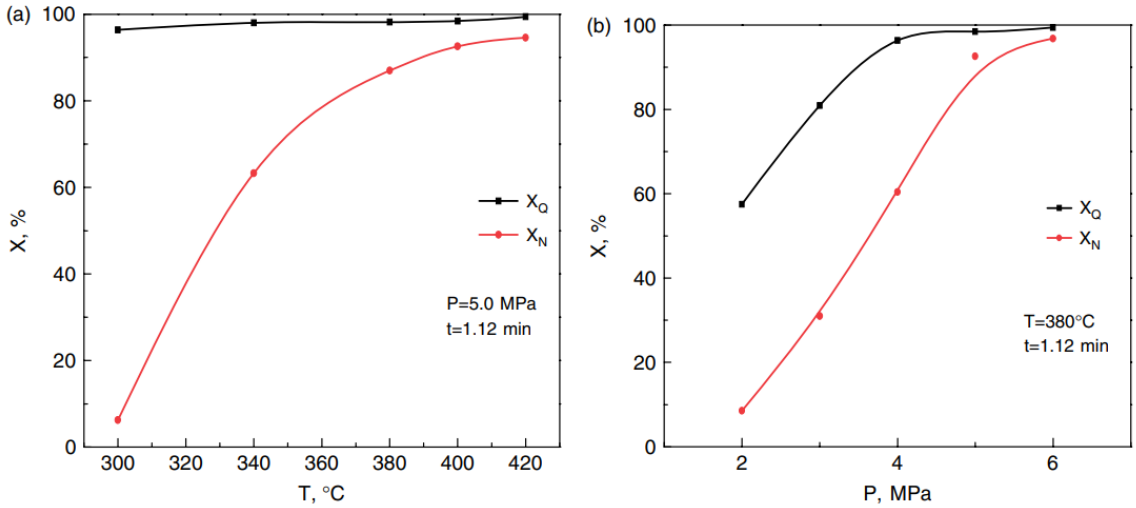

Figure 11 Hydrogenation and denitrogenation of quinoline as a function of temperature of pressure [58]

2.2.2.1.2 Indole HDN

Indole is a non-basic hetercyclic nitrogen compound which is commonly found on petroleum fractions. Around two-thirds of nitrogen in petroleum fractions is concentrated in five-membered heterocycles [61] but literature is more extensive on six-membered heterocycles.

There are several proposed reaction schemes of the HDN of indole on the literature varying in complexity between each other. Kim and Massoth [62] as well as Zhang and Oskan [63] proposed the scheme shown in Figure 12. In this reaction scheme, Indole is rapidly hydrogenated into HIN which can be then converted according to two different paths. The benzene ring can be hydrogenated and OHIN is formed, or the C-N bond of the heterocycle is broken and OEA is formed. It was assumed that OHIN reacts very fast to form OECHA which then is denitrogenated into ECHE and ECH. The intermediate compound OEA can also be converted according to two different paths. The benzene ring can by hydrogenated forming OECHA or it con by directly denitrogenated into EB. Sabo Bello, et al. [64] proposed a modified version of the mechanism shown in Figure 12. As shown in Figure 13 the denitrogenation of OECHA is not done in series but in parallel to ECHE and ECH.

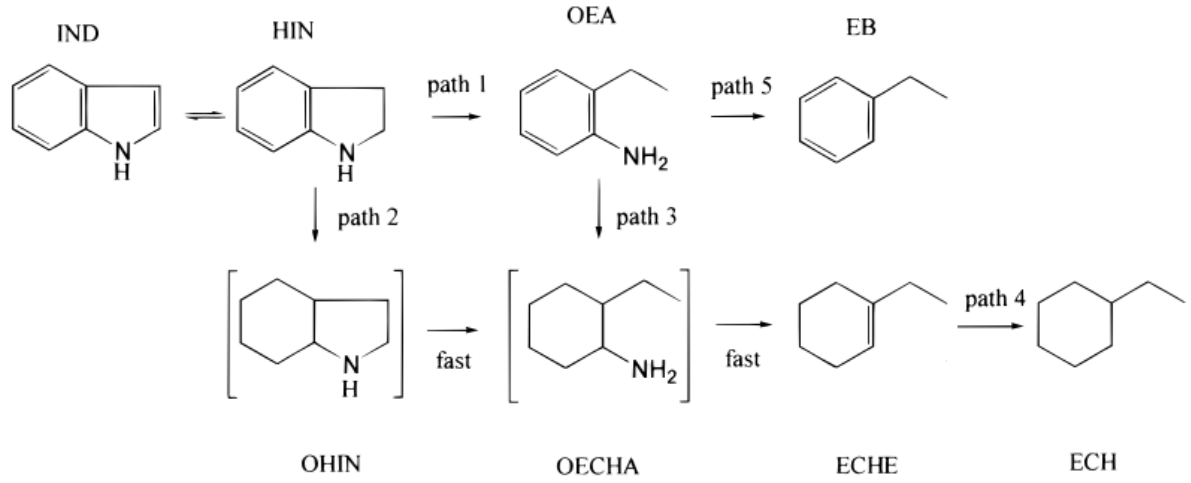

Figure 12 Simplified Indole HDN reaction scheme. Ind = Indole, HIN = Indoline, OHIN = Octahydroindoline, OEA = Orthoethylaniline, OECHA = Ethylcyclohexilaniline, EB = Ethylbenzene, ECHE = Ethylcyclohexene, ECH = Ethylcyclohexane [62]

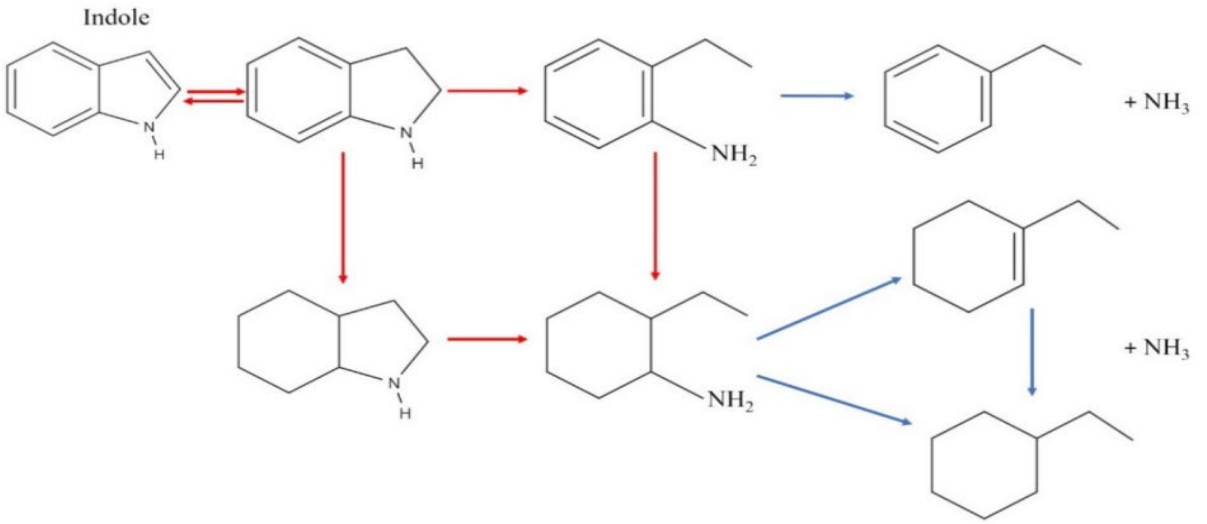

Figure 13 Modified reaction scheme of the HDN of Indole [64]

The study of Zhang and Oskan [63] was done at temperatures of 200-400°C, constant pressure of 0.8 MPa, hydrogen flow of 30-60 cm^3(STP) min^{-1} in vapour phase at a fixed bed reactor using NiMo and Mo catalysts. Benzotiophene (BT) or H_2S were used in order to provide a sulphur atmosphere. Reactant concentrations were 0.023-0.069% and balanced with H_2. As shown in Figure 14, the conversion rate of indole increases with temperature but at high temperatures decreases in the presence of sulphur. The ECH/EB ratio decreases with temperature and the effect of the presence of sulphur is more significant at lower temperatures. It was also reported that at 320°C and 0.023% loading, near 100% indole conversion was obtained but decreased to around 50% when the loading was doubled.

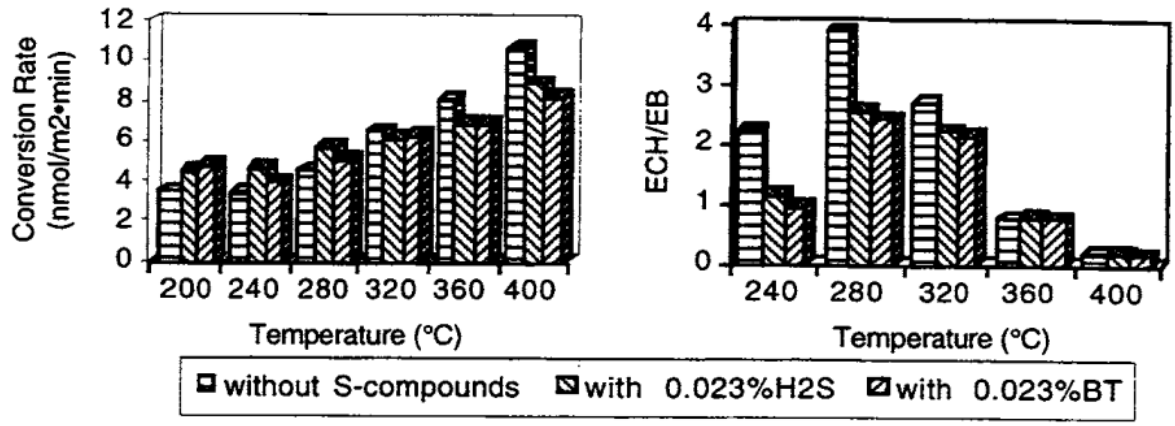

Figure 14 Indole Coversion rate vs temperature (left) and ECH/EB ratio vs temperature over a NiMo catalyst [63]

The experiments of Kim and Massoth [62] were done at 613 K and 3.5 MPa at a fixed bed reactor under vapour phase atmosphere using NiMo and CoMo catalysts. The liquid feed consisted of 0.25-0.75 wt.% Indole, 1-4 wt.% DMDS and the balance n-heptane. Hydrogen partial pressure was maintained at 3.1 MPa. As shown in Figure 15, the major product is ECH while OCHA and ECHE are intermediates. It was also reported that the highest obtained Indole conversion ad HDN were 72.3% 55.3% respectively at a space time of 1.47.

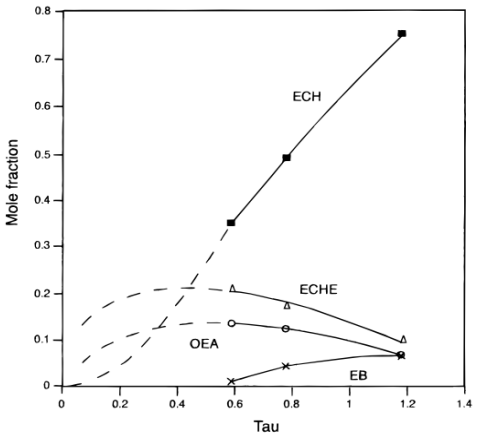

Figure 15 Product distribution (mole fraction) vs space time (kg min m^{-3}) at 0.25% Indole loading using a NiMo catalyst [62]

Bunch, et al. [65] proposed a more complex reaction scheme as shown in Figure 16. The experiments were done at 200-400°C, 100-1000 psig in a fixed bed reactor using a NiMo catalyst. H_2 flow was varied between 30-300 cm^3(STP) min^{-1}, H_2S/H_2 mole ratios of 0-0.0163 while no solvent was used. The results are shown in Figure 17. As temperature increases the conversion of Indole increases and the production rates of EB and ECH increase which is in accord with the previous studies, however in this study Indoline and OHI were detected as major products at temperatures lower than 320°C which were not detected in the previous studies. It can also be seen that the ECH/EB ratio increases in the presence of H_2S which contradicts what's reported on the study of Zhang and Oskan [63]. It was also reported that increasing pressure increases the production rate of all the intermediates and major products.

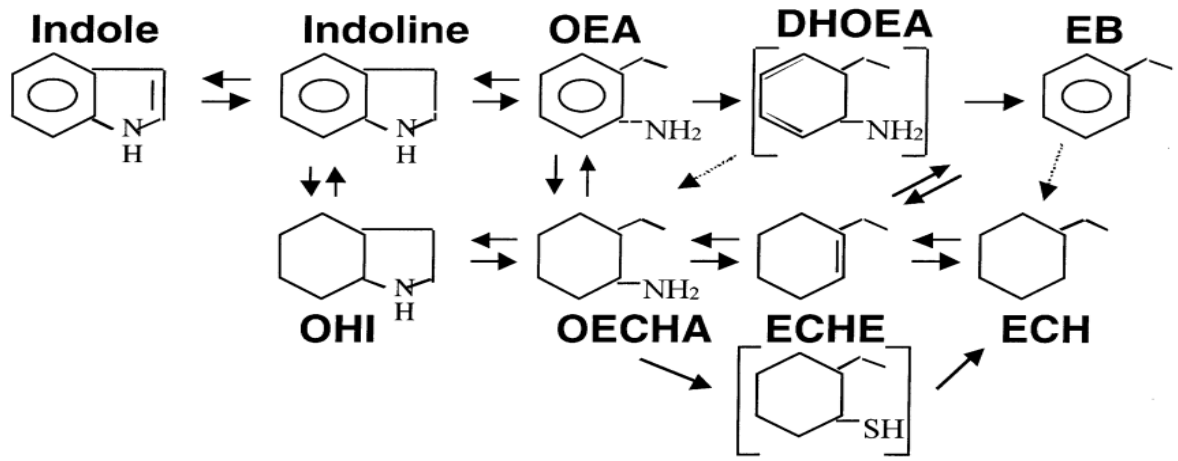

Figure 16 Complex reaction scheme for Indole HDN. OHI = Octahydroindoline, OEA = Orthoethylaniline, OECHA = Ethylcyclohexilaniline, EB = Ethylbenzene, ECHE = Ethylcyclohexene, ECH = Ethylcyclohexane, DHOEA = Dihydro-o-ethylaniline [65]

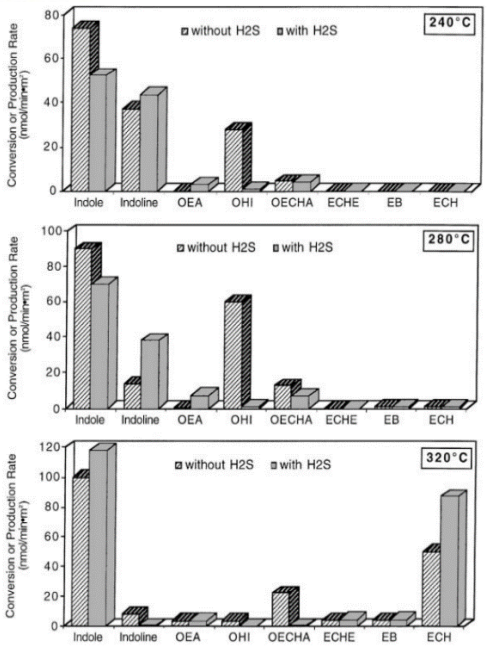

Figure 17 Variation of Indole conversion and product formation rate with temperature at 1000 psig [65]

2.2.2.1.3 HDN Kinetics

It has been stated that HDN reactions are irreversible and follow the premise that for a reaction to occur on a surface the reactants must be adsorbed over that surface in reversible equilibrium [66]. The adsorbed reactants must then be subjected to some transformation which involves adsorbed intermediates as rate-limiting steps leading to product formation [67]. Since Langmuir-Hinshelwood type of kinetics are very complex to use in real industrial feeds due to the heterogeneity of the nitrogen heterocompounds and the large amount of coefficients, attempts has been made to use Power-Law type of kinetics in order to describe HDN kinetics. Reaction orders have been reported from 1 to 1.5 with activation energies from 74 to 92 kJ mol^{-1} [67], [68] however Power-Law models are highly dependent on the experimental conditions on which the study was performed. Consequently, a study by Diaz, et al. [69] reported an activation energy of 208 kJ mol^{-1}. Due to these reasons, attempts had been made on simplified Langmuir-Hinshelwood models. Botchwey, at al. [70] and Ferdous, et al. [67] used a generalized model which includes H_2S inhibitory effects as shown in Eq. 12.

$$r_N = \frac{k_N K_N K_{H_2} P_{H_2} C_N}{1 + K_N C_N + K_{H_2} P_{H_2} + K_{H_2S} b (C_{S0} - C_{SI})} \qquad 12$$

Where r_N is the HDN reaction rate, k_N and C_N are the reaction constant of the HDN reaction and nitrogenated species concentration respectively. K_N, K_{H2} and K_{H2S} are the adsorption constants for nitrogen, hydrogen and H_2S. P_{H2} is the hydrogen partial pressure, b is a constant, C_{S0} and C_{SI} are the feed and product concentration of sulphur. Activation energies of 193.5 kJ mol^{-1} were reported for basic nitrogen heterocompounds while 93.5 kJ mol^{-1} were reported for non-basic nitrogen

heterocompounds [70]. Ferdous, et al. [67] didn't discriminated between basic and non-basic and reported a single activation energy of 110 kJ mol^{-1}. Yin, et al. [71] proposed a generalized kinetic model based on a simplified reaction scheme for carbazole HDN which is shown in Figure 18. Under this scheme, similar nitrogen heterocompounds are lumped into one parameter (N_1) while the partially hydrogenated heterocompounds are lumped into another parameter (N_2). The following assumptions are made: adsorption term of NH_3 is negligible while the adsorption constant of N_1 towards direct HDN is cero and hydrogenation and hydrogenolysis take place at different active sites. The resulting reaction rate equation is shown in Eq. 13. Activation energies of 98 kJ mol^{-1} and 130.8 kJ mol^{-1} were reported for k_1 and k_3.

$$r_N = k_1 C_{N_1} P_{H_2} + \frac{k_3 C_{N_2} P_{H_2}}{\left(1 + K_2 C_{N_1}\right)^2} \qquad 13$$

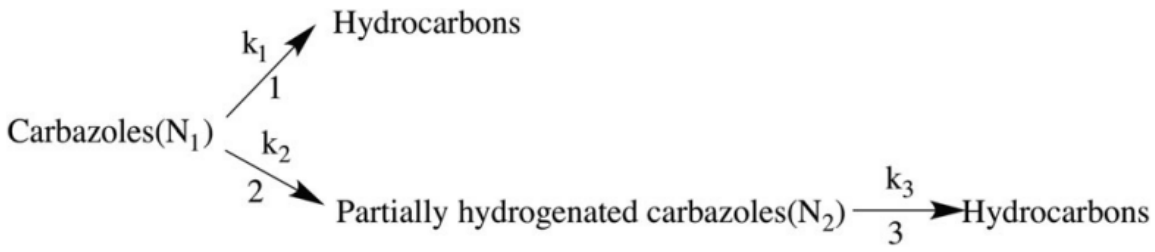

Figure 18 Simplified reaction scheme of carbazole HDN [71]

Nguyen, et al. [56] proposed a kinetic which doesn't discriminate between active sites as according to the authors, well defined catalytic sites for hydrogenation and C-N cleavage may not be an appropriate solution because the mechanisms in which both reactions occurs over a sulphide catalyst are still under debate. During catalytic operation, the MoS_2 edge undergoes constant change. Consequently, the consumption and creation of sulphur vacancies and the dissociative adsorption and release of hydrogen may transform hydrogenolysis sites into hydrogenation sites and vice-versa [56]. Other simplifying assumptions made for the development of the model are:

- Adsorption constants of H_2 and H_2S are negligible
- Volume of liquid and gas is constant during the reaction
- No internal and external diffusion limitations
- 1st order reactions
- The concentration of H_2 in the liquid phase is constant and equal to the equilibrium concentration
- Liquid-Vapor mass transfer is represented by a linear driving force

- Surface reactions are the rate-limiting step
- Competitive adsorption on the same catalytic sites between H_2, nitrogenated compounds and solvents
- System is saturated
- Generalized Langmuir-Hinshelwood formalism to express the fractional occupation of an adsorbed species

Considering these assumptions, the fractional occupation of a relevant adsorbed species is expressed in Eq. 14.

$$\Theta_i = \frac{K_i C_i}{1 + \sum_{j=1}^{n} K_j C_j} \quad 14$$

Where K_i, K_j, C_i and C_j are the adsorption constants and concentrations of species i and j. The global reaction rate for one of the adsorbed species (r_i) is defined in Eq. 15.

$$r_i = k_i \Theta_i \Theta_{H_2} \quad 15$$

As the hydrogen concentration is assumed to be constant in the liquid phase and by replacing Eq. 14 in Eq. 15 the reaction rate for any adsorbed compound is shown in Eq. 16.

$$r_i = \frac{k_i K_i C_i C_{H_2}}{\left(1 + \sum_{j=1}^{n} K_j C_j\right)^2} \quad 16$$

2.2.2.2 *Olefin Saturation*

Olefin saturation is not an application of the highest importance for industrial relevance as petroleum fractions do not contain olefins, consequently is not expected that the VGO composition show olefins. Olefin saturation gains relevance at an industrial scale after the petroleum fraction undergoes thermal or catalytic units as olefins may be formed and from a health and operational point of view might be of interest to saturate the fraction. Fractions containing olefins are unstable and the formation of polymer gums is a possibility as the exothermic character of olefin saturation is higher than HDS and HDN [39].

As explained in section 2.1.1, for this thesis, olefin saturation gains special relevance as depending on the plastic composition, the resultant PPO may contain a significant amount of olefin compounds in its composition. Consequently, saturation of these olefins is of the utmost importance to achieve the aim of this thesis.

Xin, et. al. investigated the hydrotreatment of olefins in thermally processed Bitumen. In their first research they determined that the reactivity of the olefin molecule is largely influenced by the position of the double bond. The experiments were done by hydrotreating a simulated naphta. Upgraded commercial naphta derived from Bitumen was used a feed base. The simulated naphta was prepared by adding selected olefins. The hydrotreatment was done using a commercial $NiMo/Al_2O_3$ catalyst at temperatures of 100°C to 300°C, pressures from 1.4MPa to 2.8MPa, LHSV from 0.5 to 2.5 h^{-1} and H_2/oil of 200 NL/L. By analysing the effect of temperature on olefin conversion it was possible to determine the reactivity of the selected olefins as illustrated in Figure 10. The selected diolefin was the most reactive olefin, followed by the two selected terminal olefins and the two olefins with internal double bonds. Lastly, the cycloalkene was the least reactive olefin. At 300°C all the selected olefins achieved complete conversion. Increments in pressure affects positively the olefin conversion as higher pressures favours the diffusion of hydrogen into the liquid phase, while LHSV affects negatively the olefin conversion because of lower retention times [72]. This results are also in agreement with the research of Badawi, et al. where they concluded that the reactivity of the olefin is also determined by the double bond position and molecule structure over the same catalyst [73]. It's important to notice that the selected diolefin was hydrogenated at 150°C as they present an operational problem; they can polymerize under HDS and HDN conditions and at temperatures over 350°C the formation of gum is a certainty [74]. The possible reactions on olefin saturation are alkene terminal double bond saturation (Eq. 17), alkene internal double bond saturation (Eq. 18), cycloalkene internal double bon saturation (Eq.19) and double bond migration (Eq.20) [72].

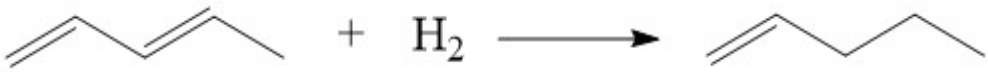

17

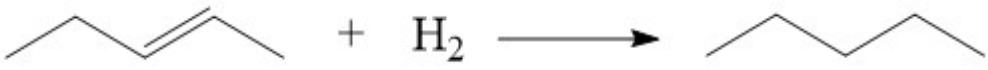

18

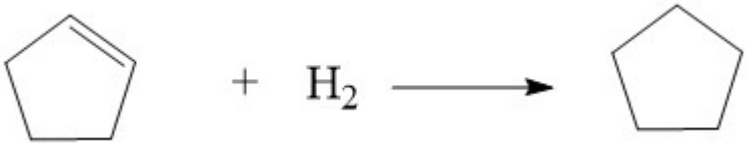

19

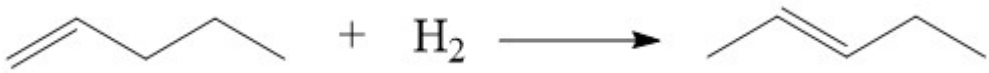

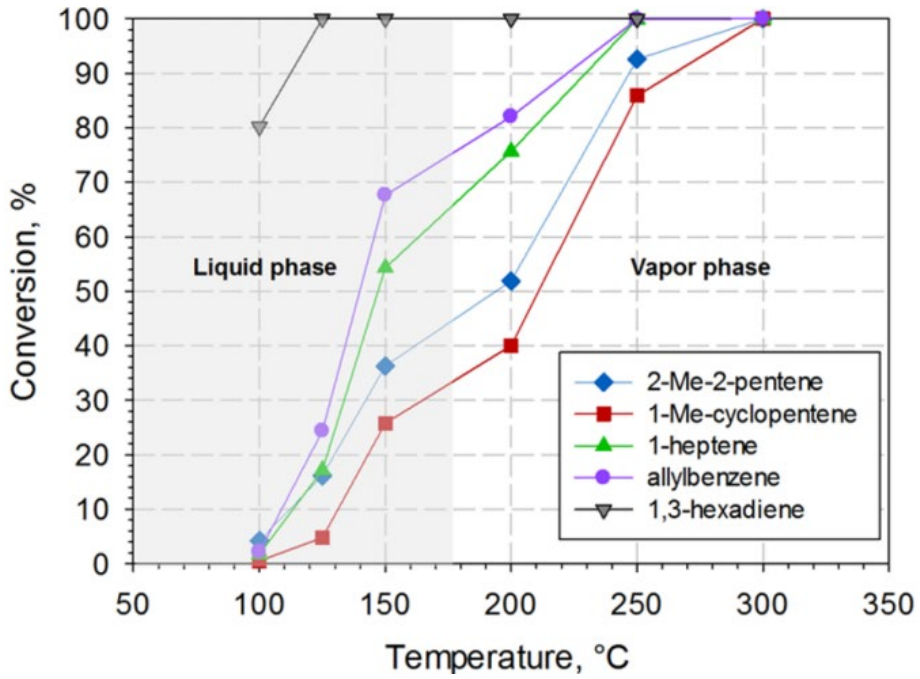

Figure 19 Effect of temperature on olefin conversion [72]

In the second research of Xin, et.al., they hydrotreated a thermally processed Bitumen in the presence of a commercially $NiMo/Al_2O_3$ catalyst. Two feeds were prepared, a light fraction with IBP of 280°C and the whole thermally processed Bitumen. The light fraction was hydrotreated at temperatures from 150°C to 300°, pressure of 3.5MPa, LHSV from 1 h^{-1} to 2 h^{-1} and H_2/oil of 400 NL/L. The whole thermally processed Bitumen was hydrotreated at temperatures from 275°C to 325°, pressure of 3.5MPa, LHSV of 1.5 h^{-1} and H_2/oil of 400 NL/L. The first result that stands out is that the olefins tended to concentrate on the light fraction. Olefin content on the light fraction was 6.30 wt %, while the whole thermally processed Bitumen had an olefin content of 1.78 wt %. As illustrated in Figure 11, at temperatures of 150°C the olefin conversion was very low for the hydrotreated light fraction as the olefin content was just over 6 wt %. As the temperature increased the olefin content diminished until it reached just under 0.5 wt % at 300°C which is a conversion of more than 90%. Similar results were obtained for the whole thermally processes Bitumen. LHSV affected negatively the olefin conversion. It is also important to mention that the hydrogen consumption increased considerably as the olefin content decreased. On the light fraction, at temperatures under 200°C the hydrogen consumption remained constant at 80-90 scf/bbl. As the temperature increased HDS, HDN and aromatic saturation also started to play a role in the hydrotreating process, reaching a hydrogen consumption of 500 scf/bbl at 300°C [75].

These results are in agreement with the previous work of Xin, et al. At low temperatures, the only olefins that were reacting were diolefins. As the temperature increased, terminal olefins and internal double bonds started reacting until at the highest temperatures the most complex olefins were hydrogenated.

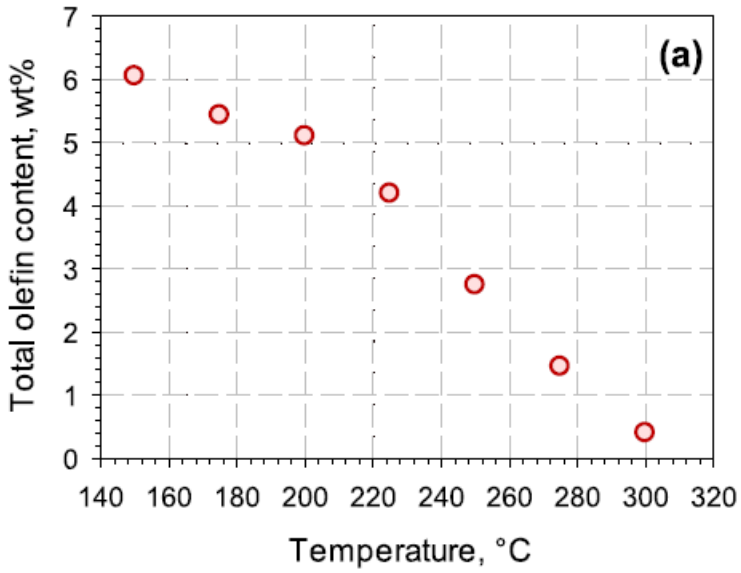

Figure 20 Effect of temperature on olefin content of the light fraction of thermally processed Bitumen [75]

There is no abundant literature on olefins hydrotreating using metal sulphides catalysts such as NiMo or CoMo which ae the typical hydrotreating catalysts because as mentioned before olefin saturation is not of special interest for industrial application of hydrotreating.

2.2.2.2.1 Olefin saturation kinetics

Olefin saturation kinetics over a sulphide catalyst was not extensively found on the literature. Badawi, et al. [73] proposed an expression based on the Langmuir-Hinshelwood theory computed with a reaction mechanism which discriminates between two types of active sites, vacancy of a metallic atom (Θ_{MV}) and sulphur anions (Θ_{S}^{-2}). The reaction scheme is shown in Eq.20-23. Under this mechanism it is assumed a heterolytic dissociation of hydrogen into a hybride on a metal vacancy (Θ_{MH}^{-}) and a proton on a sulphur anion ($\Theta_{S}^{-2}{}_{H}^{+}$), adsorption and desorption of H_2S is negligible, adsorption and desorption of hydrogen and olefins are considered to be very fast and in equilibrium, adsorption of olefins is only considered on a metal vacancy, adsorption and desorption of the solvent and the saturated olefin is not considered

$$C_{H_2} + \Theta_{MV} + \Theta_{S^{-2}} \rightleftharpoons \Theta_{MH^-} + \Theta_{S^{-2}H^+} \quad 20$$

$$C_O + \Theta_{MV} \rightleftharpoons \Theta_{MO} \quad 21$$

$$\Theta_{\mathrm{MO}} + \Theta_{H^-} \rightleftharpoons \Theta_{MOH^-} + \Theta_{MV} \quad (22)$$

$$\Theta_{MOH^-} + \Theta_{S^{-2}H^+} \rightarrow C_{OH_2} + \Theta_{MV} + \Theta_{S^{-2}} \quad (23)$$

Consequently, the reaction rate for olefin saturation is defined in Eq. 24.

$$r_{ole} = k\Theta_{OHM}\Theta_{S^{-2}H^+} \quad (24)$$

At low partial pressures of H_2S the expression on Eq. 24 is converted into Eq. 25.

$$r_{ole} = \frac{kC_O K_{OH} K_{H_2} C_{H_2} \Theta_{MT} \Theta_{ST^{-2}}}{C_O K_O + 1} \quad (25)$$

Where k is the rate constant, K_{H2} and K_{OH} are the adsorption constants for Eq. 20 and Eq. 22, C_{H2} and C_O are the concentrations of hydrogen and the olefin, Θ_{ST}^{-2} and Θ_{MT} is the total concentrations for the sulphur anions sites and metal vacancy sites respectively.

Mattson, et al. [76] proposed a reaction mechanism based on a Horiuti-Polanyi Mechanism on ethylene hydrogenation over a Pd/Al_2O_3 catalyst. The mechanism assumes that both hydrogen dissociation and olefin adsorption occur at the same sites and that the second hydrogenation (Eq. 29) is the rate-limiting step. The reaction mechanism is shown in Eq. 26-29.

$$H_{2(g)} + \mathrm{Pd}_{(s)} \rightleftharpoons 2\mathrm{H_{Pd}} \quad (26)$$

$$\mathrm{C_2H_{4(g)}} + \mathrm{Pd}_{(s)} \rightleftharpoons \pi - \mathrm{C_2H_{4Pd}} \quad (27)$$

$$\pi - \mathrm{C_2H_{4Pd}} + \mathrm{H_{Pd}} \rightleftharpoons \sigma - \mathrm{C_2H_{5Pd}} \quad (28)$$

$$\sigma - \mathrm{C_2H_{5Pd}} + \mathrm{H_{Pd}} \rightarrow \mathrm{C_2H_{6(g)}} + \mathrm{Pd}_{(s)} \quad (29)$$

In this mechanism, hydrogen dissociates and is bonded to palladium forming adsorbed hydrogen (Eq. 26). Ethylene binds to the palladium surface via π-electron donation to a single palladium atom (Eq. 27). On Eq. 28, a hydrogen atom forms a σ-bond with ethylene and the π-bond of ethylene with palladium is transformed into a σ-bond. Finally, the adsorbed σ-ethyl species undergoes an irreversible reductive elimination by addition of another adsorbed hydrogen [76]. No further development on kinetic modelling was done in this work but it is illustrative for further developments on olefin saturation kinetics.

Olefin hydrogenation kinetics may by analogue to aromatic hydrogenation kinetics. Thybaut, at el. [77] studied the hydrogenation kinetics of toluene over a Pt/ZSM-22 catalyst. The assumptions made on the reaction mechanism are as follows:

- No rate-limiting step exists: The first four hydrogen atom additions are not in quasi-equilibrium. Fifth and sixth H addition are.
- Dissociative chemisorption of H_2 and reactant are both chemisorbed on identical sites and are quasi-equilibrated.
- Desorption of the fully hydrogenated product is fast and irreversible.
- No dehydrogenated surface species are considered.

The reaction mechanism based on those assumption is shown in Eq. 30-38.

$$H_{2(g)} + 2\Theta \rightleftharpoons 2\Theta_{\mathrm{H}} \quad (30)$$

$$A_{(g)} + \Theta \rightleftharpoons \Theta_{\mathrm{A}} \quad (31)$$

$$\Theta_{\mathrm{A}} + \Theta_{\mathrm{H}} \overset{k_1}{\Leftrightarrow} \Theta_{\mathrm{AH}} + \Theta \quad (32)$$

$$\Theta_{\mathrm{AH}} + \Theta_{\mathrm{H}} \overset{k_2}{\Leftrightarrow} \Theta_{\mathrm{AH2}} + \Theta \quad (33)$$

$$\Theta_{\mathrm{AH2}} + \Theta_{\mathrm{H}} \overset{k_3}{\Leftrightarrow} \Theta_{\mathrm{AH3}} + \Theta \quad (34)$$

$$\Theta_{\mathrm{AH3}} + \Theta_{\mathrm{H}} \overset{k_4}{\Leftrightarrow} \Theta_{\mathrm{AH4}} + \Theta \quad (35)$$

$$\Theta_{\mathrm{AH4}} + \Theta_{\mathrm{H}} \rightleftharpoons \Theta_{\mathrm{AH5}} + \Theta \quad (36)$$

$$\Theta_{\mathrm{AH5}} + \Theta_{\mathrm{H}} \rightleftharpoons \Theta_{\mathrm{AH6}} + \Theta \quad (37)$$

$$\Theta_{\mathrm{AH6}} \rightarrow \mathrm{AH6}_{(\mathrm{g})} + \Theta \quad (38)$$

For finite values on the adsorption constants of Eq. 36 and Eq. 37 and under the assumptions mentioned before, the equilibrium of those reactions is shifted to the right. Consequently, the coverage of the chemisorbed hydrogenated species Θ_{AH4} and Θ_{AH5} is negligible [77]. As a result, the net rate of production of the full hydrogenated compounds is depicted in Eq. 39.

$$\mathrm{R}_{\mathrm{AH6(g)}} = k_4 \Theta_{\mathrm{AH3}} \Theta_{\mathrm{H}} \quad (39)$$

By applying pseudo-stationary state for the species Θ_{AH}, Θ_{AH2} and Θ_{AH3}, Eq. 39 becomes Eq. 40.

$$R_{AH6(g)} = k_{surf} \frac{B^3 K_A p_A \sqrt{K_{H_2} p_{H_2}} (B^3 + B^2 + B + 1)}{\left((B^3 + B^2 + B + 1)\left(1 + \sqrt{K_{H_2} p_{H_2}}\right) + K_A p_A (4B^3 + 3B^2 + 2B + 1)\right)^2} \quad 40$$

Where $B=K_{surf}\sqrt{K_{H_2} p_{H_2}}$ and the surface reaction rates are assumed to be equal.

2.2.3 Hydrotreating Catalyst

The typical hydrotreating catalyst is made out of a metal sulphide of CoMo or NiMo supported on a high surface area carrier like γ-Alumina. Sulphide CoW and NiW have shown promised in deep HDS and aromatic hydrogenation with subsequent hydrocracking at low H_2 partial pressures but they are expensive to produce and have lost industrial interest. Noble metals like Pd or Pt present a high hydrogenation activity but are prone to deactivation by sulphur compounds [78]. Typical compositions of hydrotreating catalysts are 1-4 wt. % of Ni or Co, 8-16 wt. % Mo and the balance for the support [79]. The activity of CoMo catalyst towards HDS is reported to be higher than NiMo catalysts [80] while the activity of NiMO catalysts towards HDN, HDO and olefin and aromatic saturation is reported to be higher than CoMo cataltsts [48].

It is generally accepted that the activity of the catalyst is originated in the MoS_2 bulk structure and that Ni or Co act as promoters that increases the activity of the catalyst due to high energies in the S-Mo bond that restricts adsorption of the reactants [78]. Consequently, the catalyst is produced and sold in an inactivated form because it lacks the sulphur atoms needed for the activity. The activation of the catalyst is done by reacting the inactivated form with a sulfiding agent. As shown in Figure 13, the sulfidation process involves the reduction of the metal oxides by reacting the Co/NiMo complex with H_2S and as a result the sulphur replaces the oxygen and a reorganization on the catalyst surface occurs [81].

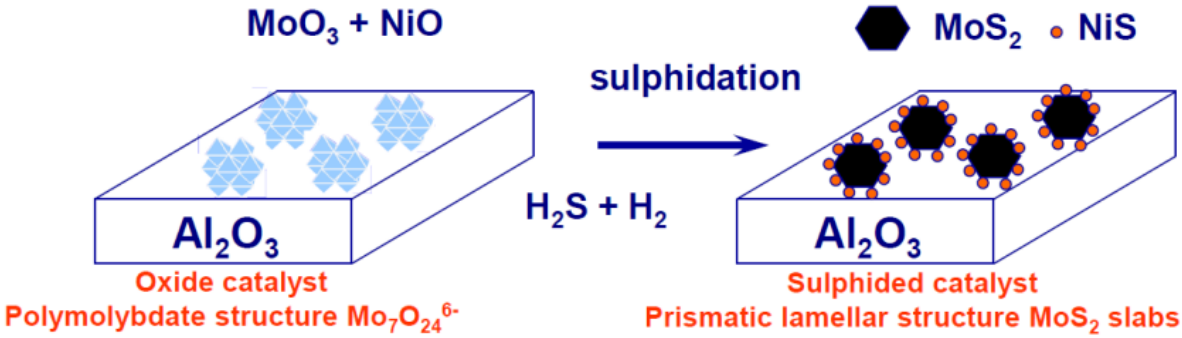

Figure 21 Schematic representation of the sulfidation of a NiMo catalyst [81]

At an industrial level, H_2S as a sulfiding agent is not used because of practical issues, instead organosulfides such as DMDS or polysolfides are used. Organosulfides are much easier to handle than H_2S and the control of the process can be better by controlling the decomposition of the organosulfide as the sulphidation process is exothermic. If the exothermicity of the process is not controlled the reoxidation of the metal is a possibility [82]. Consequently, the temperature has to be carefully increase in order to activate the hydrotreating sulfide catalyst. On Figure 14 it is shown a standard activation procedure for a hydrotreating catalyst. Under a hydrogen atmosphere the catalyst is heated to 423K at 3K m^{-1}. Once it reaches 423K, the sulfiding agent is injected and left in a plateau from 1 to 4h in order to allow complete wetting of the catalyst [82]. Then, the temperature is increased at 3K min^{-1} until 623K in order to allow the sulfiding agent to decompose. It is left for 12h and finally the temperature is decreased to the HDS test at 563K.

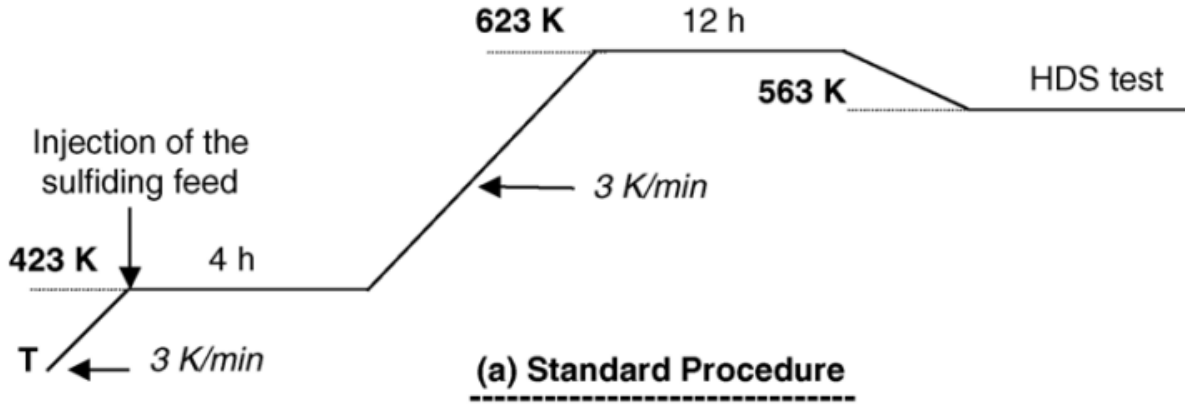

Figure 22 Standard activation procedure for a hydrotreating catalyst [82]

Ancheyta [83] proposed an activation procedure which involves a drying, soaking, sulfuding and activity test stages. The procedure shown in Figure 23 starts with a first temperature ramp from ambient conditions to 120°C at 0.5 K min^{-1} and left at those conditions for 2 h in order to remove water contained in the catalyst pores. The soaking stage begins with injecting a liquid hydrocarbon feed and the temperature is increased to 150°C at 0.5 K min^{-1} and left there for 2 h. The sulfiding stage begins by injecting a sulfiding feed which contains DMDS accounting for 2% total sulphur [83] and the temperature is increased to 260°C at 0.5 K min^{-1} and left there for 3 h. Afterwards, the temperature is again increased to 320°C at 0.5 K min^{-1} and left for 5 h. Once the sulfiding stage is over, the activation test is done according to the conditions shown in Figure 23.

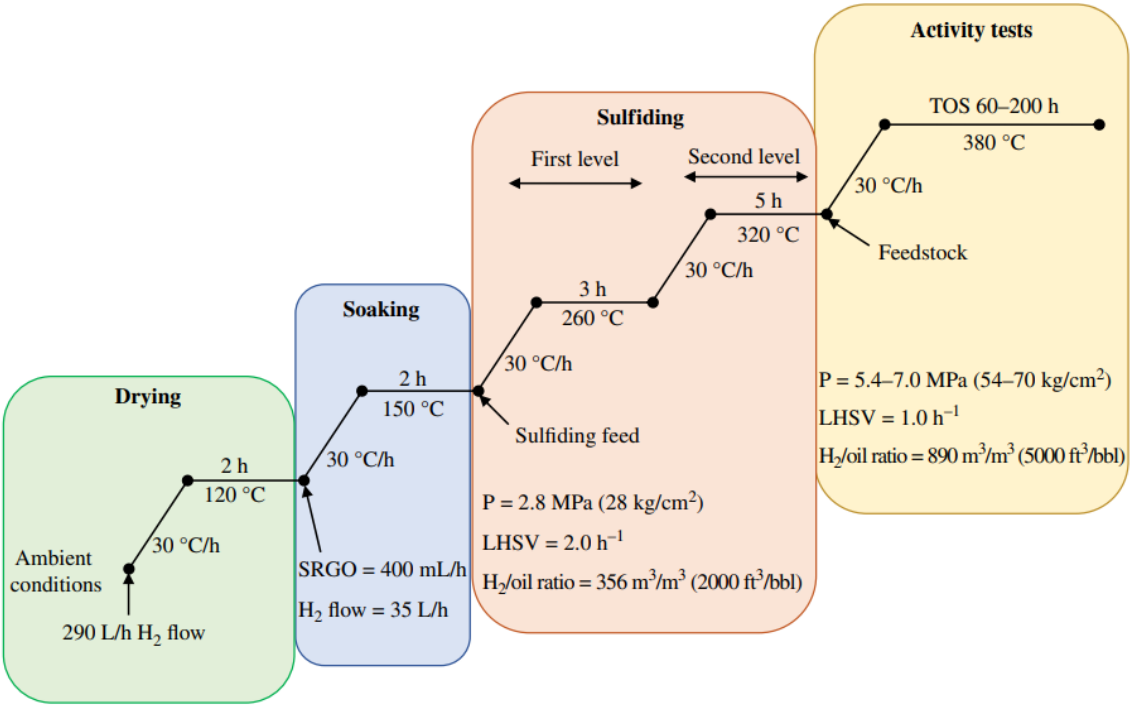

Figure 23 Alternative activation procedure for hydroreating catalyst [83]

3. Materials and methods

3.1 Set-up – Robinson Mahoney reactor

The Robinson-Mahoney set-up or "Rob2" is the set-up that is going to be used for the experimentation. It was designed with the intention of studying reactions, testing catalyst and acquiring kinetic data with the possibility of operating at high pressures (up to 120 bar) and high temperatures (up to 350°C). It is a gradient-less three phase continuously stirred tank reactor (CSTR) which makes it ideal for the hydroprocessing of petroleum fractions such as light gas oil (LGO) and VGO. A schematic view of the reactor is shown in Figure 24. The impeller revolves around the central axis in order to ensure good mixing and avoid heat and concentrations gradients. There are two tubes used for housing two thermocouples. The external thermocouple measures wall conditions while the internal thermocouple measures reactor conditions. The catalyst basket is a double wall cylinder with square pattern holed-wall which allows for the feed to flow toward the wall direction. Recirculation is formed in zones above and below the impeller; at high turbulent conditions it allows for good mixing and consequently uniform concentrations through the reactor ensured by sufficiently high mass transfer coefficient between the gas and liquid phases [84]. The reactor wall seals the reactor from the environment preventing the inlet of air into the reactor. The inlet lines of the liquid and gas feeds and the outlet line

of the product are not shown in Figure 24 which are important parts pf the reactor and will be explained in the following sections.

Figure 24 Schematic representation of the Robinson-Mahoney reactor Vessel

The process and instrumentation diagram (P&ID) of the Rob2 is shown in Figure 25. The complete set-up can be divided into three sections: feed, reaction and separation sections. The feeding section introduce the liquid and gas that are going to be feed into the reactor into the system and also preheat the liquid and gas streams. The reaction section comprises the reaction vessel as shown in Figure 24. The function of this section is self-evident. The separation section comprises all outlet lines from the reactor and the separation units. The function of this section is to separate the gas product from the liquid product. The liquid product is cooled down and collected in a vessel while the gas product is sent into the chromatograph for online analysis. After the chromatography analysis, the gas product is cooled down in a series of condensers where the condensable gases are collected in liquid phase while the non-condensable gases are vented way.

3.1.1 Feeding section

An overview of the feeding section of the set-up is shown in Figure 26. The liquid feed is contained in a bottle which can be heated with heating mantle in case the feed can solidify at environmental conditions. The feed vessel is located on a balance in order to track the real feed flow consumption and can be easily tracked via the display on the left side of the feed bottle and through the graphical

user interface. The pump (PMP-01) is located at the right side of the feed bottle. The liquid feed flow is

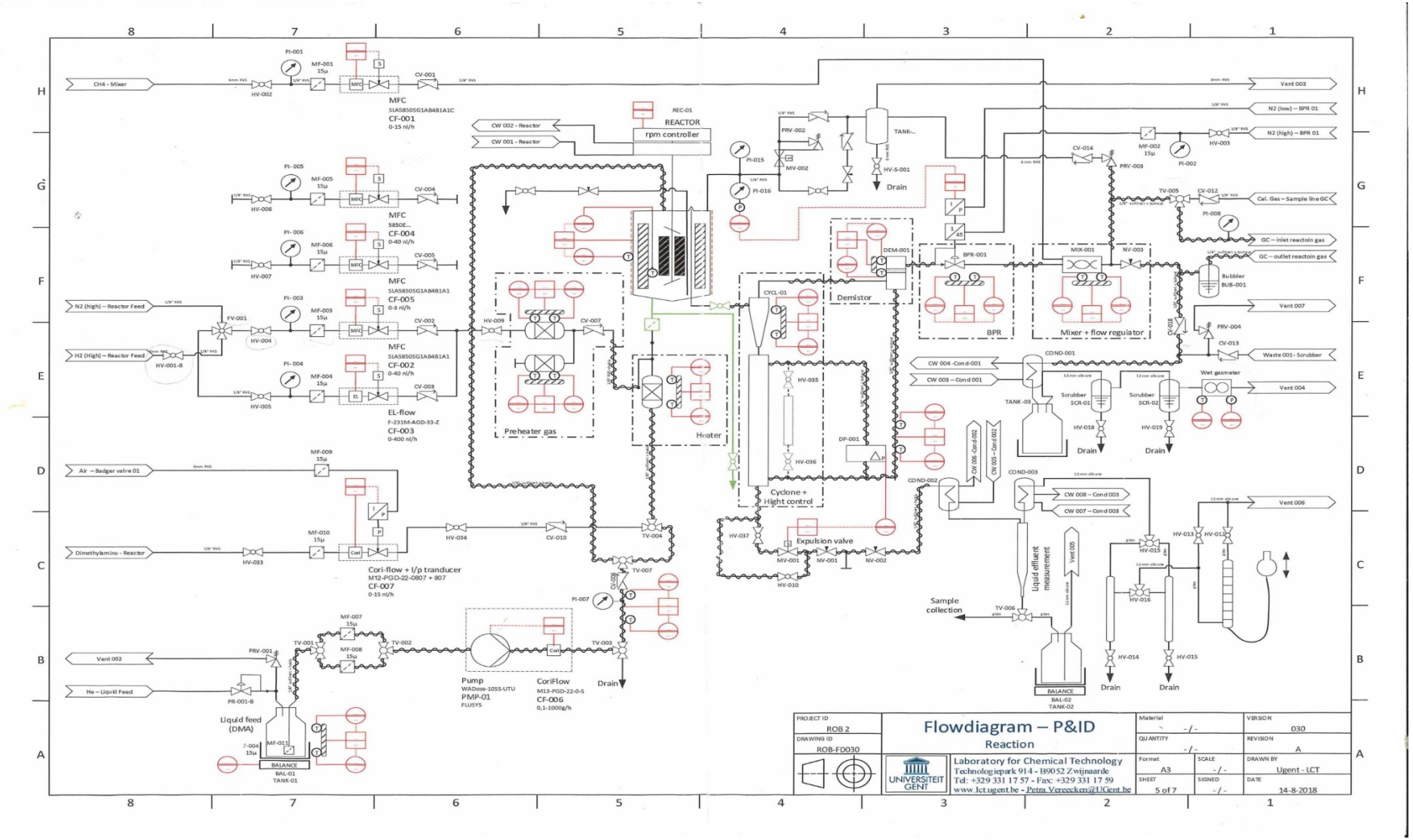
CH4 - Mixer
MFC
SIA58505G1AB4B1A1C
CF-001
0-15 nl/h
REACTOR
rpm controller
REC-01
CW 002 - Reactor
CW 001 - Reactor
MFC
5850E...
CF-004
0-40 nl/h
MFC
SIA58505G1AB4B1A1
CF-005
0-3 nl/h
MFC
SIA58505G1AB4B1A1
CF-002
0-40 nl/h
EL-flow
F-231M-AGD-33-Z
CF-003
0-400 nl/h
N2 (high) – Reactor Feed
H2 (High) – Reactor Feed
Air – Badger valve 01
Dimethylamine - Reactor
Cori-flow + I/p tranducer
M12-PGD-22-0807 + 807
CF-007
0-15 nl/h
Vent 002
He – Liquid Feed
Liquid feed
(DMA)
Pump
WADose-10SS-UTU
PMP-01
FLUSYS
CoriFlow
M13-PGD-22-0-S
CF-006
0,1-1000g/h
Drain
Preheater gas
Heater
Cyclone +
Hight control
Expulsion valve
Demistor
BPR
Mixer + flow regulator
Vent 003
N2 (low) – BPR 01
N2 (high) – BPR 01
Cal. Gas – Sample line GC
GC – inlet reactoin gas
GC – outlet reactoin gas
Bubbler
BUB-001
Vent 007
Waste 001- Scrubber
Wet gasmeter
Vent 004
Vent 006
CW 004 -Cond-001
CW 003 – Cond 001
CW 008 – Cond 003
CW 007 – Cond 003
Scrubber
SCR-01
Scrubber
SCR-02
Liquid effluent
measurement
Sample
collection
BALANCE
BAL-02
TANK-02
BALANCE
BAL-01
TANK-01
PROJECT ID
ROB 2
DRAWING ID
ROB-FD030
Flowdiagram – P&ID
Reaction
Material
-/-
QUANTITY
-/-
VERSION
030
REVISION
A
Format
A3
SCALE
-/-
DRAWN BY
Ugent - LCT
SHEET
5 of 7
SIGNED
-/-
DATE
14-8-2018
UNIVERSITEIT GENT
Laboratory for Chemical Technology
Technologiepark 914 - B9052 Zwijnaarde
Tel: +329 331 17 57 - Fax: +329 331 17 59
www.lct.ugent.be - Petra.Vereecken@UGent.be

Figure 25 P&ID Rob2

controlled with a mass flow controller (CF-006) which works based on the principle of the "Coriolis effect". The range of liquid feed flow possible is 0.01-10.00 ml min^{-1}, however the graphical user interface allows entries on mass units (g min^{-1}). Consequently, an estimation of the feed density is needed. The density of the mixture was estimated by an Aspen simulation and was found to be 0.742 g ml^{-1}. Based on this information it was possible to determine that the highest possible LHSV is 4 h^{-1} which corresponds to 10 ml min^{-1} or 7.42 g min^{-1}. The lowest possible LHSV was found to be 0.004 h^{-1} which corresponds to 0.01 ml min^{-1} or 0.00742 g min^{-1}. The H_2, N_2 and CH_4 feed lines can be seen on the right side of Figure 26. The inlet gas flows are controlled by thermal mass flow controllers; controller CF-003 is used for high flows, up to 400 Nl h^{-1} while CF-002 is used for low to middle flows, up to 40 Nl h^{-1} of H_2 and N_2. CH_4 flow is controlled by CF-001 and has an upper limit of 15 Nl h^{-1}. N_2 was used used for purging and drying purposes, CH_4 was used for the analysis in the GC while H_2 was used as a reactant.

Figure 26 Overview of the feeding section

3.1.2 Reaction section

A front view of the reaction is shown in Figure 27. The reactor itself cannot be seen in the picture as it is covered by a blue coffin which also covers the heating coils. The temperature control is done by regulating the power input to the heating coils. The temperature range allowed is 50-350°C. Pressure allowed in the reactor range from 30 bar to 120 bar and it is regulated by a back pressure regulator (BPR-001). The impeller motor is shown above the reactor and at the upper-left of the picture a reactor pressure indicator is shown. The liquid feed line enters the reactor at the top and is shown as the white line at the middle of the picture. The white colour of the liquid feed line is due to a heating coil that is wrapped around the feeding line in order to pre-heat it. The gas feed line also enters at the top of the reactor and can be seen left to the cooling water of the impeller motor. Left to the gas feed line there is a pressure relieve valve which opens at pressures higher than 120 bar. The Styrofoam covert units shown at the bottom of the reactor are already part of the separation section. The unit that is located at the middle of the picture is a drain system while the unit that is located at the down-right side of the picture is a cyclone which separates the gas and liquid products. The total volume, including catalyst basket and impeller is 250 ml, without the catalyst basket and impeller the volume was estimated to be 150 ml. The impeller speed is usually set at 1500 rpm in order to avoid gradients.

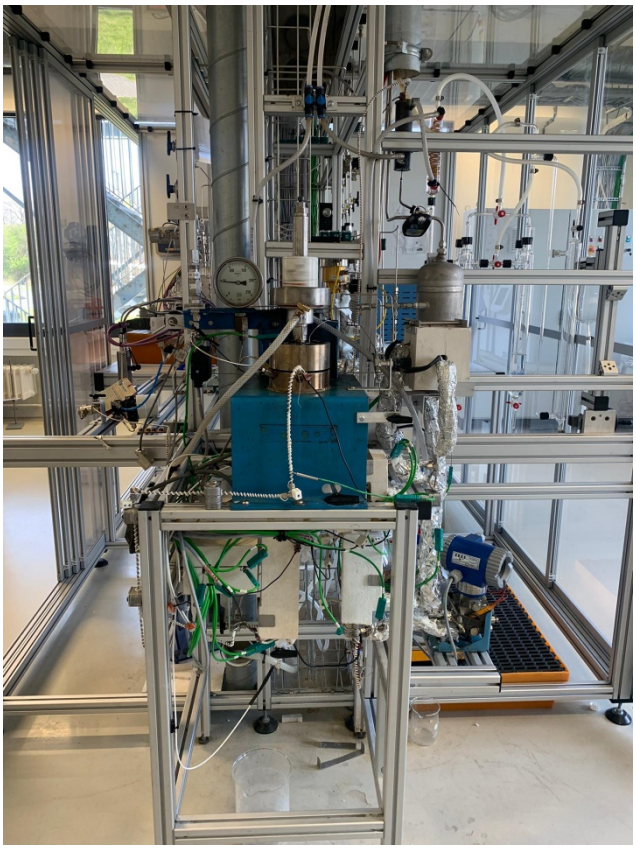

Figure 27 Front view of the reaction section

3.1.3 Separation section

The reaction products exit at the bottom of the reactor and enter a cyclone which separates the gas at the top and liquid at the bottom. The liquid product then goes into a vessel which has a level controller. Once the liquid reach a certain level it is flushed into a condenser and a collection burette and finally leading to a collection vessel which over a balance as can be seen on the bottom-left side of Figure 26. The gas product is first sent to a demister which removes entrained liquid droplets and then to a back pressure regulator (BPR-001) which decreases the pressure of the gas process stream to a pressure which is slightly higher than the atmospheric. Then the gas is sent to a mixer (MIX-001) seen as the white box in the middle of Figure 28 where the process stream can be mixed with CH_4 which can be used as internal standard for GC analysis. A needle valve (NV-003) regulates the flow that goes into GC. A pressure of 0.2-0.4 is recommended at the inlet of the GC, this pressure can be adjusted by opening or closing NV-003. The gas that does not go into the GC is sent to a condenser (COND-001) which removes entrained liquid and/or condensable gases and collected at the bottle shown in centre-down of Figure 28. After COND-001, the gas passes through two scrubbers (SCR-01 and SCR-02) which neutralizes any harmful gases such as H_2S and NH_3 by reacting those gases with a H_3PO_4 solution to neutralize NH_3 and a NaOH solution to neutralize H_2S. Finally, the neutralized gas stream is vented away.

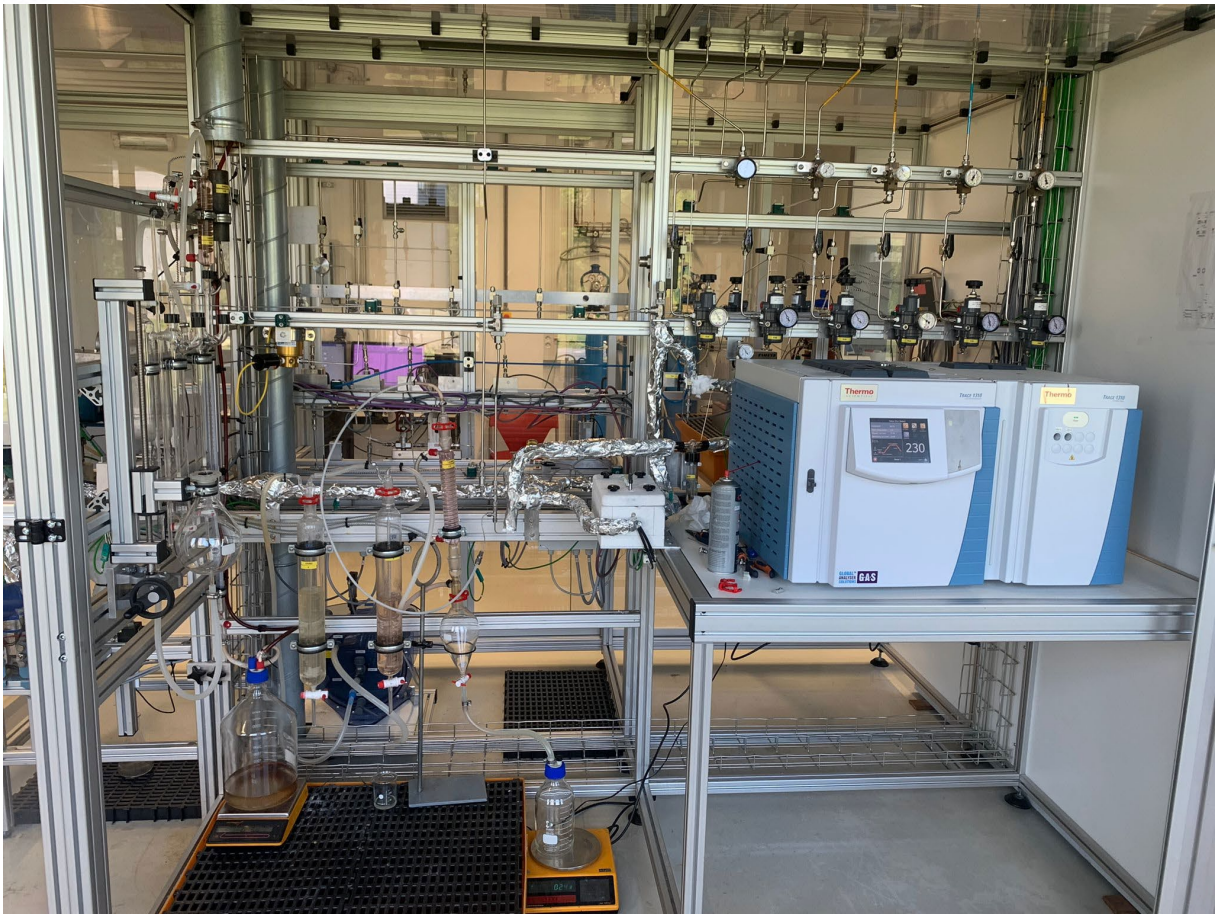

Figure 28 Front view of the separation section

3.1.3.1 *Analytic section*

The set-up is equipped with a gas chromatograph Trace 1310 from Thermo Scientific. The GC has three detectors, two TCDs and one FID. The FID detector is attached to a detailed hydrocarbon analysis (DHA) column of dimensions 100m x 0.25mm and a liquid injector module and uses helium as carrier gas. This detector is used to detect and quantify the hydrocarbons and hetero-compounds both in gas and liquid phase. The gas phase analysis is done in an online manner while the liquid phase analysis will be done in an offline manner. The Front TCD is attached to a RT-Volamine column of dimensions 30m x 0.32mm and also uses helium as carries gas. This detector is used to detect and quantify NH_3 and H_2S. The Aux TCD is attached to a Molsieve 5A, 60-80 of dimensions 3m x 1/16 SS and a Hayesep Q, 60-80 of dimensions 1m x 1/16 SS and uses argon as carrier gas. This detector will be used to detect and quantify hydrogen. All detectors are able to detect CH_4 which was used as internal standard for the gas phase analysis. The normalized composition of any compound x_i in wt.% is calculated according to Eq. 41.

$$x_i = \frac{CF_i PA_i}{\sum_{j=1}^{n} \mathrm{CF_j PA_j}} \qquad 41$$

Where CF_i is the calibration factor of the compound and PA_i is the peak area detected from the chromatogram. Experimental calibration factors of the FID detector were calculated using a calibration standard of known composition of the available compounds according to Eq. 42 [85].

$$CF_i = \frac{PA_{ref} wt_i}{PA_i wt_{ref}} \quad 42$$

Where PA_{ref} is the peak area of a reference compound, PA_i is the peak area from any compound, wt_{ref} is the composition of the reference compound in wt.% and wt_i is the composition of any compound in wt.%. The calibration factors of the FID detector for the compound not present in the calibration standard are calculated according to the correlations presented by Dierickx, et al. [85]. Calibration factors for the compounds detected on the TCDs are taken from the work of Dietz [86].

3.2 Materials

The selected olefins for the model samples were synthesis grade synthesis grade 1-Hexadecene with a purity of ≥92 wt.% and unspecified impurities. Technical grade with a purity of ≥90% 1-Octadecene and 2-octyl-1-decene, n-octadecane, 2-butyl-1-tetradecene, 2-hexyl-1-dodecene as impurities of unspecified composition. The selected nitrogenated heterocompound was synthesis grade quinoline with a purity of ≥97 wt.%. As solvents, halpasol and n-Octadecane with a purity of ≥90 wt.% were selected. Halpasol is a mixture of C_9-C_{14} paraffins. The GC/FID analysis of this solvent yielded the following composition in wt.%: 0.15% n-nonane, 7.71% n-decane, 33.29% n-undecane, 22.00% n-dodecane, 36.49% tridecane and 0.46% tetradecane. DMDS is used as a sulfiding agent for the catalyst activation procedure and for the experimental campaign. None of the chemicals were subjected to further purification processes. The suppliers and product numbers for the different chemicals used in the experimentation are listed in Table 3.

Table 3 Suppliers and product numbers of the chemicals used in the experimental campaign

CHEMICAL	PHASE (25°C)	SUPPLIER	PRODUCT NUMBER
1-HEXADECENE	Liquid	Sigma Aldrich	211-105-8
1-OCTADECENE	Liquid	Sigma Aldrich	204-012-9
QUINOLINE	Liquid	Sigma Aldrich	202-051-6
HYDROGEN	Gas	L'Air Liquide	I7005L50R2A001
DMDS			
HALPASOL	Liquid	Haltermann GmbH	AG190100TF

A commercial NiMoP/Al_2O_3 catalyst (HR-348 from PROCATALYSE) was used. The catalyst composition by weight is as follows: 10.7% Mo, 2.5% Ni and 2.64% P with a BET surface area of 164 $m^2\ g^{-1}$ [87]. The catalyst pellets were crushed and sieved to get a particle size between 600 and 720 µm.

3.3 Procedures

3.3.1 Catalyst basket preparation

The catalyst basket was prepared according to the scheme shown in Figure 29. The total height of the basket is 8 cm recommended a 1 cm height of catalyst bed in the middle of the basket. A 1.5 cm glass wool bed is located at the bottom of the basket which accounts for 4.15 g. Top of the glass wool bed, a 2 cm inert material (9.42 g) bed is located which brings the height to 3.5 cm. The inert material is porous alumina. Top of the inert bed is the catalyst bed. The mass of the catalyst is 2.58 g [46] and is mixed with 2.57 g of the inert material. Top of the catalyst bed is another 2 cm (9.99 g) bed of inert material. A final 1.5 cm bed (4.0 g) of glass wool is located at the top of the basket.

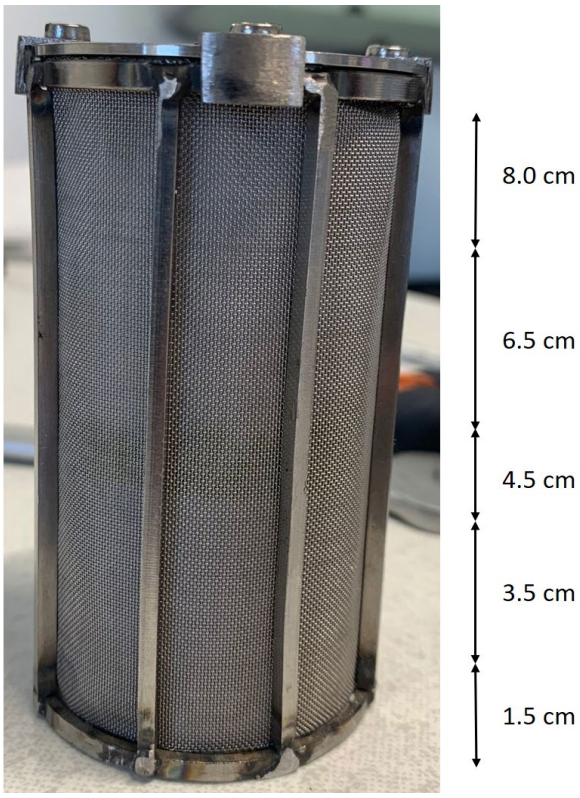

Figure 29 Catalyst basket

3.3.2 Catalyst activation

As explained in section 2.2.3 the catalyst is received in the inactivated form and was activated by in-situ sulfidation. The catalyst activation was performed based on the procedure shown in Figure 23 and is divided into drying, soaking and sulfiding procedures as shown in Figure 30. The reactor temperature was increased from ambient conditions to 200°C at 14 bar. The change made from the procedure from Ancheyta [83] was due to difficulties of the reactor to reach atmospheric pressures. Consequently, the temperature needed to be increased above the boiling point of water at 14 bar. The basket was left to

dried up for 67 min. The soaking was made at those same conditions but with the addition of a liquid feed of Halpasol at 6.66 ml min^{-1} and was left to soak for 68 min. Once the soaking was over, a sulfiding feed was added, the temperature increased to 260°C and the pressure to 28 bar. The liquid feed consisted of a mixture of Halpasol and DMDS accounting for a total of 2% sulphur in the mixture. Once it reached those conditions, it was left to sulphide for 150 min. Afterwards, the temperature was increased to 310°C and maintained for 194 min.

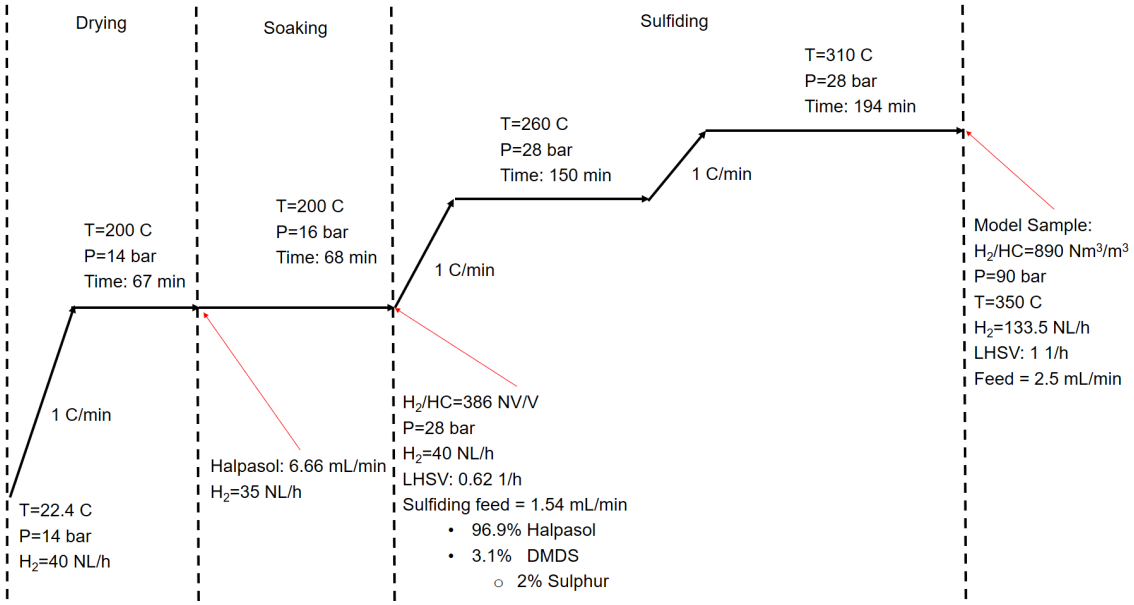

Figure 30 Catalyst activation procedure scheme

3.3.3 Activation test

An activation test was done previous to the experimental campaign in order to verify that the catalyst was effectively activated. The activation test mixture composition is shown in Table 4. Halpasol was used as solvent, decene as the compound to verify the olefin hydrogenation activity, pyridine and indole to verify the HDN activity and DMDS to provide an atmosphere in the presence of sulphur. The amount of decene added to the activation test mixture was chosen assuming a PPO/VGO mixture of 10% PPO and 90% VGO while the PPO olefin content is 58% in wt. %. The pyridine and indole content was chosen assuming 1% wt. of total nitrogen. DMDS content was chosen assuming a H_2S/Nitrogenated hetero-compounds ratio of 0.2 mol mol^{-1} [46]. The operating conditions are shown in Figure 30. They were chosen according to Figure 23 which is the procedure proposed by Ancheyta [83]. The temperature was chosen to be 350°C as it is the maximal temperature of the reactor while the pressure was chosen as 90 bar to ensure HDN activity.

Table 4 Activation test mixture composition

COMPOUND	COMPOSITION (WT. %)
NONANE	0.13%

DECANE	6.65%
UNDECANE	28.72%
DODECANE	18.99%
TRIDECANE	31.40%
TETRADECANE	0.39%
INDOLE	4.16%
PYRIDINE	2.83%
DECENE	6.04%
DMDS	0.68%

3.3.4 Experimental campaign

The feed consisted of a mixture of paraffins, olefins and nitrogenated heterocompound. The paraffins chosen were Halpasol which composition is already described in section 3.2. The chosen olefins were Hexadecene and Octadecene. Those olefins were chosen as representation of possible heavy olefins present in PPO and assumed to be in 1:1 proportion in the PPO. As nitrogenated heterocompound, Quinoline was chosen because is a typical heterocompound found in VGO. It was decided not mix different heterocompouds in order to ease the analysis of the composition of products. DMDS was added in order to provide a sulfided atmosphere in the reactor which is closer to a real operation. The composition of the feed was chosen assuming a 58 wt.% olefin content in PPO, a mixture of 80 wt.% VGO and 20 wt.% PPO, a total nitrogen content of 1 wt.% and a H_2S/Nitrogenated hetero-compounds ratio of 0.2 mol mol^{-1} as in the activation test mixture of Table 4. Consequently, the composition in wt.% of the feed is shown in Table 5 as the average of the composition of all the mixtures prepared. Small deviations between feed mixtures are present due to experimental errors while adding the compounds to the mixture. The chromatogram corresponding to the liquid feed is shown in Figure 31.

Table 5 Liquid feed composition

COMPOUND	WT. %
NONANE	0.12%
DECANE	6.02%
UNDECANE	25.99%
DODECANE	17.18%
TRIDECANE	28.41%
TETRADECANE	0.36%
QUINOLINE	9.23%
HEXADECENE	6.01%
OCTADECENE	6.02%
DMDS	0.67%

The operating conditions were chosen considering the literature and the limitations of the Set-up. As HDN reactions require more severe conditions than HDS and olefin saturation reactions it was decided

to use temperatures between 300°C and 350°C and pressure between 60 bar and 90 bar. While the reactor has an upper operating pressure of 120 bar, no pressure above 90 bar was chosen to be used due to safety reasons. The relive valve of the high pressure hydrogen line in the cylinder cabinet failed at pressures above 110 bar. Consequently, in order to not force that relive valve a limit of 90 bar was set. The LHSV was set at 1 h^{-1} and a H_2/HC ratio of 890 was chosen as typical industrial conditions according to Ancheyta [83]. For an empty reactor volume of 150 ml, the liquid feed volumetric flow is equal to 2.5 ml min^{-1} which corresponds to a H_2 flow of 133.5 NL h^{-1}. The CH_4 flow (internal standard) was set at 10 NL h^{-1}.

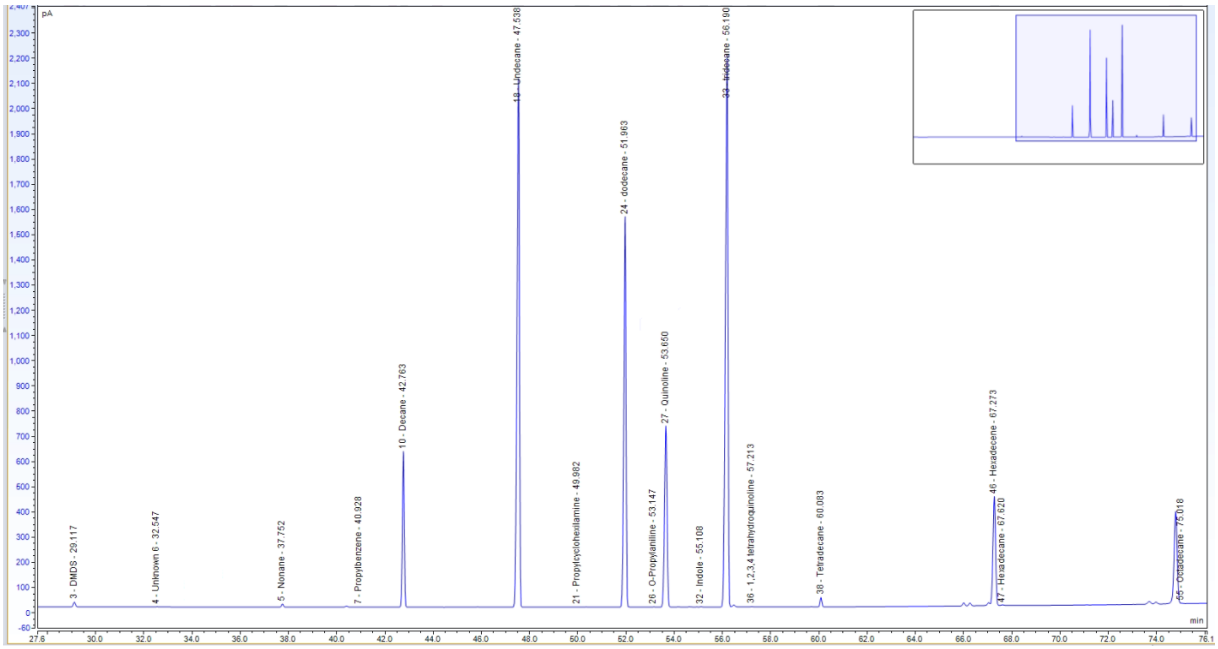

Figure 31 Liquid Feed chromatogram

It was decided to start with the highest operating pressure at 90 bar. If no deep HDN activity was observed at the proposed temperature range and 90 bar means that more severe conditions are needed for deep HDN. Since the set-up was already at the limits of temperature and pressure, the other operating variable to change was the LHSV. Consequently, after the first set of experiments at 90 bar and a LHSV of 1 h^{-1} it was decided to fix the pressure at 90 bar and vary the LHSV between 0.4 h^{-1} and 1 h^{-1}. The final experimental design is shown in Table 6.

Table 6 Choice of operating conditions

OPERATING CONDITION	EXPERIMENTS
TEMPERATURE	300-317-334-350°C
PRESSURE	90 bar
LHSV	0.4-0.7-1 h^{-1}
LIQUID FEED FLOW	1-1.75-2.5 ml min^{-1}
H_2 FLOW	53.4-90.45-133.5 NL h^{-1}

The stability of the reactor or the stationary state was checked before collecting the liquid samples and mass balances calculations. At the beginning of the experimental campaign it was decided to check for the stationary state once three consecutive chromatograms if the online gas injections were very similar but this criterion resulted to be inadequate because the product gas flow was highly irregular as shown in Figure 32. The flow measured by the wet gas meter (G) which is supposed to be only H_2 and CH_4 as the hydrocarbons are removed by the condenser while NH_3 and H_2S are removed in the scrubbers varied between 2 and 3.5 L min^{-1}. Consequently, the product gas stream of the reactor G_P that enters the mixer is also varying and hence the composition of the gas injection to the GC is also changing (See Figure 34).

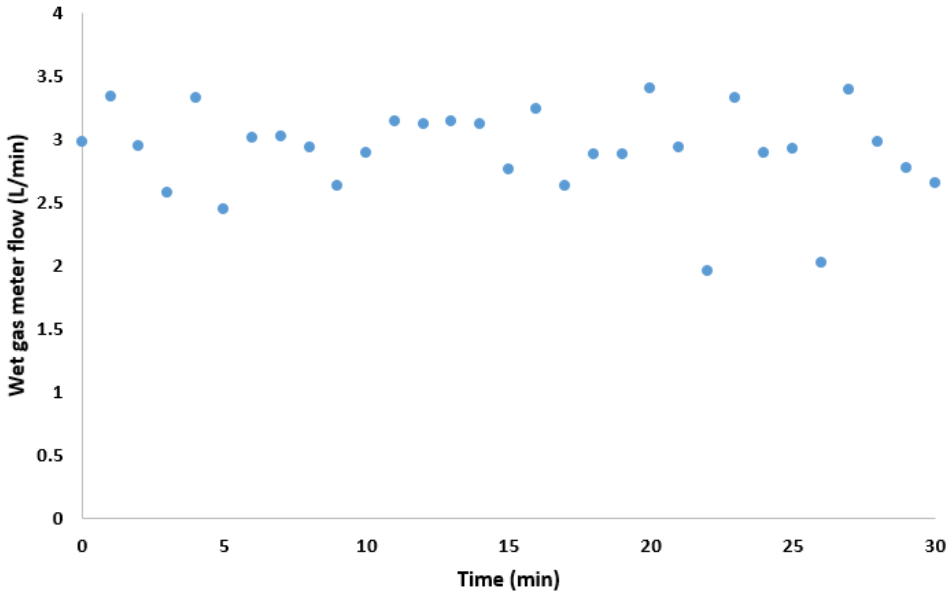

Figure 32 Gas flow measured by the wet gas meter in a 30 min time frame at a H_2 flow of 133.5 NL h^{-1}

As can be seen from Figure 33, the chromatograms from two consecutive online gas injections at 317°C, 90 bar and a LHSV of 1 h^{-1} are completely different. The difference between the chromatograms can be attributed to the reasons mentioned earlier and to the fact that the line of the reactor gas product G_P could only be heated up to 220°C which may lead to changes in the composition of the stream as the reactor temperature is different.

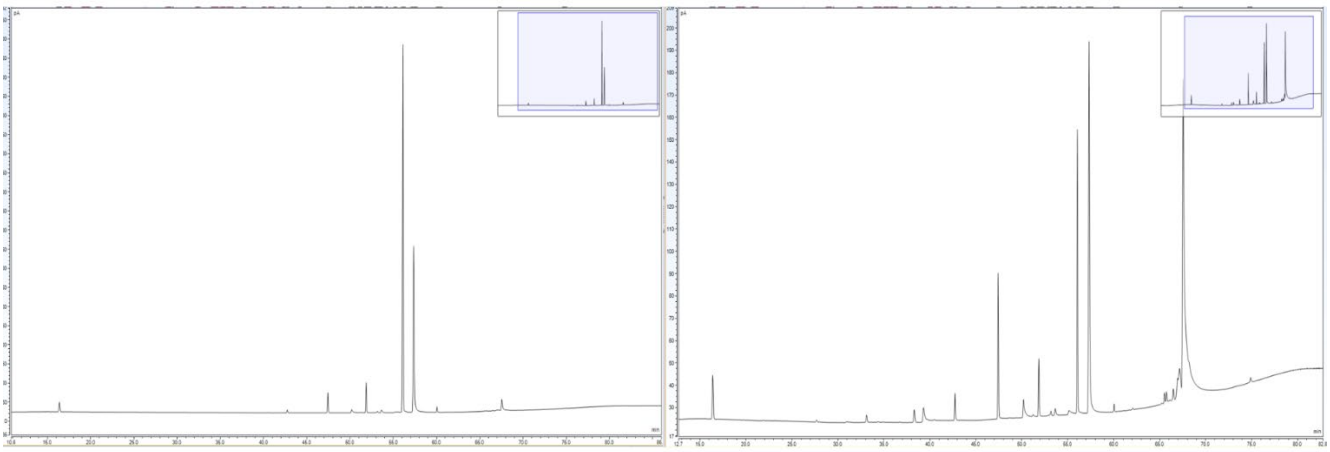

Figure 33 Two consecutive online gas injections at T=317°C, P=90 bar, LHSV=1 h^{-1}

As a result, a new criterion which was independent of the flow needed to be applied. Since NH_3 and H_2S are detected in only one detector, the stationary state can be checked by analysing the areas of these two compounds detected on the TCD. The absolute value of the areas is dependent of the flow but the ratio of the areas should be independent of the flows. Consequently, when the ratio of the peak area of NH_3 to the peak area of H_2S becomes constant, it is assumed that the reactor is at stationary state. This criterion was then validated by injecting two non-consecutive liquid samples.

4 Results and discussion

4.1 Activation test

A quantitative analysis of the activation test couldn't be done due to damage at the septum of the FID detector which lead to unreliable chromatograms of the liquid samples however, a qualitative analysis was possible to do in the regions of interest of the chromatograms. In Figure 34 left it is shown the 1-Decene and N-Decane peaks of the feed that is described in Table 4. At the right, the same peaks are shown for the liquid product. From the comparison it can be seen that the 1-Decene peak decreases considerable in the liquid product while the N-Decane increases in intensity considerably. Hence, olefin hydrogenation activity is observed.

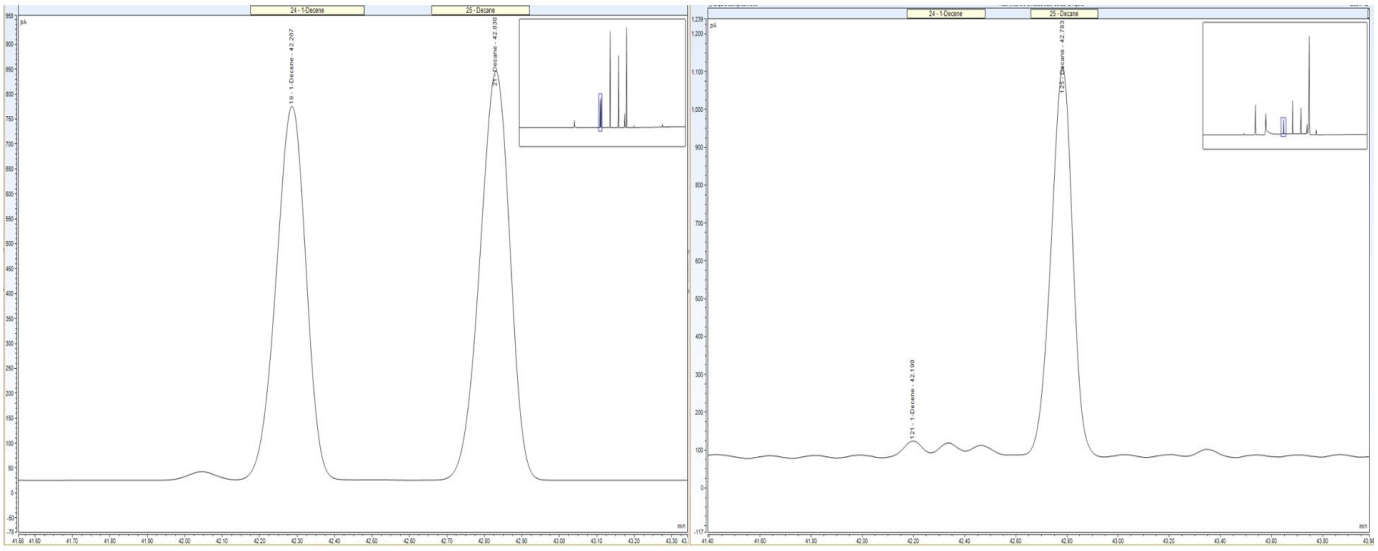

Figure 34 1-Decene and N-Decane peaks in the FID detectors during the activation test at the Feed (left) and the liquid product (right)

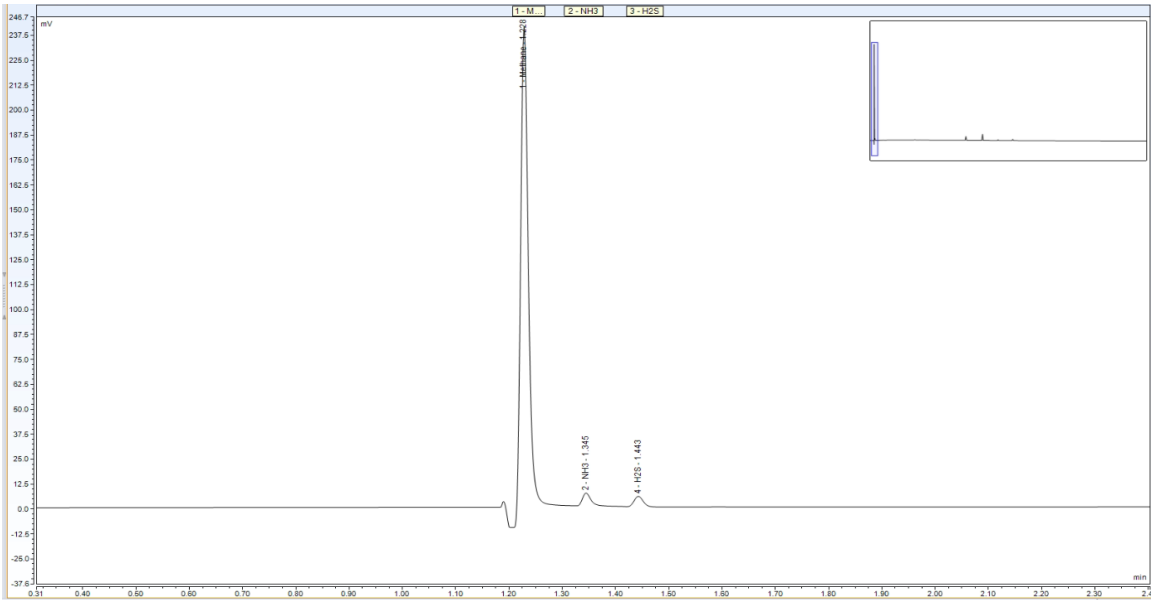

Figure 35 NH_3 and H_2S peaks at the Front-TCD of the gas product of the activation test

The HDN activity could be observed at the Front-TCD. In Figure 35 it is shown a chromatogram of the Front-TCD during the activation test of an online gas injection. It can be seen that the characteristic peak of NH_3 is being formed which leads to the observation of HDN activity. At the right of the NH_3, the H_2S peak is also observed which is evidence of the decomposition of DMDS.

4.2 Mass balances, conversion, selectivities and production rates

4.2.1 General mass balance

The general carbon mass balance is calculated according to the scheme shown in Figure 36. There are three inlet streams and three outlet streams. The liquid feed L_F mass is weighted in a balance at times

t_1 and t_2, being t_1 the initial time and t_2 the end time of the measurement. This time frame was set to be around 88 min which is the total time of the chromatograph method. Both H_2 and CH_4 are measured in NL h^{-1}, consequently by assuming ideal gas law the volumetric flow of those two inlets are converted to mass flows. The main liquid product L_{p1} is the liquid separated in the cyclone while L_{p2} is the liquid condensed from the reactor gas product stream G_p. The masses of L_{p1} and L_{p2} are both weighted in balances in times t_1 and t_2. The non-condensable gases G are measured with the wet gas meter in L min^{-1} at normal conditions, by assuming ideal gas law it is converted to mass flow. Hence, the general carbon mass balance is shown in Eq. 43.

$$L_F + H_2 + CH_4 - L_{P1} - L_{P2} - G = 0 \qquad 43$$

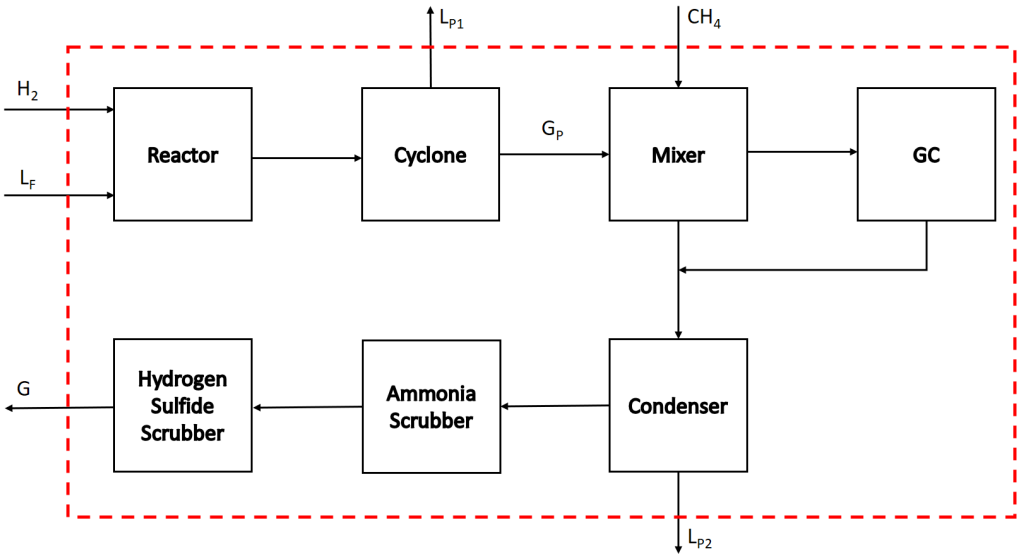

Figure 36 General mass balance scheme of the set-up

This method of calculating the mass balance closure proved to be very inconvenient due to the reasons explained in section 3.3.4. Consequently, a new methodology was needed for the mass balance closure. It was decided to close the mass balance via carbon balance of the liquid feed L_F and the liquid products L_{P1} and L_{P2}. The carbon balance was calculated according to Eq. 44.

$$CB = \left(1 - \left(\frac{\sum_{i=1}^{n} L_{FC,i} - \sum_{i=1}^{n} L_{P1C,i} + \sum_{i=1}^{n} L_{P2C,i}}{\sum_{i=1}^{n} L_{FC,i}}\right)\right)100 \qquad 44$$

Where CB is the carbon balance with a value of 100% means perfect closure and is an acceptable closure if it has deviations lower than ±5%. $L_{FC,i}$ is the carbon mass flow of compound i in the liquid feed, $L_{P1C,i}$ and $L_{P2C,i}$ are the carbon mass flow of compound i in the liquid products L_{P1} and L_{P2}

respectively. The results are shown in Figure 37. It can be seen that no carbon balance measurement felt below 95% which means that the mass balances are within the proposed criterion.

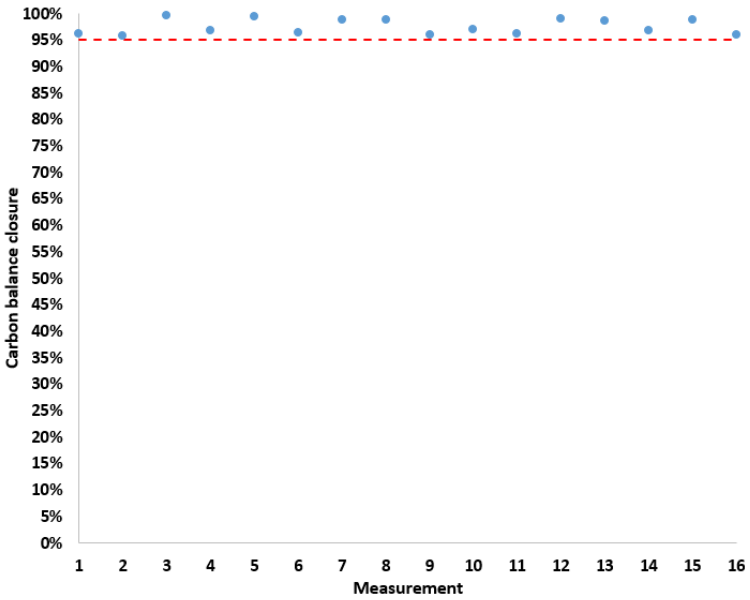

Figure 37 Carbon balance results

4.2.2 Reactor stability

As explained in section 3.3.4 the reactor stability or stationary state was validated through the analysis of the peak areas of the NH_3 and H_2S according to Eq. 45.

$$R_{\frac{NH_3}{H_2S}} = \frac{PA_{NH_3}}{PA_{H_2S}} \quad 45$$

where R is the ratio of the areas and PA are the peak areas of NH_3 and H_2S according to the subscripts. In Figure 38 it is shown a typical behavior of the ratio of the peak areas of NH_3 and H_2S. After 5 consecutive gas injections the ratio becomes constant. Once the ratio is constant, the mass balances started to be measured. In Table 7, it is shown the hydrotreated product composition of two separates mass balances at 350°C, 90 bar and a LHSV of 0.4.

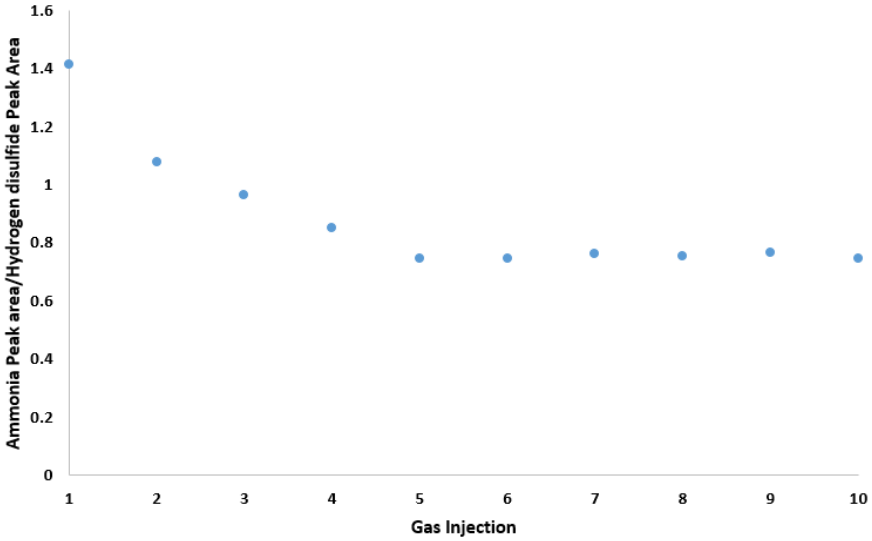

Figure 38 Reactor stability at 350°C, 90 bar LHSV=0.4

Table 7 Product composition at 350°C, 90 bar and LHSV=0.4 h^{-1}

	PRODUCT COMPOSITION (WT. %)	
COMPOUND	**Mass balance 1**	**Mass balance 3**
N-NONANE	0.11%	0.12%
N-DECANE	5.98%	5.97%
N-UNDECANE	26.16%	25.99%
N-DODECANE	17.15%	16.97%
N-TRIDECANE	28.41%	28.11%
N-TETRADECANE	0.37%	0.38%
QUINOLINE	0.25%	0.26%
HEXADECENE	0.21%	0.23%
OCTADECENE	0.15%	0.21%
DMDS	0.00%	0.00%
1,2,3,4 TETRAHYDROQUINOLINE	5.68%	5.86%
HEXADECANE	5.98%	6.08%
OCTADECANE	6.04%	6.12%
O-PROPYALNILINE	0.99%	0.92%
5,6,7,8 TETRAHYDROQUINOLINE	0.23%	0.23%
DECAHYDROQUINOLINE	0.16%	0.20%
PROPYLCYCLOHEXILAMINE	0.89%	0.96%
PROPYLCYCLOHEXANE	1.01%	0.94%
PROPOYLBENZENE	0.24%	0.44%
PROPYLCYCLOHEXENE	0.00%	0.00%

The compositions shown in Table 7 are the compositions of the liquid product at the wetted surface of the catalyst which means that they were calculated including both the main liquid product L_{P1} and the condensed gas product L_{P2} according to Figure 36. There are no major differences between the compositions of both mass balances. Consequently, it can be assumed that the reaction is at steady state and the criterion is validated. The behavior in Figure 38 shows that the concentration of NH_3 is

higher at the start of the experimental run. The first gas injection has the highest ratio and decreases until It reaches a constant value. This behavior could be explained by considering the end of the previous run. Once an experimental run is finished, the liquid and gas feed are stopped and the temperature set-point of the reactor is set at 80°C in order to stop the reactions. However, the temperature decrease is not immediate but takes time, from one to two hours depending on the cooling rate. During the time frame, the reactor is still filled with liquid that can react while the reactor temperature decreases and as there is no flow to displace that reactor volume, the reaction products are being accumulated. For that reason, the NH_3 concentration is higher than the steady state at the start of the next experimental run. It decreases while the flow displaces the accumulated product.

4.2.3 Olefin Saturation

The experimental conversions of hexadecene and octadecene are calculated considering that the reactions take place in the completely wetted catalyst [88]. As a consequence, the fraction of liquid reactant that vaporize is excluded from participating in the reaction. Therefore, given a molar feed rate of the olefin $L_{F,O}$, the molar rate that is in contact with the catalyst is $L_{F,O}$-$L_{P2,O}$ where $L_{P2,O}$ is the molar flow of the olefin that is condensed from the product gas stream G_P. Consequently, the conversion of the olefins is defined in Eq. 46.

$$X_O = \frac{L_{F,O} - L_{P1,O} - L_{P2,O}}{L_{F,O} - L_{P2,O}} \quad 46$$

The conversion of the saturated olefin, which is an alkane is calculated according to Eq. 47.

$$X_A = \frac{L_{P1,A} + L_{P2,A}}{L_{F,O} - L_{P2,O}} \quad 47$$

As there are no side or intermediate products during the saturation of an n-olefin X_O should be equal to X_A as the moles consumed of olefin should be the same as the moles produces of the respective alkane. It was found that the differences between the conversions of the olefin and the respective alkane never differed in more than ±5%.

Experimental production rates/rate of disappearance of the olefin and the respective alkane R_i, is calculated by dividing the conversion X_i by the space time. Due to the assumption made for the calculation of the conversion space time is defined as the mass of the catalyst W divided by the molar flow rate that is in contact with the catalyst [88]. Consequently, the experimental production rates R_i are calculated according to Eq. 48.

$$R_i = \frac{X_i}{\frac{W}{L_{F,O} - L_{P2,O}}} \quad (48)$$

The summarized results for the conversion of olefin hydrogenation can be found on Table 8. On Figure 39 it is shown the effect of temperature on olefin conversion. At a fixed LHSV of 1 h^{-1} the lowest olefin experimental obtained conversion was 72% for hexadecene and 74% for octadecene at 300°C. As the temperature increased, the olefin conversion increased which was expected. 95% and 96% conversion was obtained for hexadecene and octadecene respectively. It is also shown that temperature has a strong effect on olefin conversion. These results are in agreement with the work of Xin, et al. [72]. However, there are differences between the results. Xin, et al. [72] worked at lower temperatures (100-300°C) and pressures (14-28 bar) using lower olefins as feedstock. Consequently, high conversions were obtained in vapor phase reactions. As shown in Figure 19, 100% conversion was obtained at 300°C, 21 bar, LHSV of 1.5 h^{-1} for C_7 olefins while in this work conversions between 72% and 75% were obtained at 300°C for C_{16} and C_{18} n-olefins. This proves that the heavier the olefin the more difficult the hydrogenation is. However, it doesn't appear to be a significant difference between the conversions of hexadecene and octadecene. The lower conversions shown at 334°C can be attributed to unstable liquid feed flow as during the start of mass balances at those conditions there was gas trapped in the liquid pump which lead to unstable flow. After purging the pump, the stable flow returned. The effect of LHSV on olefin conversion is visualized on Figure 40. As LHSV decreases the effect of temperature on olefin conversion is less pronounced. At 0.4 h^{-1} the lowest conversion was 91.2% at 300°C. As temperature increases, the olefin conversion becomes more difficult. From 317°C to 350°C, the conversion increased from 95.1% to 97.2%. At 0.7 h^{-1} the conversion increased from 88.7% to 99.1% at 300°C and 350°C respectively. The same behavior was observed as in the case of 0.4 h^{-1}. The promoter effect of lower LHSV on olefin conversion can be attributed to higher retention times while at higher LHSV the retention time is lower. As described in Eq. 46-47, the assumption made for the olefin conversion calculation is that the reaction takes place in the liquid phase. Consequently, the fraction of the olefins that is vaporized before the reaction takes place does not participate in the reaction. Since olefins with relatively high carbon number were chosen (C_{16} and C_{18}), the vaporized fraction from the liquid feed was negligible due to high boiling points of the reactants. It varied from 0.02% to 0.6%. However, as shown in Figure 42 the ratio of the olefin molar flow condensed $L_{P2,O}$ to the olefin molar feed flow $L_{F,O}$ appears to be higher as the temperature increases which is contrary to what would be expected. If the reaction only takes place in the liquid phase, it would be expected that the vaporized fraction would increase as the temperature increases but that is what is being observed. This might be an indication that olefin hydrogenation reactions might be occurring also in the gas phase but these results are inconclusive. More experimentation would be needed to validate or invalidate

the assumption. The vaporized fraction for lower boiling compounds such as n-decane was around 25%, consequently it would be expected that for lower olefins the vaporized fraction would be higher if reaction only takes place in the liquid phase, but if the reaction also takes place in the gas phase the vaporized fraction should decrease as temperature increases because the lower the olefin the easier to saturate.

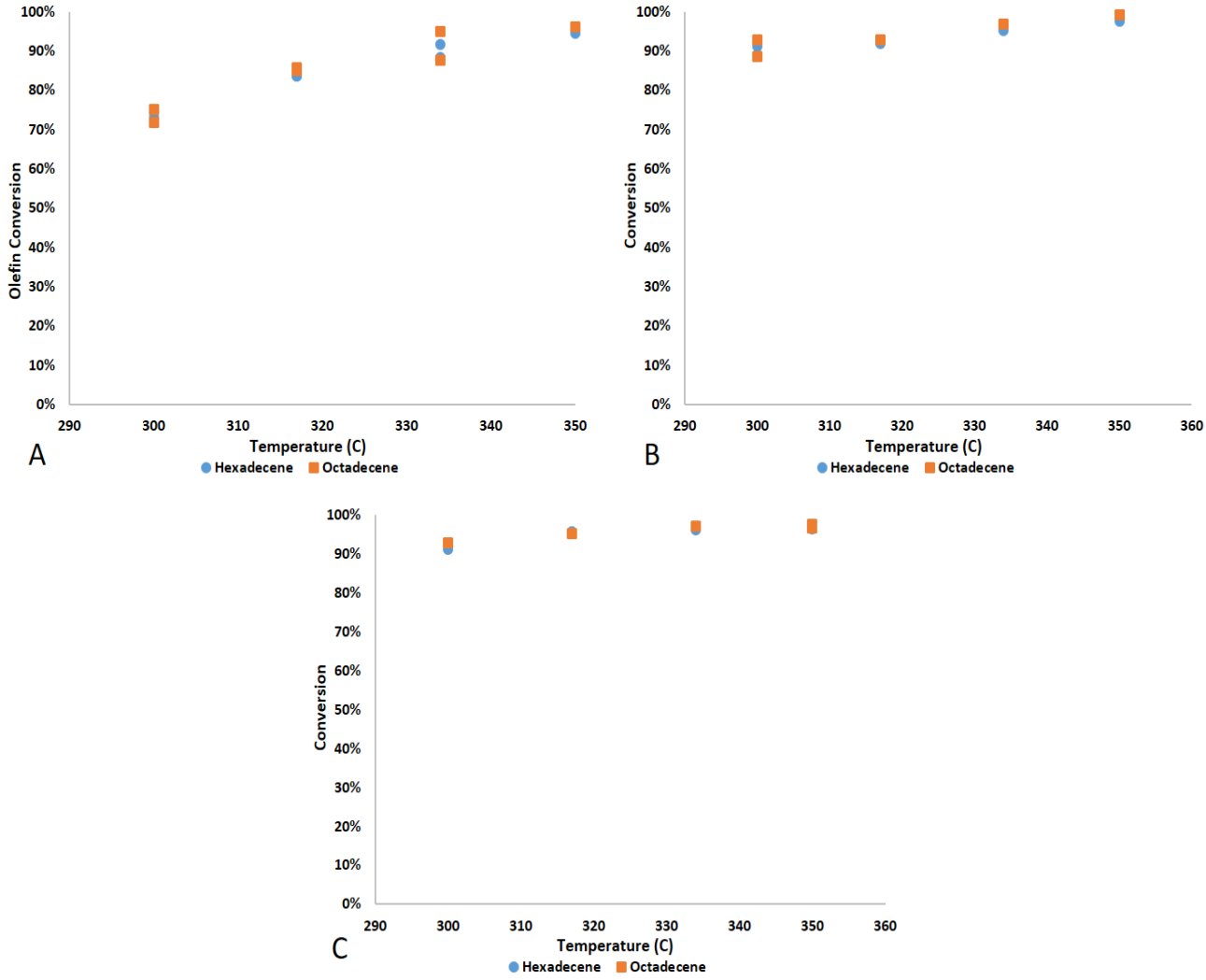

Figure 39 Olefin conversion at 90 bar as a function of the temperature. A: LHSV=1, B: LHSV=0.7, C: LHSV=0.4

Table 8 Olefin hydrogenation conversion results

	LHSV					
	1 h^{-1}		0.7 h^{-1}		0.4 h^{-1}	
TEMPERATURE (°C)	**Hexadecene**	**Octadecene**	**Hexadecene**	**Octadecene**	**Hexadecene**	**Octadecene**
300	73.7%	73.5%	89.0%	88.7%	91.2%	92.8%
317	83.6%	85.4%	92.0%	93.0%	95.7%	95.1%
334	90.1%	91.3%	95.3%	96.9%	96.1%	97.1%
350	95.6%	96.9%	97.7%	99.1%	96.5%	97.2%

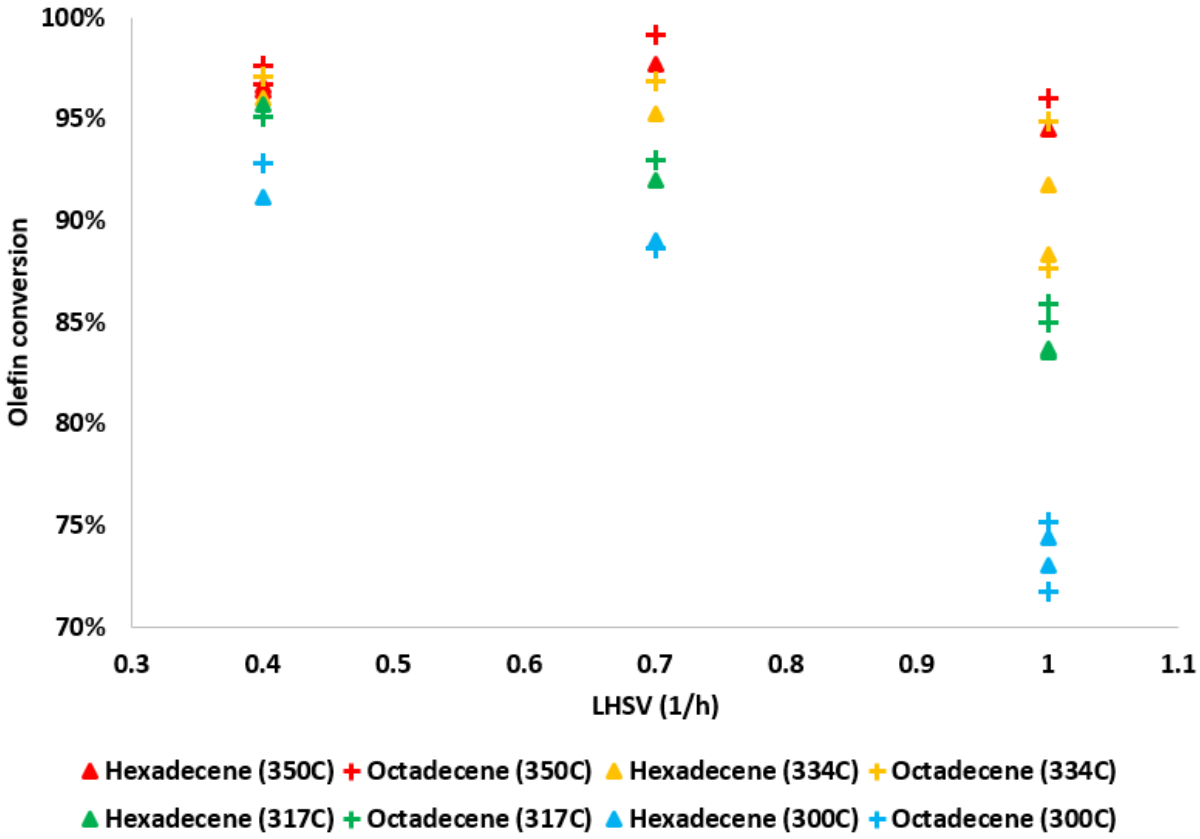

Figure 40 Olefin conversion as a function of LHSV

The total olefin content in the hydrotreated product (L_{P1} + L_{P2}) at a LHSV of 1 h^{-1} decreased from a maximal value of 3.5 wt.% at 300°C to a minimal value 0.57 wt.% at 350°C as shown in Figure 41 from an initial total olefin content of 12 wt.% in the feed according to Table 5. These results are also in according with the other work of Xin, et al [75]. As shown in Figure 20, the olefin content of a light fraction of a thermally processed bitumen decreased from 6 wt.% in the feed to 0.5 wt.% in the hydrotreated product at 300°C. From these results it can be inferred that in order to obtain near full olefins saturation conversion with carbon numbers of 16 or higher at industrially relevant space velocities temperatures of 350°C or higher. However, olefin content in PPO ranges from C_{10} to C_{20} as shown in Figure 5 and since PPO can be separated into light and heavy fractions, the choice of operating conditions in a PPO/VGO mixture if the objective is to saturate the olefins of the mixture will depend on the amount of PPO added to the mixture and carbon range of the PPO fraction. Adding lighter PPO fractions to VGO will need less severe conditions than adding heavy PPO fractions. Another important factor is the source in the PPO. As explained in section 2.1.1, the composition of the pyrolysis product will depend on the composition of the plastic feed stream of the pyrolysis process. Knowledge

of the composition of the PPO added to the VGO becomes a prerequisite if conventional hydrocracking is to be desired.

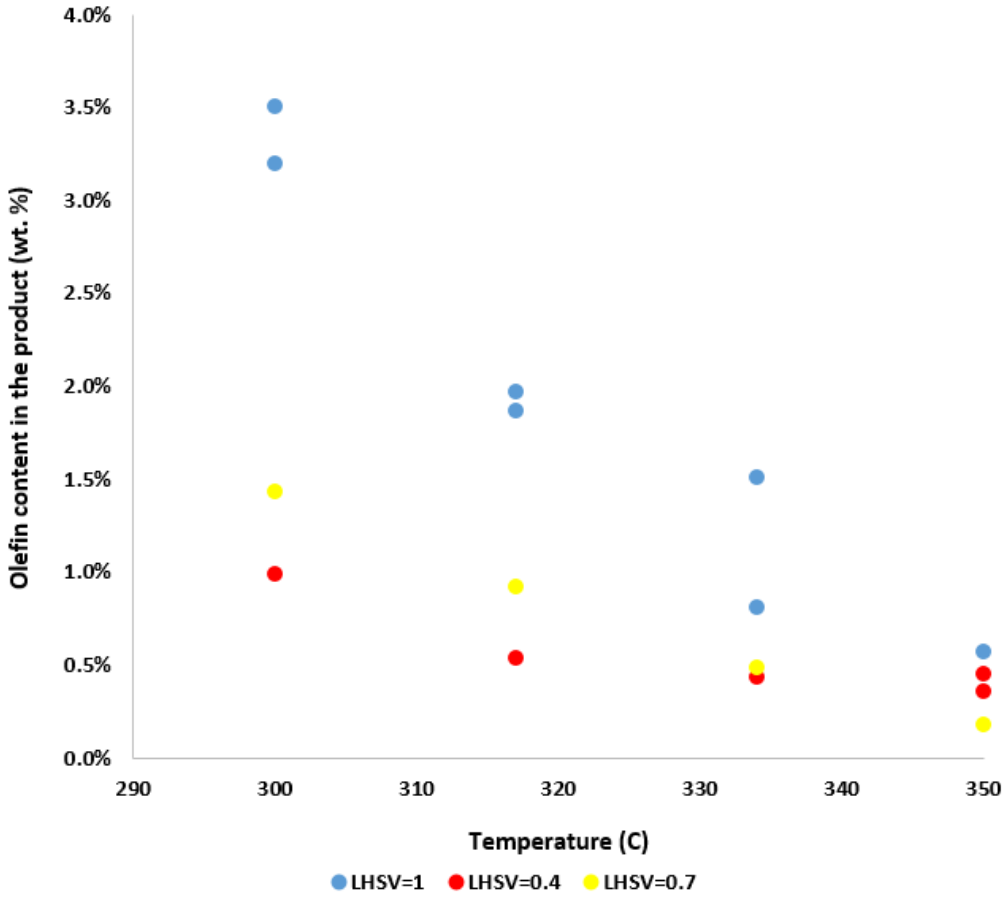

Figure 41 Total olefin content in the hydrotreated product as a function of temperature at 90 bar [1]

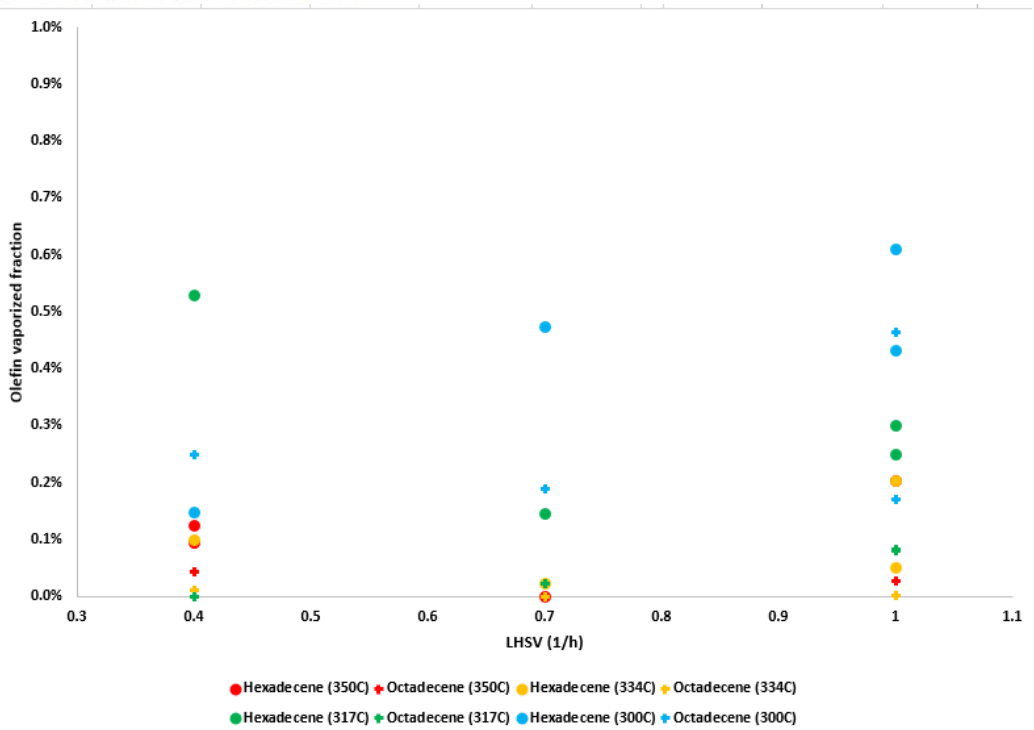

Figure 42 Olefin vaporized fraction with respect to the olefin feed flow as a function of LHSV

4.2.4 Quinoline hydrodenitrogenation

Experimental conversions of quinoline and the conversions of the respective products respective to quinoline are calculated making the same assumptions as in section 4.2.3. In Eq. 48 it is shown the calculation for quinoline conversion and in Eq. 49 for the products.

$$X_Q = \frac{L_{F,Q} - L_{P1,Q} - L_{P2,Q}}{L_{F,Q} - L_{P2,Q}} \quad 48$$

$$X_i = \frac{L_{P1,i} + L_{P2,i}}{L_{F,Q} - L_{P2,Q}} \quad 49$$

The experimental selectivity of the products of the decomposition of Quinoline are calculated according to Eq. 50. Where S_i is the selectivity with reference to Quinoline, $L_{P1,i}$ is the molar flow of compound i in the liquid product. $L_{F,Q}$ is the molar flow of Quinoline in the liquid feed, $L_{P1,Q}$ is the unreacted Quinoline in the liquid product and $L_{P2,Q}$ is the unreacted Quinoline in the condensed gas product.

$$S_i = \frac{L_{P1,i} + L_{P2,i}}{L_{F,Q} - L_{P1,Q} - L_{P2,Q}} \quad 50$$

Experimental production rates/rate of disappearance of quinoline and the respective products R_i, is calculated by dividing the conversion X_i by the space time. Due to the assumption made for the calculation of the conversion space time is defined as the mass of the catalyst W divided by the molar flow rate that is in contact with the catalyst [88]. Consequently, the experimental production rates R_i are calculated according to Eq. 51.

$$R_i = \frac{X_i}{\frac{W}{L_{F,Q} - L_{P2,Q}}} \quad 51$$

Nitrogen conversion was calculated based on the fact that 1 mole produced of the hydrocarbon products of quinolone HDN produce 1 mole of ammonia. Hence, the total moles of produced hydrocarbons are equal to the total moles of NH_3 produced. Consequently, the total amount of nitrogen in the products is known. As a result, nitrogen conversion is calculated according to Eq. 52.

$$X_N = \frac{N_{in} - N_{out}}{N_{in}} \quad 52$$

Where N_{in} is the total nitrogen in the feed and N_{out} is the total nitrogen in the product.

On Table 9 can be found the quinoline as well as product conversions and their respective selectivities at a LHSV of 1 h^{-1}. These results are also shown graphically on Figure 43 and Figure 44 for better illustration.

Table 9 Quinoline hydrodenitrogenation conversions and product selectivities at LHSV=1 h^{-1}

	CONVERSION				SELECTIVITY			
COMPOUND	**300°C**	**317°C**	**334°C**	**350°C**	**300°C**	**317°C**	**334°C**	**350°C**
QUINOLINE	95.1%	96.2%	95.6%	95.6%	-	-	-	-
14THQ	89.2%	85.7%	81.1%	72.9%	93.9%	89.0%	84.9%	76.2%
OPA	1.9%	3.2%	4.1%	6.1%	2.0%	3.3%	4.3%	6.4%
58THQ	0.2%	0.3%	1.1%	2.3%	0.2%	0.3%	1.2%	2.4%
DHQ	0.4%	0.7%	1.0%	1.6%	0.5%	0.7%	1.1%	1.6%
PCHA	2.3%	4.2%	6.1%	7.7%	2.5%	4.4%	6.4%	8.0%
PCH	0.1%	0.4%	1.2%	3.5%	0.1%	0.5%	1.3%	3.6%
PB	0.2%	0.3%	0.6%	1.3%	0.2%	0.4%	0.7%	1.4%
PCHE	0.0%	0.0%	0.0%	0.0%	0.0%	0.0%	0.0%	0.0%

Table 10 Quinoline hydrodenitrogenation conversions and product selectivities at LHSV=0.7 h^{-1}

	CONVERSION				SELECTIVITY			
COMPOUND	**300**	**317**	**334**	**350**	**300**	**317**	**334**	**350**
QUINOLINE	97.3%	96.3%	97.4%	97.5%	-	-	-	-
14THQ	84.4%	82.3%	77.8%	65.7%	86.74%	85.5%	79.8%	67.3%
OPA	7.1%	4.1%	6.0%	8.4%	7.30%	4.3%	6.1%	8.7%

58THQ	0.4%	0.2%	0.5%	1.7%	0.39%	0.2%	0.5%	1.8%
DHQ	0.6%	0.9%	1.2%	1.4%	0.57%	1.0%	1.2%	1.4%
PCHA	4.2%	6.4%	7.6%	8.5%	4.34%	6.7%	7.8%	8.7%
PCH	0.4%	1.0%	2.9%	10.4%	0.37%	1.1%	3.0%	10.7%
PB	0.2%	0.4%	0.9%	1.9%	0.24%	0.4%	0.9%	2.0%
PCHE	0.0%	0.0%	0.0%	0.0%	0.00%	0.0%	0.0%	0.0%

Quinoline conversion appears to be constant, varying between 95.1% and 96.2% conversion independent of the temperature. These results are in agreement with the results given by the work of Luan et al. [58] shown in Figure 11 and similar results for quinoline conversion were obtained by Tu, et al [89] in a batch reactor at 350°C and 30 bar using a NiMo catalyst. Temperature seem to have a low influence on quinoline conversion as at temperature above the ones used in this work; conversions can be as high as 98% [58]. The effect of temperature on product selectivities is more pronounced than in quinolone conversion as shown in Figure 43 and Figure 44. While at a LHSV of 1 h^{-1} the principal product was 14THQ at the whole range of temperatures tested, the selectivity towards this product decreased from 93.9% at 300°C to 76.2% at 350°C. LHSV does not appear to have a strong effect on quinoline conversion as conversions varied between 95.1% and 97.9% at 0.4 h^{-1} and 0.7 h^{-1} but it does have a strong effect on 14THQ selectivity. At 0.4 h^{-1}, 14THQ selectivity decreased from 84.1% to 59.6%.

Table 11 Quinoline hydrodenitrogenation conversions and product selectivities at LHSV=0.4 h^{-1}

	CONVERSION				**SELECTIVITY**			
COMPOUND	**300**	**317**	**334**	**350**	**300**	**317**	**334**	**350**
QUINOLINE	97.9%	95.1%	97.9%	97.4%	-	-	-	-
14THQ	84.1%	76.0%	71.3%	59.6%	85.8%	79.9%	72.8%	61.2%
OPA	4.6%	5.7%	8.6%	9.7%	4.7%	6.0%	8.8%	10.0%
58THQ	0.2%	0.5%	0.6%	2.4%	0.2%	0.6%	0.6%	2.4%
DHQ	0.8%	0.9%	1.3%	1.8%	0.8%	0.9%	1.3%	1.9%
PCHA	5.5%	4.9%	7.1%	9.0%	5.7%	5.2%	7.3%	9.2%
PCH	2.2%	5.3%	6.8%	10.7%	2.2%	5.5%	7.0%	10.9%
PB	1.0%	1.2%	2.6%	3.9%	1.0%	1.2%	2.6%	4.0%
PCHE	0.0%	0.0%	0.0%	0.0%	0.0%	0.0%	0.0%	0.0%

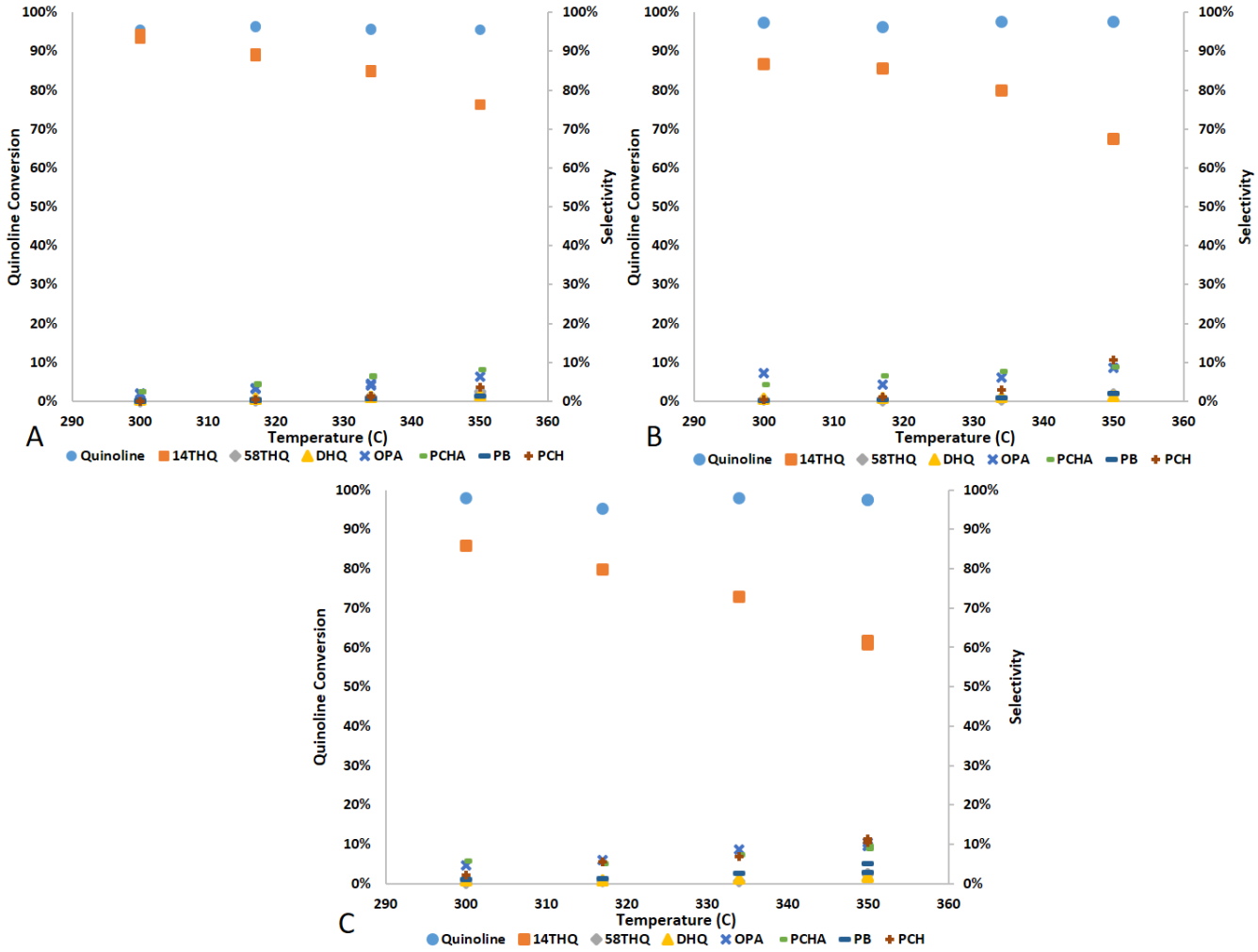

Figure 43 Quinoline conversion and product selectivity as a function of temperature. 14THQ=1,2,3,4 tetrahydroquinoline, 58THQ= 5,6,7,8 tetrahydroquinoline, OPA=orto-propylaniline, DHQ=decahydroquinoline, PCHA= propyl-cyclohexylamine, PB=propylbenzene, PCHE=propylcyclohexene, PCH=propylcyclohexane. A: LHSV=1, B: LHSV=0.7, C: LHSV=0.4

Other major products were OPA and PCHA in which the selectivities increased from 1.9% and 2.3% at 300°C to 6.4% and 8.0% at 350°C respectively. As the LHSV decreased, the selectivity towards these intermediates increased to 10.0% and 10.9% at 350°C and 0.4 h^{-1}. Minor intermediate products were 58THQ and DHQ whose selectivities increased from 0.2% and 0.4% at 300°C to 2.4% and 1.6% at 350°C respectively. LHSV doesn't have a strong effect on the selectivity of those minor intermediates. The detected denitrogenated products were PCH and PB with selectivities that increased from 0.1% and 0.2% at 300°C to 3.6% and 1.4% at 350°C respectively. LHSV does have a strong effect on PCH and PB selectivities. At 0.4 h^{-1} there was an increase from 2.2% and 1.0% at 300°C to 10.9% and 4.0% at 350°C. PCHE was not detected in none of the experimental runs. It is possible that PCHE was eluting at the same retention time as PB or that it is easily hydrogenated into PCH. The results show that 14THQ is the main product of quinoline HDN, this is in accord with the results of Tian, et al. [60], Luan, et al. [58], Nguyen, et al. [56] and Tu, et al. [89]. Since quinoline conversion is independent of temperature at the

tested temperature range, it can be deduced that it is easily hydrogenated into 14THQ while hydrogenation of 14THQ is a more difficult reaction. The hydrogenation of the hetero-cyclic aromatic ring is the prefer path towards quinoline HDN as the production 58THQ is much lower than that of 14THQ. Once 14THQ is produced, the HDN can take two different pathways. One pathway (PW1) is the subsequent hydrogenation of the benzene ring to form DHQ which then undergoes ring opening through C_{sp3}-N cleavage to form PCHA. Finally, the C-N is broken to form PCH releasing NH_3. The other pathway (PW2) according to the results is the direct hydrogenolysis of 14THQ to form OPA which is then either hydrogenated into PCHA or it can go into direct C_{sp2}-N bond cleavage to form PB releasing NH_3. According to the selectivity analysis as a function of temperature, PW1 is the prefer path towards quinoline HDN as the temperature increases. The PCH to PB ratio increases from 0.43 at 300°C to 2.60 at 350°C a 1 h^{-1}. LHSV does not increases the PHC to PB ratio which is an indication that as the temperature increases PW2 is favoured over PW1. Due to the high production of 14THQ, it can be deduced that the slowest steps from PW1 and PW2 are the benzene ring hydrogenation to DHQ and the direct hydrogenolysis to OPA respectively. DHQ and PCH shows lower selectivities than PCHA which means that ring opening is faster step than C-N cleavage however, DHQ is also being consumed in the equilibrium reaction with 58THQ as shown by the increase in selectivity of 58THQ. Since quinoline conversion is not changing with temperature, it means that the other only possible pathway towards 58THQ formation is that as temperature increases the equilibrium shifts to the left and hence 58THQ is formed. OPA selectivity is lower is than PCHA selectivity which means that either ring opening of 14THQ is more difficult than the benzene ring hydrogenation or that as temperature increases more OPA is being consumed towards PCHA.

Despite the high quinoline conversion, the total nitrogen conversion is low as shown in Figure 44. However, temperature have a strong effect on nitrogen conversion. There is an exponential increase from 0.25% at 300°C to 4.8% at 350°C at a LHSV of 1 h^{-1}. These results are much lower than those presented by Luan, et al. [58]. According to the authors, at a space time of 1.12 min which means a LHSV of 0.018 h^{-1}, at 350°C there is a nitrogen conversion of around 70%. It worth noticing that the strong effect of temperature is also evidenced. Yet, the operating conditions and the catalyst (NiW) were different. Ferdous, et al. [67] hydrotreated a heavy gas oil containing 0.3% nitrogen at operating conditions similar to the ones tested in this work. At 356°C, 94 bar and a LHSV of 0.8 h^{-1}, they obtained a 49.3% nitrogen conversion which is a value much higher than the one obtained at similar conditions in this work. While the operating conditions were similar, the catalyst used was a NiMoB catalyst and the feed was a complex mixture which does not contains olefins. As a result, the feed contains a mixture of basic and non-basic nitrogen containing hetero-compounds. As explained in the selectivity

analysis, HDN follows sequential hydrogenation, ring opening and denitrogenation. As a consequence, the presence of olefins in the feed may affect the hydrogenation of the intermediate HDN products due to competitive effects and/or hydrogen availability. Since hydrogenation of the benzene ring of a heterocyclic compound is a fundamental pathway for nitrogen removal, olefin presence may inhibit this step and consequently decreasing the total nitrogen conversion but no experiments without the presence of olefins was performed, as a result it is only a hypothesis that needs to be tested. The highest obtained nitrogen conversion was 15% at 350°C and 0.4 h^{-1}. Hence, no deep hydrodenitrogenation was achieved at the tested operating conditions. Since the Rob2 reactor has an upper limit of 350°C, the possibility to achieve higher nitrogen conversions would be to lower the LHSV to values which are not relevant industrially related. The quinoline vaporized fraction follows the same behaviour as the vaporized fractions of hexadecene and octadecene.

From the experimental results it can be deduced that the quinoline hydrodenitrogenation follows sequential hydrogenation, ring opening and denitrogenation reactions. The hydrogenation of quinoline towards 14THQ appears to be limited by equilibrium as the quinoline conversion was independent of the temperature and LHSV. However, the equilibrium is heavily shifted to the production of 14THQ. As the temperature increases, the ring opening of the fully hydrogenated intermediate (DHQ) becomes favoured over the direct hydrogenolisis of OPA and as a consequence the denitrogenation of PCHA becomes the favoured path towards quinoline hydrodenitrogenation.

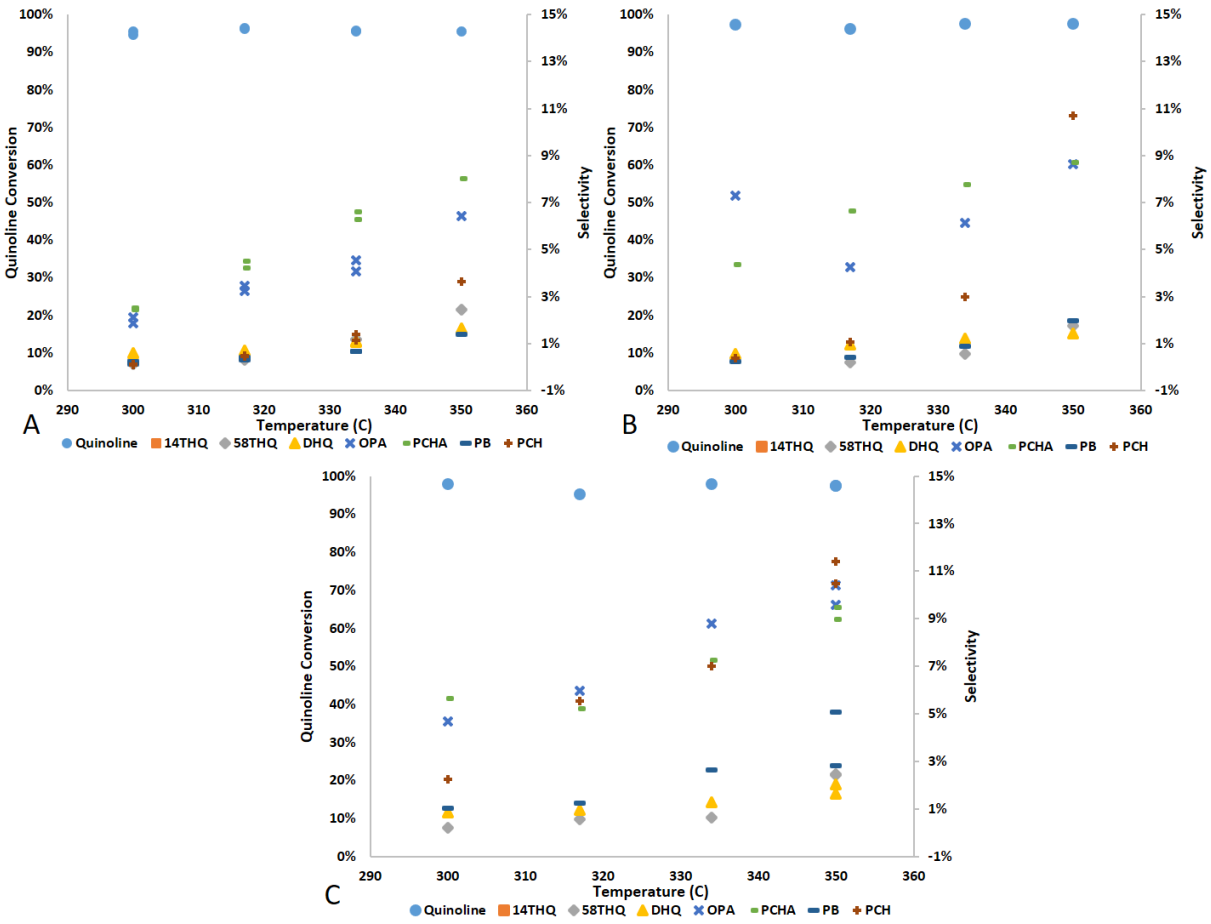

Figure 44 Quinoline conversion and close up of minor products selectivity as a function of temperature. 14THQ=1,2,3,4 tetrahydroquinoline, 58THQ= 5,6,7,8 tetrahydroquinoline, OPA=orto-propylaniline, DHQ=decahydroquinoline, PCHA= propyl-cyclohexylamine, PB=propylbenzene. A: LHSV=1, B: LHSV=0.7, C: LHSV=0.4

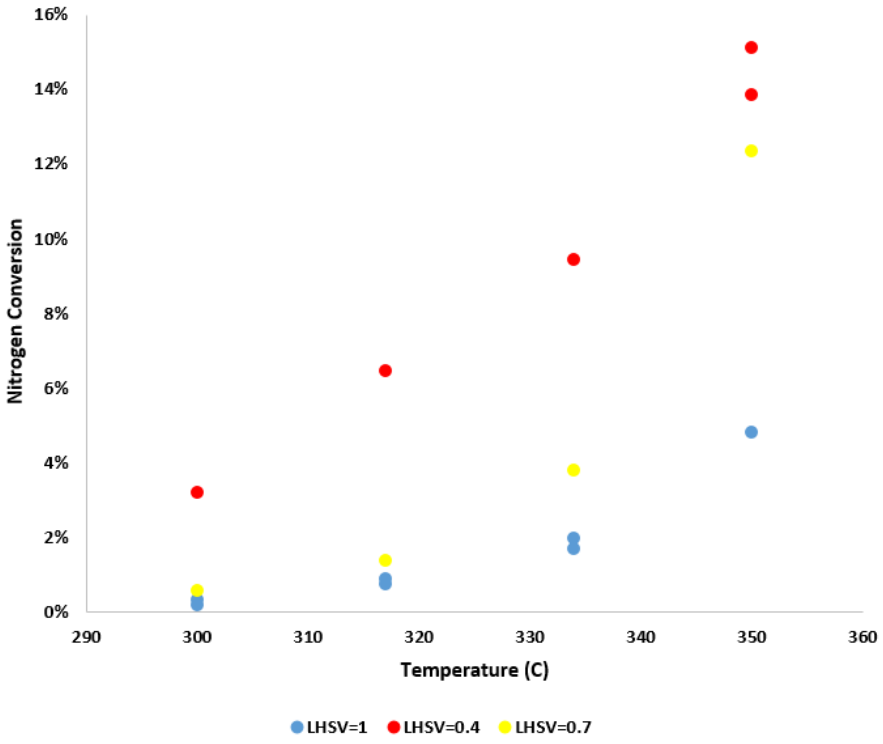

Figure 45 Nitrogen conversion as function of temperature

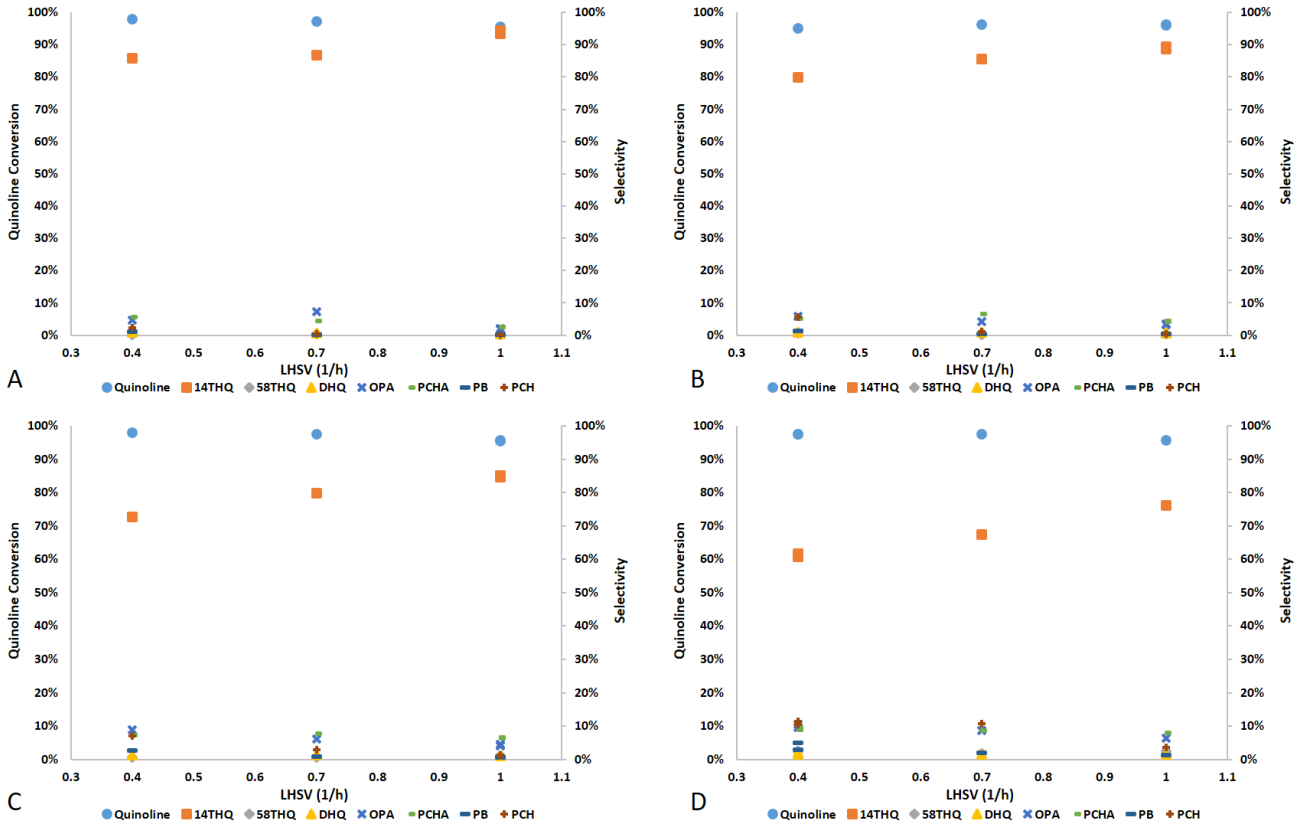

Figure 46 Quinoline conversion and products selectivity as a function of LHSV. 14THQ=1,2,3,4 tetrahydroquinoline, 58THQ= 5,6,7,8 tetrahydroquinoline, OPA=orto-propylaniline, DHQ=decahydroquinoline, PCHA= propyl-cyclohexylamine, PB=propylbenzene.A: T=300°C. B: T=317°C. C: T=334°C. D: T=350°C

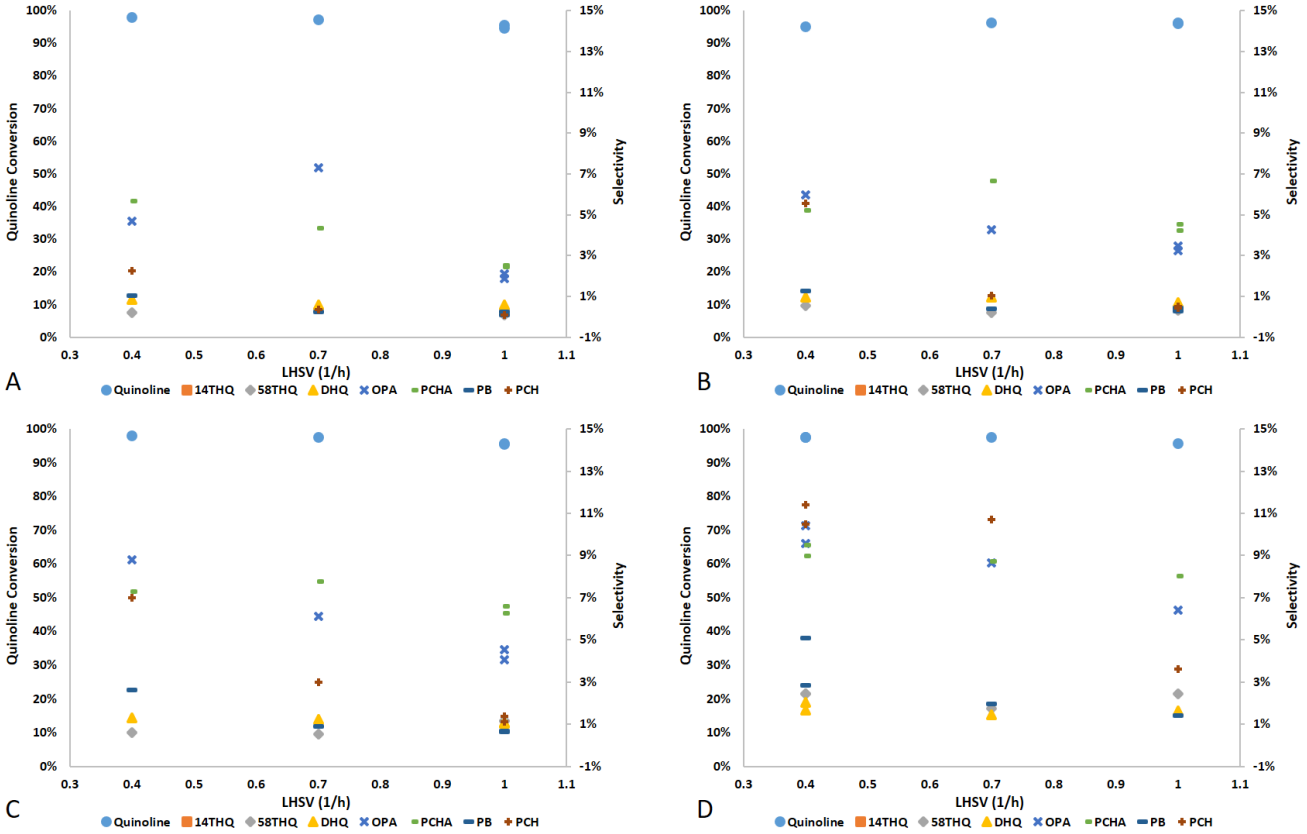

Figure 47 Quinoline conversion and close up of minor products selectivity as a function of LHSV. 14THQ=1,2,3,4 tetrahydroquinoline, 58THQ= 5,6,7,8 tetrahydroquinoline, OPA=orto-propylaniline, DHQ=decahydroquinoline, PCHA= propyl-cyclohexylamine, PB=propylbenzene. A: T=300°C. B: T=317°C. C: T=334°C. D: T=350°C

4.3 Kinetic models

4.3.1 Olefin hydrogenation kinetic models

Three different kinetic models for the olefin hydrogenation were proposed. All of them are based on the studies of Thybaut, et al. [77] and Mattson, et al. [76]. As both of these studies are based on the Horiuti-Polanyi mechanism the difference between the proposed models are on the assumptions made. The proposed reaction mechanism for the first kinetic model on olefin hydrogenation (OHKM1) is shown in Eq. 53-57. The assumptions made on this reaction mechanism are as follow:

1.1 H_2 dissociative chemisorption and olefin reactant chemisorb at identical sites (competitive chemisorption)

2.1 First hydrogenation step (Eq. 55) is the rate-limiting step and irreversible

3.1 Other surface reactions are at a quasi-equilibrated state

4.1 Alkane desorption is very fast, chemisorbed species coverage is negligible

$$C_{H_2} + 2\Theta \rightleftharpoons 2\Theta_H \qquad K_{H_2} \qquad 53$$

$$C_O + \Theta \rightleftharpoons \Theta_O \qquad K_O \qquad 54$$

$$\Theta_O + \Theta_H \rightarrow \Theta_{OH} + \Theta \qquad k_1 \qquad 55$$

$$\Theta_{OH} + \Theta_H \rightleftharpoons \Theta_{OH_2} + \Theta \qquad K_{OH} \qquad 56$$

$$\Theta_{OH_2} \rightleftharpoons C_{OH_2} + \Theta \qquad \frac{1}{K_{OH_2}} \qquad 57$$

Where C_{H2}, C_O, and C_{OH2} are the liquid phase concentrations of hydrogen, olefin and alkane (hydrogenated olefin) respectively. Θ, Θ_H, Θ_O, Θ_{OH} and Θ_{OH2} are the fractional coverage of the free active sites, chemisorbed hydrogen, chemisorbed olefin, chemisorbed mono-hydrogenated olefin and chemisorbed di-hydrogenated olefin respectively. K_{HH2}, K_O and K_{OH} are the adsorption constants of hydrogen, olefin and mono-hydrogenated olefin. K_{OH2} is the desorption constant of the di-hydrogenated olefin and k_1 is the rate constant.

By considering assumption 2.1 the reaction rate is defined in Eq. 58.

$$r_{OHKM1} = k_1 \Theta_O \Theta_H \qquad 58$$

The adsorption equilibrium constants are defined according to assumption 3.1 and are shown in Eq. 59-62.

$$K_{H_2} = \frac{{\Theta_H}^2}{C_{H_2} \Theta^2} \qquad 59$$

$$K_O = \frac{\Theta_O}{C_O \Theta} \qquad 60$$

$$K_{OH} = \frac{\Theta_{OH_2} \Theta}{\Theta_{OH} \Theta_H} \qquad 61$$

$$K_{OH_2} = \frac{\Theta_{OH_2}}{C_{OH_2} \Theta} \qquad 62$$

The total site balance is defined in Eq. 63 according to assumption 4.1.

$$\Theta_T = \Theta + \Theta_O + \Theta_H + \Theta_{OH} \qquad 63$$

Eq. 59-63 form a system of equation of 5 equations with 5 variables. By solving this system for Θ, an expression for the free sites in terms of measurable variables is obtained as shown in Eq. 64.

$$\Theta = \frac{\Theta_T K_{OH}\sqrt{K_{H_2}\mathrm{C_{H_2}}}}{K_O\mathrm{C_O}K_{OH}\sqrt{K_{H_2}\mathrm{C_{H_2}}} + K_{H_2}\mathrm{C_{H_2}}K_{OH} + K_{OH}\sqrt{K_{H_2}\mathrm{C_{H_2}}} + \mathrm{C_{OH_2}}K_{OH_2}} \quad 64$$

By replacing Eq.59, 60 and 61 in Eq. 46 the final expression for the reaction rate of OHKM1 is defined in Eq. 65.

$$r_{OHKM1} = \frac{k_1\sqrt{C_{H_2}K_{H_2}}{\Theta_T}^2 {K_{OH_2}}^2 C_{H_2}K_{H_2}K_O C_O}{\left(K_{OH}(C_O K_O + 1)\sqrt{C_{H_2}K_{H_2}} + C_{H_2}K_{H_2}K_{OH} + K_{OH_2}C_{OH_2}\right)^2} \quad 65$$

The second kinetic model for hydrogenation of olefins (OHKM2) is a variation of OHKM1. Assumption 2.1 changes from the first hydrogenation step (Eq. 55) being the rate-limiting step to the second hydrogenation step (Eq. 56) being the rate-limiting step. This assumption is now numbered 2.2. Consequently, the new rate constant and the new equilibrium constant of the mono-hydrogenated olefin (K_{OH}) are defined as shown in Eq. 66-67.

$$r_{OHKM2} = k_1\Theta_{\mathrm{OH}}\Theta_{\mathrm{H}} \quad 66$$

$$K_{OH} = \frac{\Theta_{\mathrm{OH}}\Theta}{\Theta_{\mathrm{O}}\Theta_{\mathrm{H}}} \quad 67$$

A new system of 5x5 is obtained between Eq. 59, 60, 67, 63 and 63. By solving for Θ, the expression of the free sites in OHKM2 is defined in Eq. 68.

$$\Theta = \frac{\Theta_T K_{OH}\sqrt{K_{H_2}\mathrm{C_{H_2}}}}{K_O\mathrm{C_O}K_{OH}\sqrt{K_{H_2}\mathrm{C_{H_2}}} + K_O\mathrm{C_O} + \sqrt{K_{H_2}\mathrm{C_{H_2}}} + 1} \quad 68$$

The final expression of the reaction rate of OHKM2 is then defined by replacing Eq. 59, 61 and 68 in Eq. 67 and is shown in Eq. 69.

$$r_{OHKM2} = \frac{\mathrm{k_1}K_{H_2}\mathrm{C_{H_2}}{\Theta_T}^2 K_O\mathrm{C_O}K_{OH}}{\left(K_O\mathrm{C_O}K_{OH}\sqrt{K_{H_2}\mathrm{C_{H_2}}} + K_O\mathrm{C_O} + \sqrt{K_{H_2}\mathrm{C_{H_2}}} + 1\right)^2} \quad 69$$

The third model OHKM3 takes different assumptions into consideration which are as follow:

1.3 H_2 dissociative chemisorption and olefin reactant chemisorb at identical sites (competitive chemisorption) and quasi-equilibrated.

2.3 Desorption of the alkane product (di-hydrogenated olefin) is fast and irreversible

3.3 Hydrogenated chemisorbed species are in quasi-stationary

4.3 No rate-limiting step

Consequently, the reaction mechanism is different from the one shown for models OHKM1 and OHKM2. The mechanism is shown in Eq. 70-74.

$$\mathrm{C_{H_2}} + 2\Theta \rightleftharpoons 2\Theta_{\mathrm{H}} \qquad K_{H_2} \quad 70$$

$$C_O + \Theta \rightleftharpoons \Theta_O \qquad K_O \qquad 71$$

$$\Theta_O + \Theta_H \rightleftharpoons \Theta_{OH} + \Theta \qquad K_1 \qquad 72$$

$$\Theta_{OH} + \Theta_H \rightleftharpoons \Theta_{OH_2} + \Theta \qquad K_2 \qquad 73$$

$$\Theta_{OH_2} \rightarrow C_{OH_2} + \Theta \qquad 74$$

Since the chemisorbed hydrogenated species are not assumed to be in quasi-equilibrium but in quasi-stationary state, the parameter defining Eq. 72-73 are not adsorption constant but equilibrium constants K_1 and K_2 respectively. For definite values of K_1 and K_2 the equilibrium is shifted to the right [77] and considering assumption 2.3 the rate constant becomes Eq. 75.

$$r_{OHKM3} = k_2 \Theta_{OH} \Theta_H \qquad 75$$

Where k_2 is the rate constant of Eq. 74. The adsorption constant of hydrogen and the olefin reactant are already defined in Eq. 59-60. The balance for the chemisorbed hydrogenated species are defined in Eq. 76-77 according to assumption 3.3.

$$k_1 \Theta_O \Theta_H + \frac{k_2 \Theta_{OH_2} \Theta}{K_2} - \frac{k_1 \Theta_{OH} \Theta}{K_1} - k_1 \Theta_{OH} \Theta_H = 0 \qquad 76$$

$$k_2 \Theta_{OH} \Theta_H - \frac{k_2 \Theta_{OH_2} \Theta}{K_2} = 0 \qquad 77$$

By solving Eq. 59-60 for Θ_H and Θ_O and replacing them in Eq. 76-77, the balances of the hydrogenated species are expressed in a system of two equations and two variables. By solving this system for the chemisorbed hydrogenated; these are left in terms of measurable variables and the free sites Θ as shown in Eq. 78-79.

$$\Theta_{OH} = \sqrt{K_{H_2} C_{H_2}} \Theta C_O K_1 K_O \qquad 78$$

$$\Theta_{OH_2} = K_{H_2} C_{H_2} K_2 \Theta C_O K_1 K_O \qquad 79$$

The total site balance must now include the coverage of the di-hydrogenated chemisorbed olefin because of assumption 3.3, hence the total site balance is expressed in Eq. 80.

$$\Theta_T = \Theta + \Theta_O + \Theta_H + \Theta_{OH} + \Theta_{OH_2} \qquad 80$$

By replacing Eq. 59, 60, 78 and 79 into Eq. 80 an expression for the free sites is obtained as shown in Eq. 81.

$$\Theta = \frac{\Theta_T}{C_O C_{H_2} K_1 K_2 K_O K_{OH} K_{H_2} + \sqrt{K_{H_2} C_{H_2}} C_O K_1 K_O + C_O K_O + \sqrt{K_{H_2} C_{H_2}} + 1} \quad 81$$

Finally, replacing Eq. 59, 60 and 80 into 75 a final expression for OHKM3 is obtained as shown in Eq. 82.

$$r_{OHKM3} = \frac{k_2 C_{H_2} K_{H_2} \Theta_T{}^2 C_O K_1 K_O}{\left(C_O C_{H_2} K_1 K_2 K_O K_{OH} K_{H_2} + \sqrt{K_{H_2} C_{H_2}} C_O K_1 K_O + C_O K_O + \sqrt{K_{H_2} C_{H_2}} + 1\right)^2} \quad 82$$

4.3.2 Quinoline HDN kinetic model

A kinetic model for the quinoline HDN is proposed based on the reaction scheme shown in Figure 44. This proposed reaction scheme was based on the experimental results shown in section 4.2.4. The assumptions made for this model are based on the work of Nguyen, et al. [56] described in section 2.2.2.1.3 but some differences are made. The assumptions made for this model are as follow:

- Coverages of H_2S and NH_3 are negligible
- Same active site for hydrogenation and C-N cleavage
- Surface reactions are rate limiting steps
- Competitive adsorption between H_2, N-heterocompounds and hydrocarbons
- No consideration on solvent adsorption
- Generalized Langmuir-Hinshelwood formalism to express the coverage of the relevant species

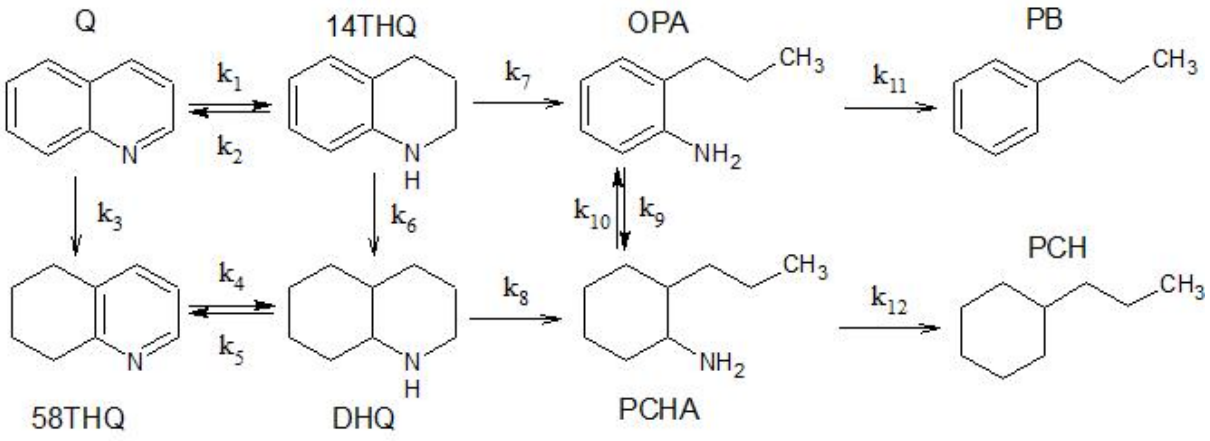

Figure 48 Proposed Quinoline HDN reaction scheme based on the experimental results

The production rates of the compounds according to the scheme shown in Figure 44 are listed in Eq. 83-90

$$R_Q = r_2 - r_1 - r_3 \quad (83)$$

$$R_{14THQ} = r_1 - r_2 - r_6 - r_7 \quad (84)$$

$$R_{58THQ} = r_3 + r_5 - r_4 \quad (85)$$

$$R_{OPA} = r_7 + r_{10} - r_9 - r_{11} \quad (86)$$

$$R_{DHQ} = r_4 + r_6 - r_5 - r_8 \quad (87)$$

$$R_{PCHA} = r_8 + r_9 - r_{10} - r_{12} \quad (88)$$

$$R_{PB} = r_{11} \quad (89)$$

$$R_{PCH} = r_{12} \quad (90)$$

By replacing the definition of the reaction rates r_i defined in Eq.16 into the production rates then become Eq. 91-98.

$$R_Q = \frac{K_{H_2}C_{H_2}(K_Q(k_1+k_3)C_Q - C_{14THQ}K_{14THQ}k_2}{\left(C_{DHQ}K_{DHQ} + C_{OPA}K_{OPA} + C_{PB}K_{PB} + C_{PCH}K_{PCH} + C_{PCHA}K_{PCHA} + C_QK_Q + K_{H_2}C_{H_2} + C_{14THQ}K_{14THQ} + C_{58THQ}K_{58THQ} + 1\right)^2} \quad (91)$$

$$R_{14THQ} = \frac{K_{H_2}C_{H_2}(-K_{14THQ}(k_2+k_6+k_7)C_{14THQ} + K_QC_Qk_1)}{\left(C_{DHQ}K_{DHQ} + C_{OPA}K_{OPA} + C_{PB}K_{PB} + C_{PCH}K_{PCH} + C_{PCHA}K_{PCHA} + C_QK_Q + K_{H_2}C_{H_2} + C_{14THQ}K_{14THQ} + C_{58THQ}K_{58THQ} + 1\right)^2} \quad (92)$$

$$R_{58THQ} = \frac{K_{H_2}C_{H_2}(C_{DHQ}K_{DHQ}k_5 + K_QC_Qk_3 - K_{58THQ}C_{58THQ}k_4)}{\left(C_{DHQ}K_{DHQ} + C_{OPA}K_{OPA} + C_{PB}K_{PB} + C_{PCH}K_{PCH} + C_{PCHA}K_{PCHA} + C_QK_Q + K_{H_2}C_{H_2} + C_{14THQ}K_{14THQ} + C_{58THQ}K_{58THQ} + 1\right)^2} \quad (93)$$

$$R_{OPA} = \frac{K_{H_2}C_{H_2}(K_{OPA}(k_9+k_{11})C_{OPA} - K_{PCHA}C_{PCHA}k_{10} - K_{14THQ}C_{14THQ}k_7)}{\left(C_{DHQ}K_{DHQ} + C_{OPA}K_{OPA} + C_{PB}K_{PB} + C_{PCH}K_{PCH} + C_{PCHA}K_{PCHA} + C_QK_Q + K_{H_2}C_{H_2} + C_{14THQ}K_{14THQ} + C_{58THQ}K_{58THQ} + 1\right)^2} \quad (94)$$

$$R_{DHQ} = \frac{K_{H_2}C_{H_2}(K_{DHQ}(k_5+k_8)C_{OPA} - K_{14THQ}C_{14THQ}k_6 - K_{58THQ}C_{58THQ}k_4)}{\left(C_{DHQ}K_{DHQ} + C_{OPA}K_{OPA} + C_{PB}K_{PB} + C_{PCH}K_{PCH} + C_{PCHA}K_{PCHA} + C_QK_Q + K_{H_2}C_{H_2} + C_{14THQ}K_{14THQ} + C_{58THQ}K_{58THQ} + 1\right)^2} \quad (95)$$

$$R_{PCHA} = \frac{K_{H_2}C_{H_2}(-K_{PCHA}(k_{10}+k_{12})C_{PCHA} - K_{OPA}C_{OPA}k_9 - K_{DHQ}C_{DHQ}k_8)}{\left(C_{DHQ}K_{DHQ} + C_{OPA}K_{OPA} + C_{PB}K_{PB} + C_{PCH}K_{PCH} + C_{PCHA}K_{PCHA} + C_QK_Q + K_{H_2}C_{H_2} + C_{14THQ}K_{14THQ} + C_{58THQ}K_{58THQ} + 1\right)^2} \quad (96)$$

$$R_{PB} = \frac{K_{H_2}C_{H_2}K_{OPA}C_{OPA}k_{11}}{\left(C_{DHQ}K_{DHQ} + C_{OPA}K_{OPA} + C_{PB}K_{PB} + C_{PCH}K_{PCH} + C_{PCHA}K_{PCHA} + C_QK_Q + K_{H_2}C_{H_2} + C_{14THQ}K_{14THQ} + C_{58THQ}K_{58THQ} + 1\right)^2} \quad (97)$$

$$R_{PCH} = \frac{K_{H_2} C_{H_2} K_{PCHA} C_{PCHA} k_{12}}{\left(C_{DHQ}K_{DHQ} + C_{OPA}K_{OPA} + C_{PB}K_{PB} + C_{PCH}K_{PCH} + C_{PCHA}K_{PCHA} + C_Q K_Q + K_{H_2}C_{H_2} + C_{14THQ}K_{14THQ} + C_{58THQ}K_{58THQ} + 1\right)^2} \quad 98$$

4.4 Parameter estimation

Athena visual studio was used to estimate the model parameters by minimizing the objective function shown in Eq. 99 employing a non-linear least square algorithm.

$$SSQ = \sum_{i=1}^{nob} \sum_{j=1}^{nresp} \left(R_{i,j} - \widehat{R_{i,J}}\right)^2 \rightarrow Min \quad 99$$

The parameters were assessed by their statistical and physical significance and The global significance of regression was confirmed by the resulting F- value, which is defined as the ratio of the sum of squares of the regression and the residual sum of squares, divided by their respective degrees of freedom, while the student t-test was used to assess the statistical significance of the individual parameters [84].

The reparametrization of the rate constants and adsorption constant were carried out according to Eq. 100-101 [88].

$$k = k_{Tm}\exp\left(-\frac{E_a}{R}\left(\frac{1}{T} - \frac{1}{T_m}\right)\right) \quad 100$$

$$A = A_{Tm}\exp\left(-\frac{\Delta H_a}{R}\left(\frac{1}{T} - \frac{1}{T_m}\right)\right) \quad 101$$

Where Tm is the average temperature of the whole temperature range in which the experiments were carried out. k_{Tm} is the value of the rate constant at Tm and Ea is the activation energy. A_{Tm} is the value of the adsorption constant at Tm and ΔHa is the adsorption enthalpy.

Since the kinetic models are in terms of concentrations which have units mol volume^{-1}, the molar flows at the outlet need to be converted in concentrations. As the volumetric flow at the surface of the wetted catalyst at a fixed molar flow depends on the operating conditions, density is needed to convert the molar flow in concentration. The density was estimated using Aspen plus. It was also assumed that the changes in composition due to the change in LHSV is negligible to the density. The densities at the different conditions are shown in Table 12.

Table 12 Product density estimated with Aspen plus

TEMPERATURE (°C)	DENSITY (KG M^{-3})

300	520
317	497
334	473
350	446

The concentrations of the compounds that could be detected in both liquid products do not present a problem as the molar flows are known. Concentration of the reactants was calculated including only the molar flow of L_{P1} while the concentrations of products was calculated including both L_{P1} and L_{P2}. Hydrogen concentration in the liquid phase was more difficult to determine as the molar flow cannot be detected in L_{P1} and L_{P2} and quantification via gas injections and measurements was not possible due to reasons already explained. As a result, it was decided to use the two film theory assuming that the reaction is much slower than the mass transfer so that the amount of any compound that reacts during its mass transfer is negligible [90]. Consequently, the concentration of hydrogen at the bulk C_B of the liquid phase can be calculated according to Eq. 102

$$N_i = k_{La}(C_I - C_B) \qquad 102$$

Where N_i is the molar flux through the film and it is assumed to be equal to the reacted hydrogen which can be estimated by stoichiometry of the reactants and products. k_{La} is the mass transfer coefficient and was taken from the literature as 0.013 s^{-1} [84]. The concentration at the interface C_I was estimated using henry coefficients H taken from the literature [91].

The total number of parameters according to the proposed kinetic models amounted to 58 which is a number too high for 16 experiments. The results of that parametrization were discarded as they had no statistical or physical significance. Consequently, a reduction of the number of parameters was done based on the following assumptions.

- Rate and adsorption constants of hexadecene and octadecene are equal
- Parametrization of olefin consumption rate was done with total olefin concentrations
- 14THQ, 58THQ and DHQ are lumped into one pseudo-compound called HYDROG
- OPA and PCHA are lumped into one pseudo-compound called RO
- PB and PCH are lumped into one pseudo-compound called HC
- Quinoline hydrodenitrogenation follows the reaction scheme shown in Figure 49
- The total H_2 concentration in the liquid phase is constant and equal to equilibrium

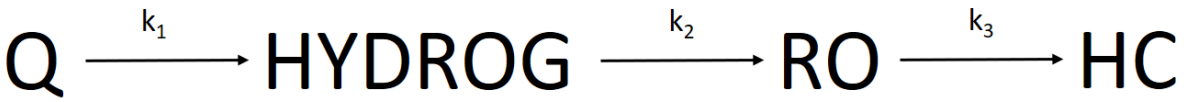

Figure 49 Simplified quinoline hydrodenitrogenation reaction scheme by lumping products

Consequently, the production/consumption rates of the quinoline hydrodenitrogenation are shown in Eq. 103-106.

$$R_Q = \frac{(K_Q(k_1)C_Q)}{\left(C_Q K_Q + C_{HYDROG} K_{HYDROG} + C_{RO} K_{RO} + C_{HC} K_{HC}\right)^2} \quad 103$$

$$R_{HYDROG} = \frac{(K_Q(k_1)C_Q - C_{HYDROG} K_{HYDROG} k_2)}{\left(C_Q K_Q + C_{HYDROG} K_{HYDROG} + C_{RO} K_{RO} + C_{HC} K_{HC}\right)^2} \quad 104$$

$$R_{HYDROG} = \frac{(C_{HYDROG} K_{HYDROG} k_2 - C_{RO} K_{RO} k_3)}{\left(C_Q K_Q + C_{HYDROG} K_{HYDROG} + C_{RO} K_{RO} + C_{HC} K_{HC}\right)^2} \quad 105$$

$$R_{HYDROG} = \frac{(C_{RO} K_{RO} k_3)}{\left(C_Q K_Q + C_{HYDROG} K_{HYDROG} + C_{RO} K_{RO} + C_{HC} K_{HC}\right)^2} \quad 106$$

The new total number of parameters is reduced to 24.

4.4.1 Olefin saturation parameter estimation results

The results of the parameter estimation for the two proposed model for olefin saturation are shown in Table 13. Activation energies for both models are around 20000 kmol kJ^{-1} with an estimated rate constant ktm at the average temperature Tm of 598.15K of 0.8 kmol m^{-3} h^{-1} and 4.1 kmol m^{-3} h^{-1} for OHKM1 and OHKM2 respectively however no t-value was estimated for ktm in both models. For OHKM2, only the Ea was statistically significant and the adsorption constant at Tm of the first hydrogenation step. OHKM1 estimated that the Ea, adsorption enthalpies of H_2, olefin, the chemisorbed alkane, the adsorption constants at Tm of hydrogen and olefin are statistically significant. Figure 6 shows the parity plots for OHKM1 (Top) and OHKM2 (Bottom). Neither of the models achieve an accurate prediction of the consumption rates of olefins. However, OKHM1 has a better performance than OHKM2 as evidenced by their F-values of 81 and 20 respectively but are low values for both models. The difficulty to predict the olefin consumption rate may be due to the low number of experiments and to the fact that the operating conditions achieved high conversions on all experiments preventing to observe the behavior of olefin conversion accurately.

Table 13 Olefin saturation parameter estimation results

	OHKM1			OHKM2		
Parameter	**Value**	**t-value**	**95% CI**	**Value**	**t-value**	**95% CI**
ktm (kmol kg_{cat}^{-1} h^{-1})	0.8	n.e.	n.e.	4.1	n.e.	n.e.
Ea (kmol kJ^{-1})	20420.6	34.4	10260.0	19464.8	47.6	409.3
AtmH_2 (m^3 $kmol^{-1}$)	367.7	n.e.	n.e.	1773.8	n.e.	n.e.
ΔH_2 (kmol kJ^{-1})	-369415.0	-2.7	1313.0	-943.5	n.e.	n.e.
AtmO (m^3 $kmol^{-1}$)	311.6	3.5	195.8	0.1	n.e.	n.e.
ΔHO (kmol kJ^{-1})	-39666.5	-2.5	17780.0	-36.5	n.e.	n.e.
AtmOH (m^3 $kmol^{-1}$)	53.0	n.e.	n.e.	134.7	5.5	134.7
ΔHOH (m^3 $kmol^{-1}$)	-28675.0	n.e.	n.e.	-29.1	n.e.	n.e.
AtmOH_2 (kmol m^{-3})	134.4	n.e.	n.e.	n.a.	n.a.	n.a.
ΔHOH_2 (m^3 $kmol^{-1}$)	-42106.5	-3.2	29190.0	n.a.	n.a.	n.a.

n.e.: not estimated, n.a.: not applicable

Figure 51 shows the residuals as a function of the two varied operating conditions, temperatures and LHSV. Temperature does show signs of systematic errors as the residuals are not randomly distributed. For both models, at 317°C the residuals are the lowest and are increased as the temperature increases. The reason for this is probably that at high temperatures the experimental results showed that the experimental conversions are less affected by temperature. Consequently, it is difficult to find an accurate behaviour of the consumption rate as a function of the temperature. Working at less severe conditions such as lower temperatures, lower pressures and higher LHSV might give better information for parameter estimation as conversions would be lower. LHSV also shows signs of systematic error as at LHSV of 1 h^{-1} the model tends to underestimate the consumption rate of olefins. That condition was the first to be tested and there were problems with the liquid pump. The flow of liquid feed to the reactor was highly unstable which might explain why at that LHSV there is a systematic error. By adjusting the PID parameters, a more stable flow was obtained for the other two LHSV tested. OHKM3 was not tested due to lack of time. But trying other models is also a way to eliminate systematic errors.

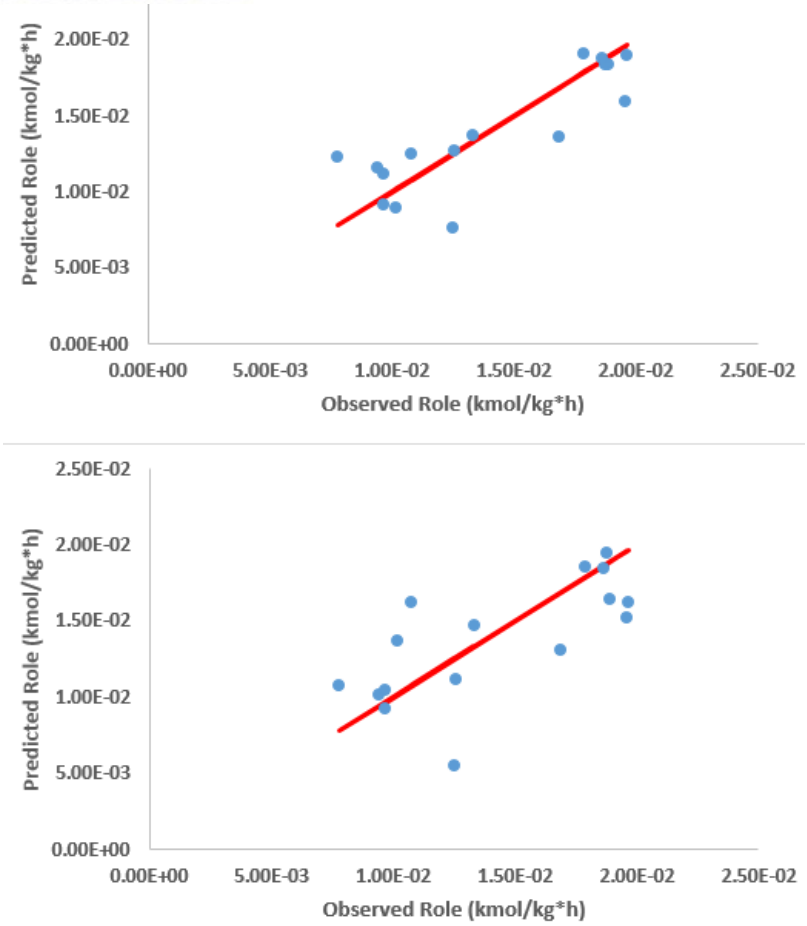

Figure 50 Parity plots for olefin saturation. Top: OHKM1, Bottom: OHKM2

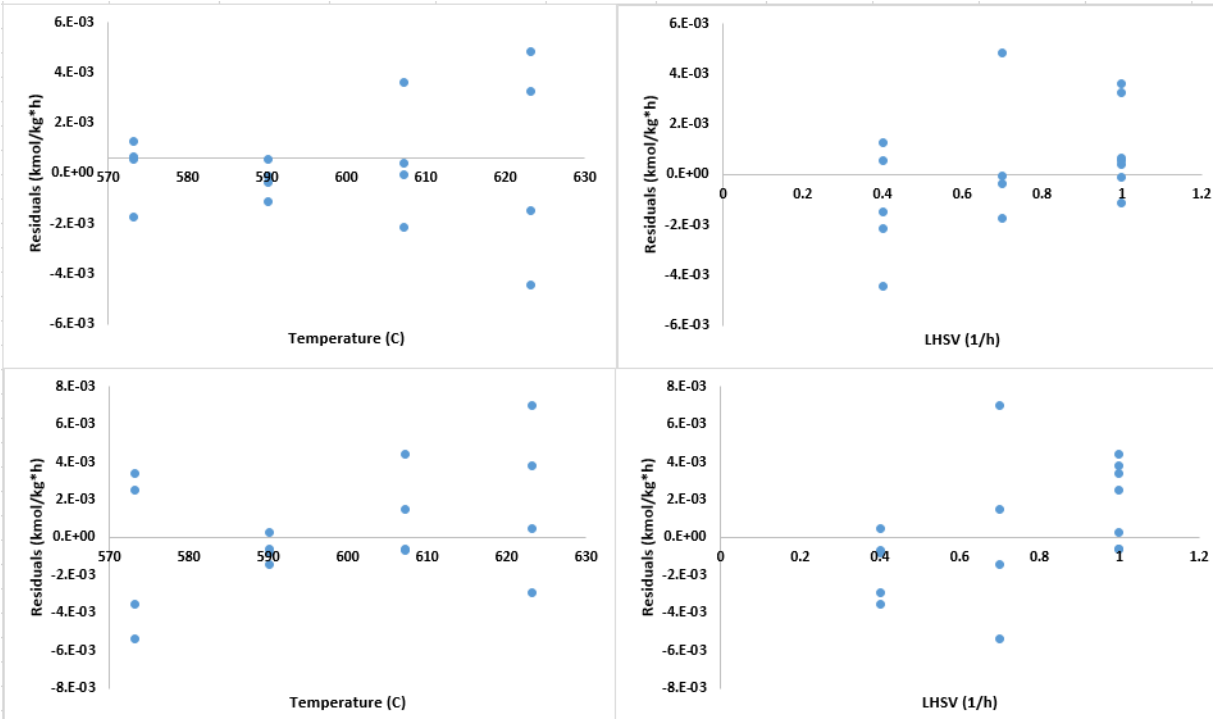

Figure 51 Residual analysis for olefin saturation. Top: OHKM1, Bottom: OHKM2

4.4.2 Quinoline hydrodenitrogenation parameter estimation results

Table 14 shows the parameter estimation for the quinoline hydrodenitrogenation model. No activation energy for quinoline hydrogenation was estimated. This was probably due to the fact that as shown in the experimental results, the quinoline conversion was constant independent of the temperature. The adsorption constant at Tm and adsorption enthalpy of quinoline was found to be not statistically significant as well as the adsorption enthalpy of the HYDROG pseudo-compounds. Activation energies from reaction 2 and 3 which are the ring opening of the HYDROG pseudo-compound and the denitrogenation reactions were found to be lower than the value presented by Nguyen, et al. [56]. The values of the rate constants are in the same order of magnitude however the values of the adsorption constants at Tm are 3 order of magnitude higher than those presented by Nguyen, et al [56] while the adsorption enthalpy of Q is 1 order of magnitude lower and the adsorption enthalpy of HYDROG was negligible. Adsorption enthalpies for RO and HC are in the same order of magnitude.

The parity plots (Figure 52) show that the model cannot predict accurately the consumption/production rates evidenced by a low F-value of 210. The low number of experiments, the limited operating conditions tested, experimental errors and the simplification made on the reaction scheme contribute to the failure of the model as evidenced by the residual analysis in Figure 53 and Figure 54 which show signs of systematic errors in the prediction of the production rates of RO and HC. More experiments at less and more severe conditions are needed in order to observe the accurate behaviour of quinoline consumption and hydrocarbon production as a function of temperature. Lumping the intermediates and final products into pseudo-compounds may also not had been the best way to reduce the number of parameters. Maybe by equalling reaction constants of similar reactions would have been a better strategy.

Table 14 Quinoline hydrodenitrogenation parameter estimation results

Parameter	Value	t-value	95% CI
ktm_1 (kmol kg_{cat}^{-1} h^{-1})	186.36	3.15	118.70
Ea_1 (kmol kJ^1)	0.00	n.e.	n.e.
ktm_2 (kmol kg_{cat}^{-1} h^{-1})	53.89	1.91	36.62
Ea_2 (kmol kJ^1)	51550.32	2.27	8118.00
ktm_3 (kmol kg_{cat}^{-1} h^{-1})	5.48	2.72	15.20
Ea_3 (kmol kJ^1)	92126.54	2.44	41590.00
Atm_Q (m^3 $kmol^{-1}$)	100000.00	n.e.	n.e.
ΔH_Q (kmol kJ^1)	-1345.75	n.e.	n.e.
Atm_{HYDROG} (m^3 $kmol^{-1}$)	1880.46	2.30	2901.00
ΔH_{HYDROG} (kmol kJ^1)	0.00	n.e.	n.e.
Atm_{RO} (m^3 $kmol^{-1}$)	26701.64	5.19	10320.00
ΔH_{RO} (kmol kJ^1)	-34678.36	-2.27	30630.00

Atm_{HC} (m^3 $kmol^{-1}$)	36306.15	3.46	21020.00
ΔH_{HC} (kmol kJ^{1})	-80256.40	-2.44	65960.00

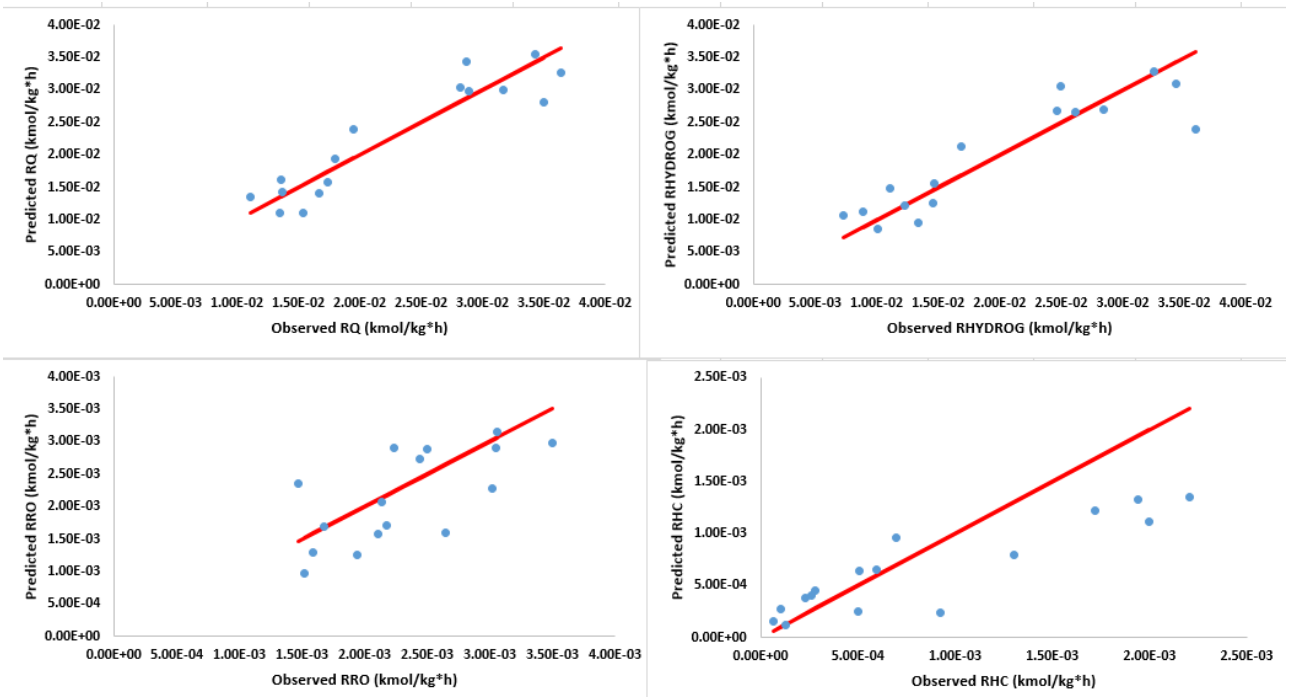

Figure 52 Parity plots for quinoline hydrodenitrogenation

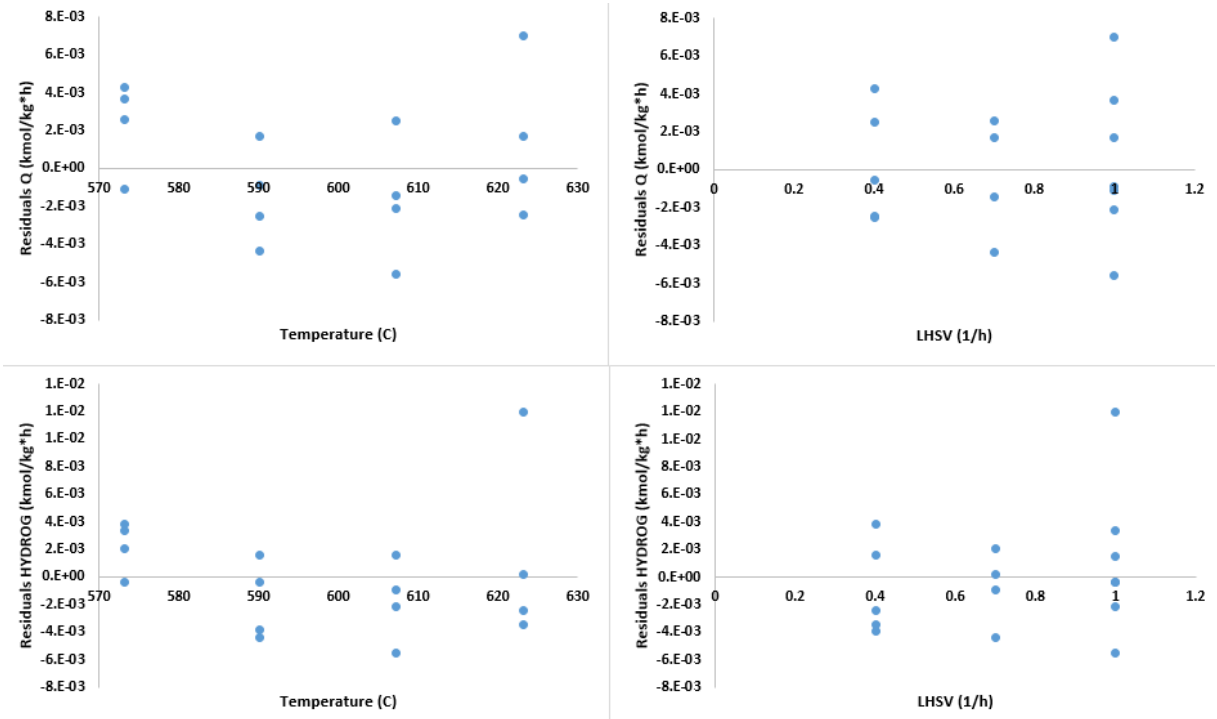

Figure 53 Residuals of Q and HYDROG as a function of temperature and LHSV

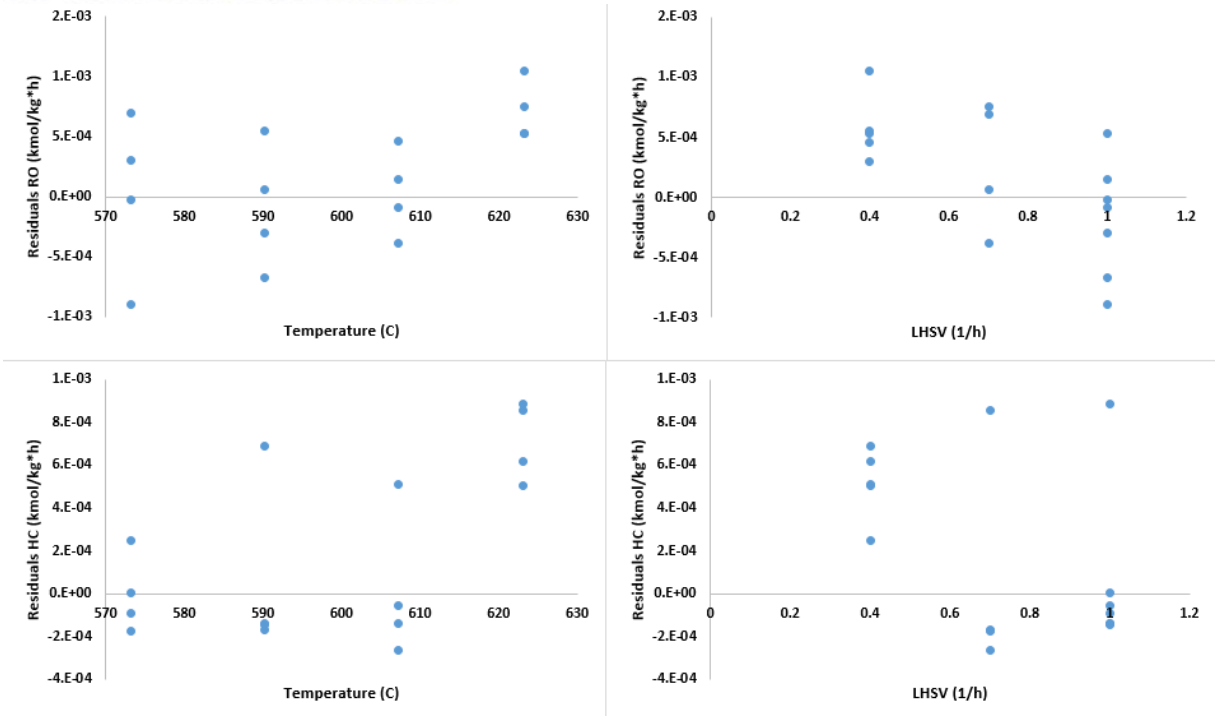

Figure 54 Residuals of RO and HC as a function of temperature and LHSV

5 Conclusion

At the tested operating conditions, high but not full olefin conversions were obtained. There was no difference between the conversions of the selected olefins. High temperatures and low LHSV favor the conversion of olefins. Deep hydrodenitrogenation was not successfully achieved. Conditions more severe than the limits of the set-up are needed or not industrially relevant LHSV as low LHSV and high temperature favors the denitrogenation process. However, from the experimental results can be concluded that the quinoline hydrodenitrogenation follows a sequential hydrogenation, ring opening and denitrogenation process. The most difficult reaction appears to be the ring opening of 14THQ. It is also suggested that the presence of olefins affects the hydrogenation and ring opening steps of the hydrodenitrogenation reactions as lower nitrogen conversions than those presented in the literature were obtained. However, experiments in the absence of olefins are needed to verify if the olefins hydrogenation does or does not affect the hydrodenitrogenation of quinoline. The results of the kinetic modelling, while not successful are inconclusive as there were too few experiments and too many parameters to be estimated at the limited operating conditions that were tested which prevented to reach a definite conclusion on the assumptions made. Conditions less severe are needed to understand correctly the behavior of olefins and quinoline conversion accurately. Conditions more severe are needed to understand the behavior of the quinoline hydrodenitrogenation minor intermediates. The experimental results showed that the more severe the conditions the production

of intermediates increases but as eventually they must be denitrogenated it means that the selectivity towards these intermediates should decrease at some point. All of this data was not integrated into the model as such experimental results were not obtained affecting the parameter estimation.

The experimental results are relevant to understanding the hydrotreating and hydrocracking of mixtures of VGO and PPO. Not negligible amounts of olefins and low nitrogen conversions are obtained at typical hydrotreating operating conditions. Consequently, feeding a mixture of VGO and PPO which was hydrotreated at typical operating conditions to a hydrocracking unit may have a negative effect on a standard hydrocracking process. It is important to keep researching on how mixing VGO with PPO affects hydrotreating at typical operating conditions. Unconventional nitrogen hetero-compounds such as nitriles are present in PPO, thus understanding the hydrodenitrigenation of nitriles is of relevance as well as oxygenated hetero-compounds which are not usually found in VGO. Model compounds offer a simpler way to understanding reaction mechanisms that can be used in simulation models. The effect of combined aromatic and olefin saturation must also be researched as well as combined with hydrodesulphurization and hydrodenitrogenation. Understanding these effects becomes a necessity in order to maximize to paraffin yield in the hydrocracking process as well as avoid catalyst deactivation.

6 References

[1] "Global plastic production 1950-2020," *Statista*. https://www.statista.com/statistics/282732/global-production-of-plastics-since-1950/ (accessed Oct. 25, 2021).
[2] "Publicaciones :: PlasticsEurope," *Plastic Europe*, 2019. https://www.plasticseurope.org/es/resources/publications/1804-plastics-facts-2019 (accessed Apr. 29, 2021).
[3] J. R. Jambeck *et al.*, "Plastic waste inputs from land into the ocean," *Science*, vol. 347, no. 6223, pp. 768–771, Feb. 2015, doi: 10.1126/science.1260352.
[4] O. Valerio, R. Muthuraj, and A. Codou, "Strategies for polymer to polymer recycling from waste: Current trends and opportunities for improving the circular economy of polymers in South America," *Current Opinion in Green and Sustainable Chemistry*, vol. 25, Jul. 2020, doi: 10.1016/j.cogsc.2020.100381.
[5] K. Ragaert, L. Delva, and K. Van Geem, "Mechanical and chemical recycling of solid plastic waste," *Waste Management*, vol. 69, pp. 24–58, Nov. 2017, doi: 10.1016/j.wasman.2017.07.044.
[6] UNEP, "Plastic Waste Background Report," UNEP, Basel, Feb. 2020.
[7] BASF, "Chemical recycling of plastic waste." https://www.basf.com/global/en/who-we-are/sustainability/we-drive-sustainable-solutions/circular-economy/mass-balance-approach/chemcycling.html (accessed Apr. 29, 2021).
[8] D. van der Hoeven, "Chemical recycling of mixed plastic waste," *Bio Based Press*, Dec. 07, 2019. https://www.biobasedpress.eu/2019/12/chemical-recycling-of-mixed-plastic-waste/ (accessed Apr. 29, 2021).
[9] C. Huang, A. Gujar, and M. Rodgers, "Methods of producing liquid hydrocarbon fuels from solid plastic wastes," US9200207B2, Dec. 01, 2015 Accessed: Apr. 29, 2021. [Online]. Available: https://patents.google.com/patent/US9200207B2/en
[10] T. Thiounn and R. C. Smith, "Advances and approaches for chemical recycling of plastic waste," *Journal of Polymer Science*, vol. 58, no. 10, pp. 1347–1364, 2020, doi: https://doi.org/10.1002/pol.20190261.
[11] A. Northemann, "Recovery of styrene from waste polystyrene," US5672794A, Sep. 30, 1997 Accessed: Apr. 29, 2021. [Online]. Available: https://patents.google.com/patent/US5672794A/en
[12] A. Lopez-Urionabarrenechea, I. de Marco, B. M. Caballero, M. F. Laresgoiti, and A. Adrados, "Catalytic stepwise pyrolysis of packaging plastic waste," *Journal of Analytical and Applied Pyrolysis*, vol. 96, pp. 54–62, Jul. 2012, doi: 10.1016/j.jaap.2012.03.004.
[13] M. Martynis, Mulyazmi, E. Winanda, and A. N. Harahap, "Thermal Pyrolysis of Polypropylene Plastic Waste into Liquid Fuel: Reactor Performance Evaluation," *IOP Conf. Ser.: Mater. Sci. Eng.*, vol. 543, p. 012047, Jun. 2019, doi: 10.1088/1757-899X/543/1/012047.
[14] D. Almeida and M. de F. Marques, "Thermal and catalytic pyrolysis of plastic waste," *Polímeros*, vol. 26, pp. 44–51, Mar. 2016, doi: 10.1590/0104-1428.2100.
[15] K. Van Geem, "Light olefin production," in *Sustainable Chemical Production Processes*, Gent: UGent, 2016.
[16] P. Robinson, "Hydroconversion processes and technology for clean fuel and chemical production," 2011. doi: 10.1533/9780857093783.3.287.
[17] M. Giachino, "HANDBOOK OF PETROLEUM REFINING PROCESSES", Accessed: Sep. 05, 2021. [Online]. Available: https://www.academia.edu/23228512/HANDBOOK_OF_PETROLEUM_REFINING_PROCESSES_www_chemicalebooks_com_
[18] I. Vollmer *et al.*, "Beyond Mechanical Recycling: Giving New Life to Plastic Waste," *Angewandte Chemie International Edition*, vol. 59, no. 36, pp. 15402–15423, 2020, doi: 10.1002/anie.201915651.
[19] S. Papari, H. Bamdad, and F. Berruti, "Pyrolytic Conversion of Plastic Waste to Value-Added Products and Fuels: A Review," *Materials*, vol. 14, p. 2586, May 2021, doi: 10.3390/ma14102586.

[20] "Recycling and recovery routes of plastic solid waste (PSW): A review - ScienceDirect." https://www.sciencedirect.com/science/article/pii/S0956053X09002190 (accessed Nov. 04, 2021).
[21] S. Papari, K. Hawboldt, and R. Helleur, "Pyrolysis: A Theoretical and Experimental Study on the Conversion of Softwood Sawmill Residues to Biooil," *Industrial & Engineering Chemistry Research*, vol. 54, p. 150112111040005, Jan. 2015, doi: 10.1021/ie5039456.
[22] "Development and Validation of a Process Model To Describe Pyrolysis of Forestry Residues in an Auger Reactor | Energy & Fuels." https://pubs.acs.org/doi/10.1021/acs.energyfuels.7b01263 (accessed Nov. 04, 2021).
[23] M. Heydariaraghi, S. Ghorbanian, A. Hallajisani, and A. Salehpour, "Fuel properties of the oils produced from the pyrolysis of commonly-used polymers: Effect of fractionating column," *Journal of Analytical and Applied Pyrolysis*, vol. 121, pp. 307–317, Sep. 2016, doi: 10.1016/j.jaap.2016.08.010.
[24] S. Lovett, F. Berruti, and L. A. Behie, "Ultrapyrolytic Upgrading of Plastic Wastes and Plastics/Heavy Oil Mixtures to Valuable Light Gas Products," *Ind. Eng. Chem. Res.*, vol. 36, no. 11, pp. 4436–4444, Nov. 1997, doi: 10.1021/ie970109o.
[25] P. Kannan, A. Al Shoaibi, and C. Srinivasakannan, "Temperature Effects on the Yield of Gaseous Olefins from Waste Polyethylene via Flash Pyrolysis," *Energy Fuels*, vol. 28, no. 5, pp. 3363–3366, May 2014, doi: 10.1021/ef500516n.
[26] J. Aguado, D. P. Serrano, and J. M. Escola, "Catalytic Upgrading of Plastic Wastes," in *Feedstock Recycling and Pyrolysis of Waste Plastics*, John Wiley & Sons, Ltd, 2006, pp. 73–110. doi: 10.1002/0470021543.ch3.
[27] K.-H. Lee, "Thermal and Catalytic Degradation of Waste HDPE," in *Feedstock Recycling and Pyrolysis of Waste Plastics*, John Wiley & Sons, Ltd, 2006, pp. 129–160. doi: 10.1002/0470021543.ch5.
[28] A. A. Garforth, S. Ali, J. Hernández-Martínez, and A. Akah, "Feedstock recycling of polymer wastes," *Current Opinion in Solid State and Materials Science*, vol. 8, no. 6, pp. 419–425, Dec. 2004, doi: 10.1016/j.cossms.2005.04.003.
[29] C. G. Pernalete, J. Ibáñez, P. S. F. Mendes, K. M. Van Geem, and J. W. Thybaut, "Hydrocracking of complex mixtures: From bulk properties, over fundamental kinetics to detailed product composition," *Catalysis Today*, vol. 378, pp. 189–201, Oct. 2021, doi: 10.1016/j.cattod.2021.06.010.
[30] W. Wang, Y. Liu, Z. Liu, and S. Tian, "Detailed Chemical Composition of Straight-Run Vacuum Gas Oil and Its Distillates as a Function of the Atmospheric Equivalent Boiling Point," *Energy Fuels*, vol. 30, no. 2, pp. 968–974, Feb. 2016, doi: 10.1021/acs.energyfuels.5b02803.
[31] H. Dao Thi, M. R. Djokic, and K. M. Van Geem, "Detailed Group-Type Characterization of Plastic-Waste Pyrolysis Oils: By Comprehensive Two-Dimensional Gas Chromatography Including Linear, Branched, and Di-Olefins," *Separations*, vol. 8, no. 7, Art. no. 7, Jul. 2021, doi: 10.3390/separations8070103.
[32] T. Li, T. Shoinkhorova, J. Gascon, and J. Ruiz-Martínez, "Aromatics Production via Methanol-Mediated Transformation Routes," *ACS Catal.*, vol. 11, no. 13, pp. 7780–7819, Jul. 2021, doi: 10.1021/acscatal.1c01422.
[33] J. A. Onwudili, N. Insura, and P. T. Williams, "Composition of products from the pyrolysis of polyethylene and polystyrene in a closed batch reactor: Effects of temperature and residence time," *Journal of Analytical and Applied Pyrolysis*, vol. 86, no. 2, pp. 293–303, Nov. 2009, doi: 10.1016/j.jaap.2009.07.008.
[34] F. Pinto, P. Costa, I. Gulyurtlu, and I. Cabrita, "Pyrolysis of plastic wastes. 1. Effect of plastic waste composition on product yield," *Journal of Analytical and Applied Pyrolysis*, vol. 51, no. 1, pp. 39–55, Jul. 1999, doi: 10.1016/S0165-2370(99)00007-8.
[35] H. Jia, H. Ben, Y. Luo, and R. Wang, "Catalytic Fast Pyrolysis of Poly (Ethylene Terephthalate) (PET) with Zeolite and Nickel Chloride," *Polymers (Basel)*, vol. 12, no. 3, p. 705, Mar. 2020, doi: 10.3390/polym12030705.

[36] M. Kusenberg *et al.*, “A comprehensive experimental investigation of plastic waste pyrolysis oil quality and its dependence on the plastic waste composition,” *Fuel Processing Technology*, vol. 227, p. 107090, Mar. 2022, doi: 10.1016/j.fuproc.2021.107090.
[37] I. Fechete, “Paul Sabatier – The father of the chemical theory of catalysis,” *Comptes Rendus Chimie*, vol. 19, Oct. 2016, doi: 10.1016/j.crci.2016.08.006.
[38] A. Sztejnberg, “Vladimir Nikolayevich Ipatieff (1867-1952) -The Eminent Russian-American Chemist of the First Half of the XX Century,” vol. 4, pp. 71–81, Mar. 2020, doi: 10.13128/Substantia-647.
[39] P. Kokayeff, S. Zink, and P. Roxas, “Hydrotreating in Petroleum Processing,” in *Handbook of Petroleum Processing*, S. A. Treese, P. R. Pujadó, and D. S. J. Jones, Eds. Cham: Springer International Publishing, 2015, pp. 361–434. doi: 10.1007/978-3-319-14529-7_4.
[40] “US leads global refinery hydrotreater unit capacity.” https://www.offshore-technology.com/comment/us-global-refinery-hydrotreater-capacity/ (accessed Nov. 09, 2021).
[41] F. Adam, F. Bertoncini, C. Dartiguelongue, K. Marchand, D. Thiébaut, and M.-C. Hennion, “Comprehensive two-dimensional gas chromatography for basic and neutral nitrogen speciation in middle distillates,” *Fuel*, vol. 88, no. 5, pp. 938–946, May 2009, doi: 10.1016/j.fuel.2008.11.032.
[42] G. C. Laredo, P. M. Vega-Merino, F. Trejo-Zárraga, and J. Castillo, “Denitrogenation of middle distillates using adsorbent materials towards ULSD production: A review,” *Fuel Processing Technology*, vol. 106, pp. 21–32, Feb. 2013, doi: 10.1016/j.fuproc.2012.09.057.
[43] A. Stanislaus, A. Marafi, and M. S. Rana, “Recent advances in the science and technology of ultra low sulfur diesel (ULSD) production,” *Catalysis Today*, vol. 153, no. 1, pp. 1–68, Jul. 2010, doi: 10.1016/j.cattod.2010.05.011.
[44] G. H. C. Prado, Y. Rao, and A. de Klerk, “Nitrogen Removal from Oil: A Review,” *Energy Fuels*, vol. 31, no. 1, pp. 14–36, Jan. 2017, doi: 10.1021/acs.energyfuels.6b02779.
[45] F. Jiménez, V. Kafarov, and M. Nuñez, “Modeling of industrial reactor for hydrotreating of vacuum gas oils: Simultaneous hydrodesulfurization, hydrodenitrogenation and hydrodearomatization reactions,” *Chemical Engineering Journal*, vol. 134, no. 1, pp. 200–208, Nov. 2007, doi: 10.1016/j.cej.2007.03.080.
[46] C. S. Raghuveer, J. W. Thybaut, R. De Bruycker, K. Metaxas, T. Bera, and G. B. Marin, “Pyridine hydrodenitrogenation over industrial NiMo/γ-Al2O3 catalyst: Application of gas phase kinetic models to liquid phase reactions,” *Fuel*, vol. 125, pp. 206–218, Jun. 2014, doi: 10.1016/j.fuel.2014.02.017.
[47] A. Parulkar, J. A. Thompson, M. Hurt, B.-Z. Zhan, and N. A. Brunelli, “Improving Hydrodenitrogenation Catalyst Performance through Analyzing Hydrotreated Vacuum Gas Oil Using Ion Mobility–Mass Spectrometry,” *Ind. Eng. Chem. Res.*, vol. 57, no. 27, pp. 8845–8854, Jul. 2018, doi: 10.1021/acs.iecr.8b01038.
[48] I. Mochida and K.-H. Choi, “An Overview of Hydrodesulfurization and Hydrodenitrogenation,” *Journal of the Japan Petroleum Institute*, vol. 47, no. 3, pp. 145–163, 2004, doi: 10.1627/jpi.47.145.
[49] C. Mase *et al.*, “Molecular Characterization of a Mixed Plastic Pyrolysis Oil from Municipal Wastes by Direct Infusion Fourier Transform Ion Cyclotron Resonance Mass Spectrometry,” *Energy Fuels*, vol. 35, no. 18, pp. 14828–14837, Sep. 2021, doi: 10.1021/acs.energyfuels.1c01678.
[50] C. Schaller, D. Rogez, and A. Braig, “Hindered amine light stabilizers in pigmented coatings,” *Journal of Coatings Technology Research*, vol. 6, pp. 81–88, Mar. 2009, doi: 10.1007/s11998-008-9130-8.
[51] B. L. Kaul, “Coloration of plastics using organic pigments,” *Review of Progress in Coloration and Related Topics*, vol. 23, no. 1, pp. 19–35, 1993, doi: 10.1111/j.1478-4408.1993.tb00093.x.
[52] W. Ścierski, “Migration of Sulfur and Nitrogen in the Pyrolysis Products of Waste and Contaminated Plastics,” *Applied Sciences*, vol. 11, no. 10, Art. no. 10, Jan. 2021, doi: 10.3390/app11104374.
[53] H. Toraman, T. Dijkmans, M. Djokic, K. Van Geem, and B. Marin, “Detailed compositional characterization of plastic waste pyrolysis oil by comprehensive two-dimensional gas-chromatography

coupled to multiple detectors," *Journal of chromatography. A*, vol. 1359, Jul. 2014, doi: 10.1016/j.chroma.2014.07.017.
[54] S. Kim, N. Lee, and J. Lee, "Pyrolysis for Nylon 6 Monomer Recovery from Teabag Waste," *Polymers*, vol. 12, no. 11, Art. no. 11, Nov. 2020, doi: 10.3390/polym12112695.
[55] J. Ancheyta, A. Alvarez-Majmutov, and C. Leyva, "Hydrotreating of oil fractions," 2016, pp. 295–329. doi: 10.1002/9781119248491.ch13.
[56] M.-T. Nguyen, M. Tayakout-Fayolle, G. D. Pirngruber, F. Chainet, and C. Geantet, "Kinetic Modeling of Quinoline Hydrodenitrogenation over a NiMo(P)/Al2O3 Catalyst in a Batch Reactor," *Ind. Eng. Chem. Res.*, vol. 54, no. 38, pp. 9278–9288, Sep. 2015, doi: 10.1021/acs.iecr.5b02175.
[57] S. H. Yang and C. N. Satterfield, "Catalytic hydrodenitrogenation of quinoline in a trickle-bed reactor. Effect of hydrogen sulfide," *Ind. Eng. Chem. Proc. Des. Dev.*, vol. 23, no. 1, pp. 20–25, Jan. 1984, doi: 10.1021/i200024a004.
[58] "Hydrodenitrogenation of quinoline and its intermediates over sulfided NiW/γ-Al2O3 in the absence and presence of H2S - Luan - 2009 - Asia-Pacific Journal of Chemical Engineering - Wiley Online Library." https://onlinelibrary.wiley.com/doi/10.1002/apj.322 (accessed Mar. 31, 2022).
[59] Q. Wei *et al.*, "Hydrodenitrogenation of basic and non-basic nitrogen-containing compounds in coker gas oil," *Fuel Processing Technology*, vol. 129, pp. 76–84, Jan. 2015, doi: 10.1016/j.fuproc.2014.08.001.
[60] S. Tian, X. Li, A. Wang, Y. Chen, H. Li, and Y. Hu, "Hydrodenitrogenation of Quinoline and Decahydroquinoline Over a Surface Nickel Phosphosulfide Phase," *Catal Lett*, vol. 148, no. 6, pp. 1579–1588, Jun. 2018, doi: 10.1007/s10562-018-2370-z.
[61] H. Topsoe, B. S. Clausen, and F. E. Massoth, *Hydrotreating catalysis*. Berlin; New York: Springer, 1996.
[62] S. C. Kim and F. E. Massoth, "Kinetics of the Hydrodenitrogenation of Indole," *Ind. Eng. Chem. Res.*, vol. 39, no. 6, pp. 1705–1712, Jun. 2000, doi: 10.1021/ie9906518.
[63] L. Zhang and U. S. Oskan, "Hydrodenitrogenation of indole over NiMo sulfide catalysts," Art. no. CONF-960652-, Dec. 1996, Accessed: Apr. 04, 2022. [Online]. Available: https://www.osti.gov/biblio/468034
[64] S. S. Bello *et al.*, "A Review on the Reaction Mechanism of Hydrodesulfurization and Hydrodenitrogenation in Heavy Oil Upgrading," *Energy Fuels*, vol. 35, no. 14, pp. 10998–11016, Jul. 2021, doi: 10.1021/acs.energyfuels.1c01015.
[65] A. Bunch, L. Zhang, G. Karakas, and U. Ozkan, "Reaction network of indole hydrodenitrogenation over NiMoS/γ-Al 2O 3 catalysts," *Applied Catalysis A-general - APPL CATAL A-GEN*, vol. 190, pp. 51–60, Jan. 2000, doi: 10.1016/S0926-860X(99)00270-7.
[66] C. I. Chu and I. Wang, "Kinetic study on hydrotreating," *ACS Publications*, May 01, 2002. https://pubs.acs.org/doi/pdf/10.1021/i200017a020 (accessed Apr. 29, 2022).
[67] D. Ferdous, A. K. Dalai, and J. Adjaye, "Hydrodenitrogenation and Hydrodesulfurization of Heavy Gas Oil Using NiMo/Al2O3 Catalyst Containing Boron: Experimental and Kinetic Studies," *Ind. Eng. Chem. Res.*, vol. 45, no. 2, pp. 544–552, Jan. 2006, doi: 10.1021/ie050094r.
[68] "Comparison of Hydrodenitrogenation of Basic and Nonbasic Nitrogen Compounds Present in Oil Sands Derived Heavy Gas Oil | Energy & Fuels." https://pubs.acs.org/doi/10.1021/ef0001484 (accessed Apr. 29, 2022).
[69] R. A. Diaz-Real, R. S. Mann, and I. S. Sambi, "Hydrotreatment of Athabasca bitumen derived gas oil over nickel-molybdenum, nickel-tungsten, and cobalt-molybdenum catalysts." https://in.booksc.eu/book/29218717/d00316 (accessed Apr. 29, 2022).
[70] "Two-Stage Hydrotreating of Athabasca Heavy Gas Oil with Interstage Hydrogen Sulfide Removal: Effect of Process Conditions and Kinetic Analyses | Industrial & Engineering Chemistry Research." https://pubs.acs.org/doi/10.1021/ie030857f (accessed Apr. 29, 2022).
[71] Y. Yin *et al.*, "Kinetics toward mechanism and real operation for ultra-deep hydrodesulfurization and hydrodenitrogenation of diesel," *AIChE Journal*, vol. 67, no. 7, p. e17188, 2021, doi: 10.1002/aic.17188.

[72] Q. Xin, A. Alvarez-Majmutov, H. D. Dettman, and J. Chen, “Hydrogenation of Olefins in Bitumen-Derived Naphtha over a Commercial Hydrotreating Catalyst,” *Energy Fuels*, vol. 32, no. 5, pp. 6167–6175, May 2018, doi: 10.1021/acs.energyfuels.8b00344.
[73] M. Badawi, L. Vivier, and D. Duprez, “Kinetic study of olefin hydrogenation on hydrotreating catalysts,” *Journal of Molecular Catalysis A: Chemical*, vol. 320, no. 1, pp. 34–39, Apr. 2010, doi: 10.1016/j.molcata.2009.12.012.
[74] A. Lengyel, S. Magyar, D. Kalló, and J. Hancsók, “Catalytic Coprocessing of Delayed Coker Light Naphtha with Light Straight-run Naphtha/FCC Gasoline,” *Petroleum Science and Technology*, vol. 28, pp. 946–954, Apr. 2010, doi: 10.1080/10916460902937059.
[75] Q. Xin, A. Alvarez-Majmutov, R. Gieleciak, J. Chen, and H. Dettman, “Hydrotreating of Olefins in Thermally Processed Bitumen under Mild Conditions,” *Energy & Fuels*, vol. 33, Mar. 2019, doi: 10.1021/acs.energyfuels.9b00157.
[76] B. Mattson *et al.*, “Heterogeneous Catalysis: The Horiuti-Polanyi Mechanism and Alkene Hydrogenation,” *Journal of Chemical Education*, vol. 90, pp. 613–619, May 2013, doi: 10.1021/ed300437k.
[77] J. Thybaut, M. Saeys, and B. Marin, “Hydrogenation kinetics of toluene on Pt/ZSM-22,” *Chemical Engineering Journal*, vol. 90, pp. 117–129, Nov. 2002, doi: 10.1016/S1385-8947(02)00073-6.
[78] L. Coulier, “Hydrotreating model catalysts : from characterization to kinetics,” *Journal of Economic Psychology - J ECON PSYCH*, Jan. 2001.
[79] B. Zhang, “Hydroprocessing and the Chemistry,” in *Hydroprocessing Catalysts and Processes: The Challenges For Biofuels Production*, 2018, pp. 1–56. doi: 10.1142/9781786344847_0001.
[80] J. van Gestel, L. Finot, J. Leglise, and J. C. Duchet, “CoMo/Al2O3 VERSUS NiMo/Al2O3 SULPHIDE CATALYSTS : SENSITIVITY TO REACTION CONDITIONS FOR HDS AND HYDROGENATION,” *Bulletin des Sociétés Chimiques Belges*, vol. 104, no. 4–5, pp. 189–195, 1995, doi: 10.1002/bscb.19951040403.
[81] A. C. Vicente da Silva, “Study of the liquid activation of CoMo and NiMo catalysts,” Tecnico Lisboa, 2014. Accessed: Dec. 02, 2021. [Online]. Available: https://www.semanticscholar.org/paper/Study-of-the-liquid-activation-of-CoMo-and-NiMo/51e72665cf7d3dd7c488acf2b87393f42f287021
[82] S. Texier, G. Berhault, G. Pérot, and F. Diehl, “Activation of alumina-supported hydrotreating catalysts by organosulfides or H2S: Effect of the H2S partial pressure used during the activation process,” *Applied Catalysis A: General*, vol. 293, pp. 105–119, Sep. 2005, doi: 10.1016/j.apcata.2005.07.026.
[83] J. Ancheyta, *Experimental Methods for Evaluation of Hydrotreating Catalysts*, 1st ed. Mexico City: Wiley, 2020. Accessed: Mar. 28, 2022. [Online]. Available: https://www.wiley.com/en-be/Experimental+Methods+for+Evaluation+of+Hydrotreating+Catalysts-p-9781119517993
[84] J. Lauwaert, C. S. Raghuveer, and J. W. Thybaut, “A three-phase Robinson-Mahoney reactor as a tool for intrinsic kinetic measurements: Determination of gas-liquid hold up and volumetric mass transfer coefficient,” *Chemical Engineering Science*, vol. 170, pp. 694–704, Oct. 2017, doi: 10.1016/j.ces.2017.02.041.
[85] “On-line gas chromatographic analysis of hydrocarbon effluents : Calibration factors and their correlation - ScienceDirect.” https://www.sciencedirect.com/science/article/pii/S002196730186965X (accessed May 25, 2022).
[86] W. A. Dietz, “Response Factors for Gas Chromatographic Analyses,” *Journal of Chromatographic Science*, vol. 5, no. 2, pp. 68–71, Feb. 1967, doi: 10.1093/chromsci/5.2.68.
[87] E. Kordouli, B. Pawelec, C. Kordulis, A. Lycourghiotis, and J. L. G. Fierro, “Hydrodeoxygenation of phenol on bifunctional Ni-based catalysts: Effects of Mo promotion and support,” *Applied Catalysis B: Environmental*, vol. 238, pp. 147–160, Dec. 2018, doi: 10.1016/j.apcatb.2018.07.012.

[88] V. Vanrysselberghe and G. F. Froment, “Hydrodesulfurization of Dibenzothiophene on a CoMo/Al2O3 Catalyst: Reaction Network and Kinetics,” *Ind. Eng. Chem. Res.*, vol. 35, no. 10, pp. 3311–3318, Jan. 1996, doi: 10.1021/ie960099b.

[89] C. Tu, S. Liu, C. Liu, X. Wu, Q. Chen, and W. Huang, “Single-Pot Synthesis of NiMo-Al2O3 Catalyst for Quinoline Hydrodenitrogenation,” *Energy Fuels*, vol. 35, no. 2, pp. 1120–1128, Jan. 2021, doi: 10.1021/acs.energyfuels.0c03186.

[90] “Chemical Reactor Analysis and Design, 3rd Edition | Wiley,” *Wiley.com*. https://www.wiley.com/en-us/Chemical+Reactor+Analysis+and+Design%2C+3rd+Edition-p-9780470565414 (accessed Jun. 17, 2022).

[91] Y. Guo, L. Zhao, C. Dai, B. Chen, and X. Fang, “H2 Solubility and Mass Transfer in Diesel: An Experimental and Modeling Study,” *Energy & Fuels*, vol. 30, Jul. 2016, doi: 10.1021/acs.energyfuels.6b00733.

FACULTY OF ENGINEERING AND ARCHITECTURE

Experimental study and kinetic modelling of combined deep hydrodenitrogenation and olefin saturation

Klaus Jacobs Cruz

Student Number: 02007302

Supervisors: Prof. Dr. Ir. Joris Thybaut, Prof. Dr. Ir. Kevin Van Geem

Councellors: Ir. Cesar Pernalete

Master's dissertation submitted in order to obtain the academic degree of
Master of Science in Chemical Engineering

Academic Year 2021-2022

GHENT UNIVERSITY